POLITECNICO DI TORINO

Corso di Laurea Magistrale in Ingegneria per L'ambiente e il Territorio

Tesi di Laurea Magistrale

Influence of the Rio Pontè on the integrity of the Serre la Voute A32 viaduct: effect of sediment transport and river instabilities

Supervisor:

Prof. Roberto Revelli

Co-Supervisor:

Andrea Valente Arnaldi

Candidate:

Dailis Ortega Leguia

March 2021

ABSTRACT

This work aims to verify the influence of the Rio Pontè, a tributary of the Dora Riparia river, on the current integrity of the structures constituting the Serre la Voute A32 viaduct, located in the municipality of Salbertrand (Torino) under the presumptions on instability and erosion phenomena due to the sediment transport and the fluvial dynamics of the river. The behavior of the so mentioned waterway will be analyzed with particular attention to the hydraulic behavior and the dynamics of solid transport. Particularly, it is intended to determine the erosion in the riverbed, specifically in correspondence with the structures of interest, whose integrity can be influenced by the fluvial dynamics, these structures correspond to two pillars, and two abutments built in reinforced concrete and footing on micro-piles of variable length, determined by the depth of the rigid and compact substrate. A Hydraulic and Sediment Transport model will be built to be implemented with the HEC-RAS numerical software which is worldwide use in the engineering field. The results obtained will be analyzed to evaluate the need for implementation of works aimed at reducing hydrogeological risk and consolidation of the slopes corresponding to critical areas, such as the implementation of geosynthetics for erosion control for the protection of the viaduct structures.

ACKNOWLEDGEMENTS

Throughout the writing of this thesis, I have received a great deal of support and assistance. I would like to thank first my supervisor, Professor Roberto Revelli, Co-Supervisor Andrea Valente Arnaldi, and AVA teamwork whose expertise and support were key in the development of this thesis.

I am grateful to all of those with whom I have had the pleasure to work during this and other projects along during my Bachelor's and Master's studies. Especially, to the professors in the Environmental and Land Engineering department at Politecnico di Torino and the Environmental and Civil Engineering department at Universidad Tecnológica de Bolivar, to whom I will always be deeply thankful for having shared their expertise in their courses.

I would like to acknowledge my colleague Geraldine at Politecnico di Torino and my friends at Universidad Tecnológica de Bolivar for their wonderful collaboration and company in and outside the classroom.

I am deeply grateful to my family for all the support they have shown me through this project, and during these seven years of learning and professional growth. I would like to thank my mother, father, and sisters Dayana and Daniela, whose love and support are with me in all my endeavors.

TABLE OF CONTENTS

INTRODUCTION

Soil erosion by water remains an important engineering issue, being capable of affecting natural, agricultural, and urban environments due to its impact on flood risk, loss of topsoil, sedimentation of waterways, influence on instability phenomena (landslides), and damage to infrastructure such as roads, buildings, and utility supply networks. Furthermore, the flow conditions and sediment size distribution define the bedform and shape of a river, these bedforms have an influence on the resistance to the flow and thus can alter the flow depth significantly. Thereby, the study of the movement of sediment particles under the influence of gravity and fluid drag constitutes a field of important interest.

This work arises from the need to verify the influence of the Rio Pontè, a tributary of the Dora Riparia river, on the current integrity of the structures constituting the Serre la Voute A32 viaduct, located in the municipality of Salbertrand (Torino), this infrastructure is presumed to be at risk of instability and erosion phenomena due to the sediment transport and the fluvial dynamics of the river.

It is intended, with this work to analyze the behavior of the so mentioned waterway, regarding the hydraulic behavior and the dynamics of solid transport. Particularly, it is intended with this Thesis to determine the erosion in the riverbed, specifically in correspondence with the structures of interest, whose integrity can be influenced by the fluvial dynamics, these structures correspond to two pillars, and two abutments built in reinforced concrete and footing on micropiles of variable length, determined by the depth of the rigid and compact substrate.

To carry out this study, this thesis aims to build an appropriate model to be implemented with the HEC-RAS numerical software, used worldwide in the engineering field. The results obtained will be analyzed to evaluate the need to implement works aimed at reducing hydrogeological risk and consolidation of the slopes corresponding to critical areas.

Preliminary critical areas will be identified in the first part of this Thesis. The following analysis will be based on geological and geotechnical studies carried out for this purpose,

following a respective survey campaign for the geological and geotechnical characterization of the materials present on-site, as well as their geometric configuration, in order to verify the stability of the slopes on which the viaduct pillars foundations are found, in seismic conditions or in the presence of intense and prolonged rainy events, as well as in their absence. A Hydrological Model will be built next, which will provide the bases and input data for the Hydraulic Model and Sediment Transport Model presented as follows in this Thesis. Identified solutions for the verified critical areas will be presented in the final part.

CHAPTER 1: INITIAL ASSESSMENT

1.1. TERRITORIAL FRAMEWORK

The area of concern is located in correspondence with the watershed of Rio Pontè located in the south-eastern of the municipal area of Salbertrand (TO), on the Cozie Alps slopes, about 70 km away from Turin city. The area develops in a Northwest - Southeast direction in correspondence with a side valley that opens onto the left side of the Val di Susa. The Pontè river is therefore a left tributary of the Dora Riparia river. The valley under study is bounded to the north by the ridge that develops at the entrance to the Serre la Voute tunnel, to the east by the ridge that crosses the Deveys' hamlet, and to the south by the delta section.

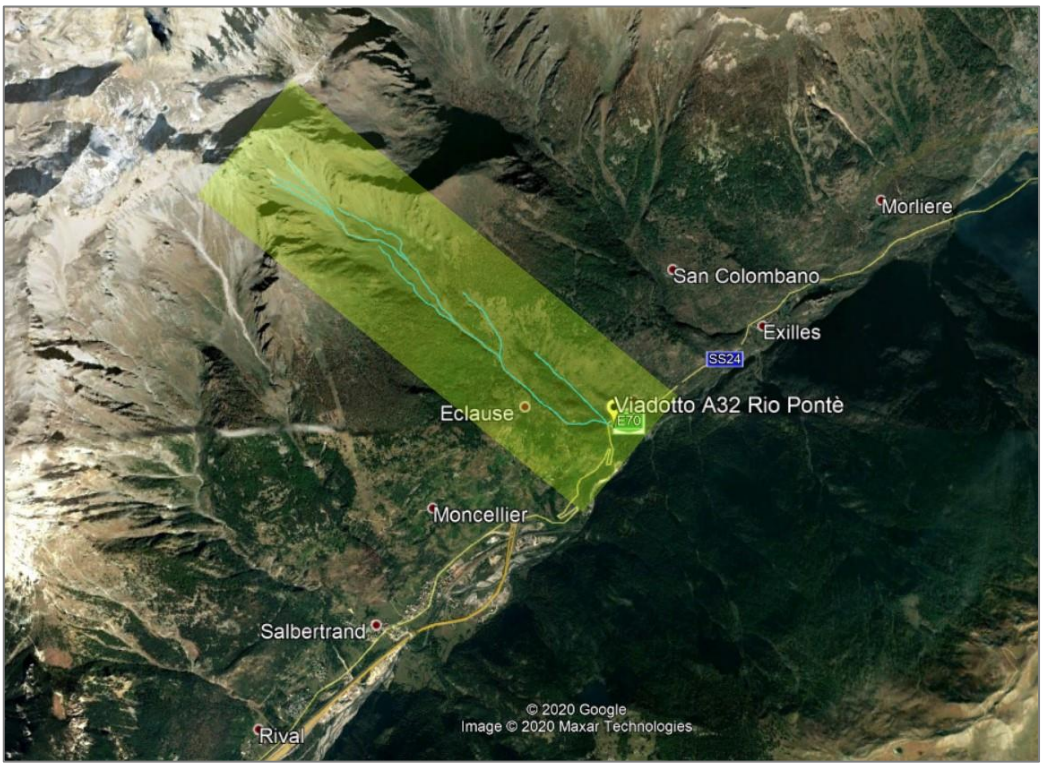

Figure 1. Territorial framework of the study area.

The planned interventions are located exclusively in the vicinity of the pillars of the Serre la Voute viaduct of the A-32 Turin - Bardonecchia highway, with UTM coordinates 335412.12 m E - 4994813.10 m N approximately, located in the southern sector of the catchment area covered by this study, as shown in Figure 1.

The Rio Pontè, which is the object of study in this document, is a small torrential tributary of the Dora Riparia river, having a basin area of about 4.3 km2, characterized by poor hierarchization of the drainage. The aforementioned tributary is located on the left bank, near the municipal border between Salbertrand and Exilles.

The Dora Riparia river runs through the entire valley of the Susa Valley until it flows into the Turin plain. The catchment area of the aforementioned waterway occupies an area of approximately 1,321 km2 and develops in an area between the altitudes of 3,583 m a.s.l. and 224 m a.s.l. (E. Gallo, D. Ganora, F. Laio, A. Masoero & P. Claps, 2014). Average rainfall varies from 800 mm/year to just over 1000 mm / year. The hydrographic basin of the Dora Riparia River is shown in Figure 2.

The main tributaries of the Dora Riparia river, which determine a considerable contribution, are both located on the left bank and are the Dora di Bardonecchia and the Cenischia stream, which flow into the main channel respectively in the municipalities of Oulx and Susa.

The hydraulic regime is of the permanent snowy river type, normally characterized by a main maximum in late spring due to precipitation and the melted snow accumulated on the ground during winter, a secondary peak due to autumn rainfall, and two minimums, one more evident in winter and one of greater importance, at the end of summer, when even at higher altitudes the snow is completely melted.

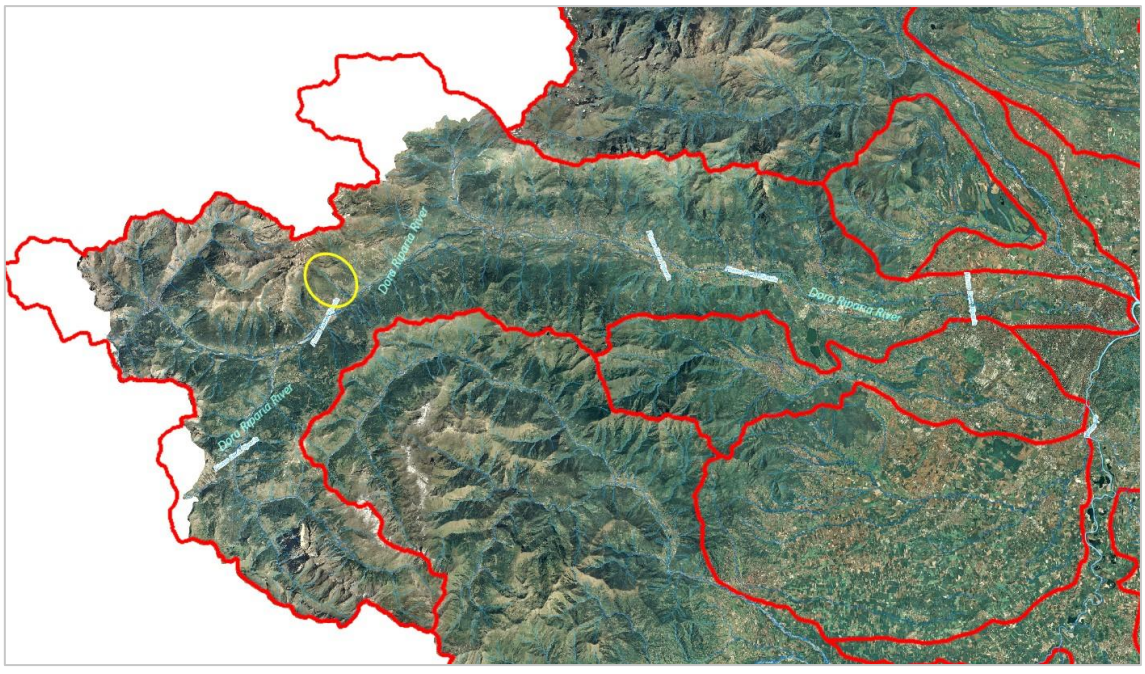

Figure 2. Hydrographic basin of the Dora Riparia river, Study area marked in yellow.

1.2. ANALYSIS OF THE STATE OF THE SITE

The valley conforming the area under study is characterized by slopes with variable steepness, interrupted by local slope breaks from upstream to downstream. This valley is intersected by the Rio Pontè bounded to the north by the head of the river, to the west by the ridge that develops at the entrance to the Serre la Voute tunnel, to the east from the ridge crossing the Deveys hamlet and to the south from the closing section of the basin.

There's a presence of elevated acclivity characterizing the head of the hydrological basin, which decreases at lower altitudes. The sector immediately upstream of the area near the viaduct is characterized by a greater steepness in the vicinity of the sectors most affected by the waterway under examination, while the surrounding area shows various slope breaks due to the presence of terraces operated by the anthropic action. The entire basin is crossed by the Pontè river, a left tributary of the Dora Riparia, which has the typical physical, morphological, and flow characteristics of mountain waterways basins. The riverbed is extremely sharp, especially immediately upstream of the area subjected to interventions and with high differences in height characterized by slope breaks with less steepness.

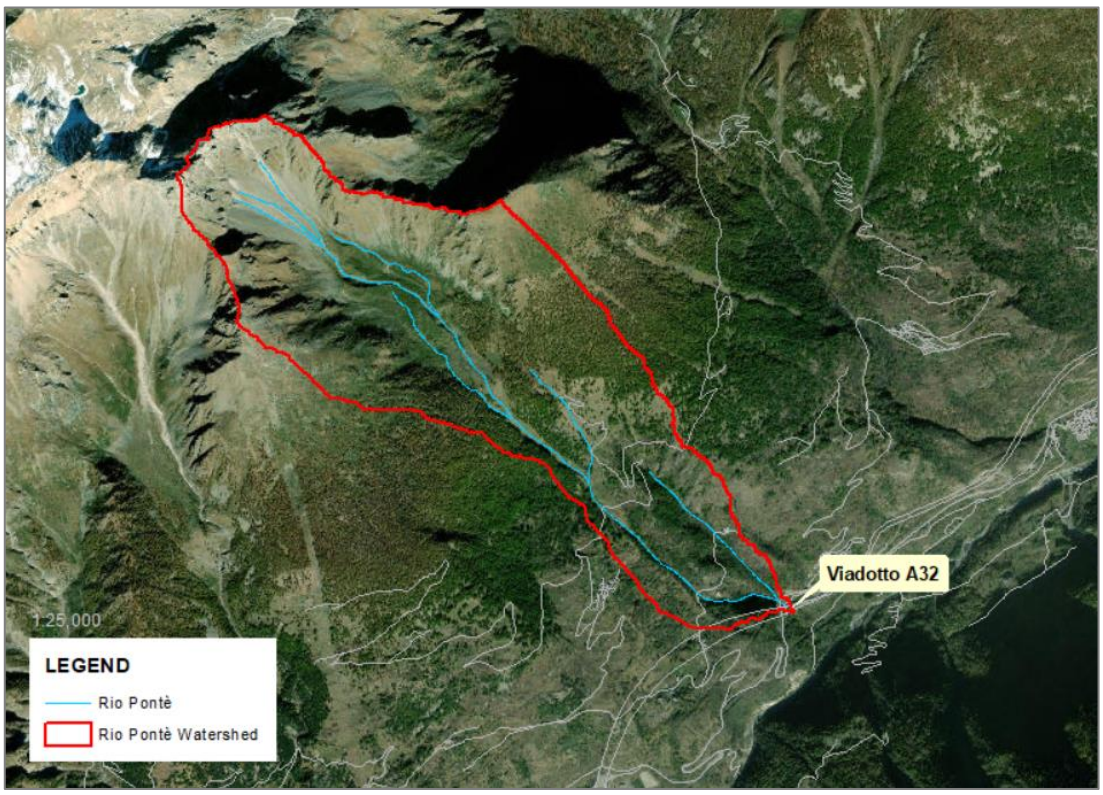

Figure 3. Rio Pontè watershed

Critical issues were identified both in the right and left banks of the Rio Pontè. On the right bank, the criticalities are mainly due to the sliding downstream of the surface material constituting the bank itself and to a lesser extent to the erosion at the foot of the aforementioned bank, caused by the action of the stream. During high-intensity meteoric events, this phenomenon is mainly evidenced, the rainfall action causes a widespread runoff along the slope and an increase in the erosive intensity of the river. Therefore, there is at the foot of the slab of the viaduct's abutments, a superficial sliding which has resulted in the loss of part of the support of the work downstream, creating a modest instability. This phenomenon is developed with different intensities in correspondence with the two abutments in question so that the upstream abutment is more compromised by the disruption phenomenon than the one located further downstream. Abutments on the right bank of the river are shown in Figure 4 and Figure 5.

The main criticality on the left bank is linked to the solid transport and its deposition during flood events, in correspondence with the pillar located further downstream (Pillar B), which is located almost inside the riverbed (Figure 6). The morphology of the site is characterized by a decrease in the slope of the riverbed, by a smaller incision in the watercourse, and by the consequent increase in the runoff section that causes an accumulation of transport material against the Pillar B and its immediate surroundings. Referring to Pillar A, there's no presence of any criticalities because of the location of the pillar which is at a much higher elevation respecting the riverbed thus being not influenced by the river dynamics.

The structures in question are based on micropiles of variable length, which are set at a depth such as to make them integral with the rigid and compact substrate. This peculiarity allows to exclude the presence of serious problems of instability of the structural works in question, in fact, the only criticalities found are essentially linked to superficial and modest instability phenomena.

Figure 4. Abutment A, located upstream on the right bank of rio Pontè

Figure 5. Abutment B, Located downstream on the right bank of rio Pontè.

Figure 6. Pillar B, located downstream on the left bank of rio Pontè.

Figure 7. Debris accumulation near the valley pillar on the left bank of rio Pontè. Presence of heterometric blocks (max 3x3x1.5 m) in a sandy-gravelly matrix.

Generally, the Rio Pontè develops along with sectors of medium-high steepness, deeply engraved, interspersed with slopes with less steepness or with rock jumps. The riverbed is mainly made up of abundant coarse material mobilized and deposited by the stream itself during its evolution, while outcrops of the lithoid substrate which are modeled and eroded by the waters of the river are rarely observed. In areas where the Rio Pontè is more

marked and bordered by steep slopes, it is not uncommon to reach debris, branches, and trunks coming from the adjacent slopes, as well as transported by avalanches, along the river channel (Figure 7).

Along the riverbed, mainly in correspondence with the crossings (road and fords), there are different types of hydraulic engineering interventions, such as wooden bridles and re-profiling of the riverbed (Figure 8), designed to protect the most vulnerable elements from debris flows and flood events. The triggering of a debris flow is a function of the geotechnical and hydrogeological characteristics of the material that constitutes the cover and of the volume of water present in the triggering area. These two elements are controlled by factors such as the topography as well as the shape and inclination of the slope, the vegetation, and the geological and structural conditions of the substrate. Given the high steepness of the slope, the strong incision of the river and the abundance of movable material, the basin of the Rio Pontè is an area at risk, as has already been demonstrated by the presence of debris flow deposits upstream of the provincial road which leads to the “Grange della Valle” hamlet. It is notable in Figure 10 the presence of large blocks immersed in a finer sandy matrix. Along the banks, long cords develop parallel to the river channel.

Figure 8. wooden bridle located upstream along the forest road

Figure 9. Riverbed of rio Pontè between the main road and the forest road.

Figure 10. Deposit of debris flow.

1.3. CRITICAL ISSUES IDENTIFIED IN THE STUDY AREA

As already mentioned in the previous section, the main problems encountered in the area under analysis are prevalently due to high-intensity meteoric events causing the surface material of the bank to slide downstream, the runoff along the slope produced by precipitations, intervene in an increase of the erosive intensity of the river. The transport and deposition phenomena during torrential flood events represent another fundamental problem in the study area.

The accumulation present on-site consists of blocks of extremely variable dimensions, from decimetric to plurimetric, immersed in a scarce fine fraction mainly sandy and gravelly.

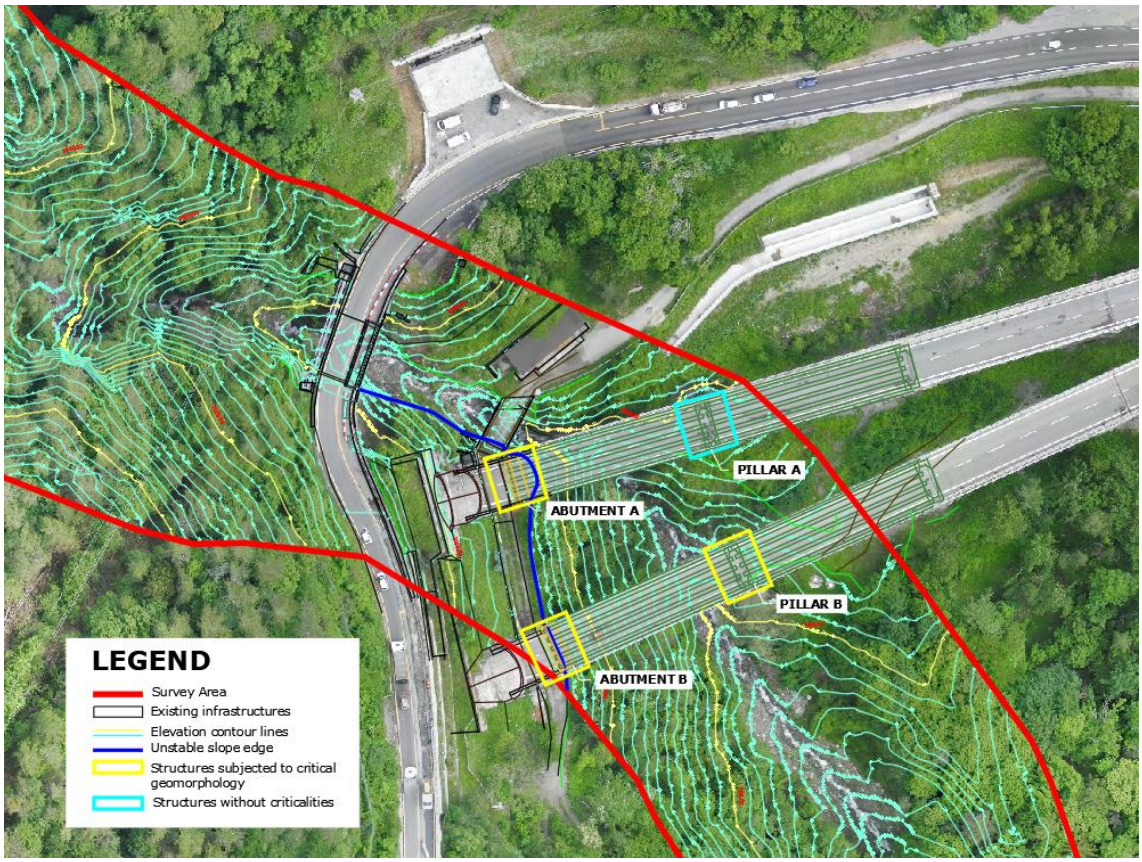

Figure 11. Identification of the criticalities in the study area

The abutments designated as Abutment A (located upstream) and Abutment B (located downstream), as shown in Figure 11, present a modest instability at the base caused by the sliding of surface material. Abutment A happens to be more affected by this instability phenomena.

The pillar located further downstream, almost inside the riverbed, designated as Pillar B, is mostly affected by the accumulation of transported material against it and its surrounding areas.

With the foregoing, it should be noted that the analysis of this work will be based on these structures and their proper protection against instability phenomena. In the next chapters, the characteristics of the study area are described further, from which it will be possible to build the hydraulic model to determine the solid transport in the riverbed of the channel. In Chapter 4 and Chapter 5 of this document, this model and its respective results are discussed in greater detail.

CHAPTER 2: CHARACTERIZATION OF THE STUDY AREA

2.1. WATERSHED CHARACTERIZATION

2.1.1. MORPHOMETRY

The Morphometric analysis of watershed is a method for the identification of the relationship of different aspects in the area, watershed could be then evaluated in various geomorphological and topographical conditions. The indices of watershed morphometry make possible the interpretation of the shape and hydrological characteristics of a river basin. The morphometric analysis of watershed helps to know the aspects of linear, areal, and relief parameters, it gives an idea about the characteristics of the discharge basin regarding slope, topography, soil condition, runoff characteristics, surface water potential, etc.

LINEAR ASPECTS

Stream Order (U): Indicates the level of branching in a river system. The smallest permanent streams are called “first order”. Two first order streams join to form a larger, second order stream; two second order streams join to form a third order, and so on. Smaller streams entering a higher-ordered stream do not change their order number (Strahler, 1964). The drainage network of the study area is of a second order basin as illustrated in Figure 12.

Stream Number (Nu): It refers to the total number of streams corresponding to each order. The number of streams gradually decreases as the stream order increases. The total stream number of the basin under study is thirteen.

Stream Length (Lu): The length of a stream is represented by the total length of all streams in a particular order (Horton, 1945). Generally, with an increase in stream order, the total length of stream segments decreases; the total length of stream segments is high in first order and decreases with the increase in stream order (Aldharab et al., 2018;

Waikar and Nilawar 2014). Stream length in the study area was considered according to Horton with the helping of ArcGIS tools, the total stream length on the study area is 9.03 Km.

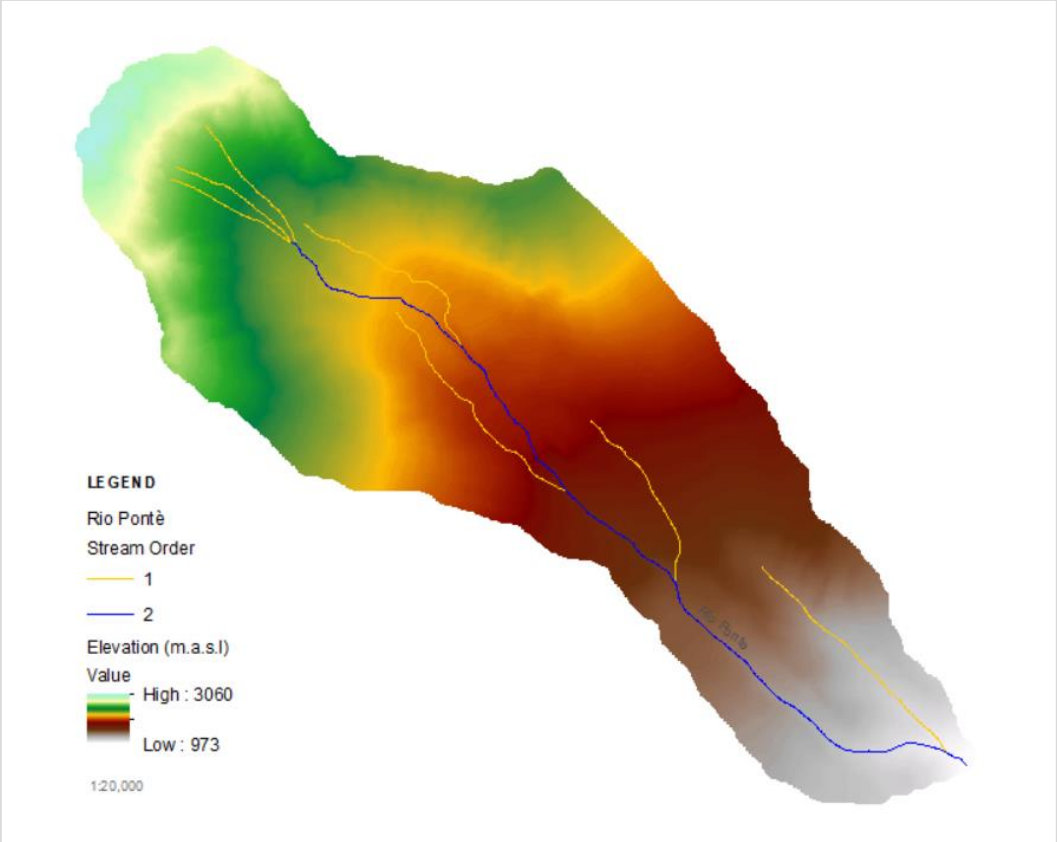

Figure 12. Identification of the stream order of the basin.

Linear aspects are summarized in Table 1:

Area (Km2)	Length (Km)	Stream numbers in different orders			Order wise total stream length (Km)		
		1	2	Total	1	2	Total
3.7	4.37	7	6	13	5.41	3.63	9.03

Table 1. Linear aspects of Pontè River watershed.

AREAL ASPECTS

Drainage density (Dd): defined by Horton (1945) as the total length of channels (Lu) in a catchment divided by the area (A) of the catchment. Drainage density factor is generally linked to climate, rock types, terrain relief, vegetation cover, infiltration capacity, surface roughness, and run-off intensity index. The drainage density is controlled principally by

two morphological factors which are the gradient of slope and relative relief. The drainage density of the basin under study is equal to 2.44. Smith (1950) was categorizing the drainage density into five different texture classes; these are shown in Table 2.

Drainage Density (Km/sq.km)	Texture
< 2	Very Coarse
2 - 4	Coarse
4 - 6	Moderate
6 - 8	Fine
> 8	Very fine

Table 2. Drainage density classification after Smith, 1950

Form Factor (Ff): It is defined as the ratio of the basin area to the square of the basin length. Form factor was introduced by Horton (1945) to predict the flow intensity of the basin. The higher values of form factor represent the basins with low peak flow for a shorter period; the lower values of the form factor represent the basins with low peak flow for a longer period. In an elongated basin, it is easy to manage the flash flood flows than those on the circular basins (Nutiyal, 1994). The value of form factor (Ff) for Rio pontè basin is 0.2 which indicates the elongated shape.

Elongation Ratio (Re): This was proposed by Schumn (1956) as the ratio between the diameters of a circle equal to the area of the drainage basin with the maximum length of that particular basin. Generally, it varies from 0.6 to 1.0 because of a wide diversity of climatic conditions and lithology. Three classes of elongation ratios can be defined: circular >0.9, oval 0.9 to 0.8, and less elongated <0.7; values close to 1.0 are normally found in regions of very low relief while values of 0.6 to 0.8 are frequently associated with the moderated to high relief and steep ground slope (Strahler, 1964). Frequently, circular basins are more efficient in the discharge of run-off than that of the elongated basin (Singh and Singh, 1997). With higher values of elongation ratio, there's high infiltration capacity and low runoff, while lower values are characterized by high susceptibility to sediment load and erosion process (Reddy et al., 2004). Elongation of the Pontè river basin is equal to 0.5 which suggests their susceptibility to erosion and sedimentation load.

Circularity Ratio (Cr): Defined as the ratio of the drainage basin area to the area of a circle with a circumference as the perimeter of the basin by Miller, (1953) and Strahler, (1964). Circularity ratio is influenced by the lithological character of the drainage basin;

length and frequency of stream network; geological structures; land use and land cover; climate; relief and slope of the drainage basin. The circularity ratio of the Pontè river is around 0.25 which means it is not representing a circular form.

Areal aspects are summarized in Table 3:

Drainage density (Km/Km2)	Elongation ratio	Circularity ratio	Form factor
3.7	0.5	0.25	0.19

Table 3. Areal Aspects of Pontè river watershed.

RELIEF ASPECTS

Relief aspects of the drainage basin are the function of the elevation measurements at several points in the watershed or along the drainage channel. The Relief aspects of the basin in question are summarized in Table 4.

Basin relief (R): Parameter that is used to know the extent denudation characteristics of the basin, and in the interpretation of the geomorphic developments and landform characteristic of the drainage basin. Basin relief refers to the elevation changes between the highest points on the ridge and the lowest points on the valley floor of the slope gradient of the channel that controls the flood pattern and the number of sediments which get transported (Hadley and Schumn, 1961). The value of relief for the basin in question is equal to 2010 m.a.s.l.

Relief Ratio (Rr): Presented by Schumn (1956) as the maximum relief in the drainage basin to the horizontal distance along the longest dimension of the drainage basin parallel to the mainline (Albaroot et al., 2018). Relief ratio is useful to measure the general steepness of the drainage basin; it is also closely related to the peak discharge and runoff intensity (Kumar A. et, 2015). The value of relief ratio for the Pontè river basin is equal to 0.5 which indicates steep slope and high relief (2010 m).

Slope (S): Refers to the inclination extent of the topographic landforms to the horizontal surface. Slope analysis is one of the essential parameters in morphometric studies; it is an important parameter to analyze the land use of any terrain. The slope is affected by lithology, climate, metrological parameters, runoff, vegetation, geological structures, and processes of denudation. Highest value of the slope is indicative of higher run-off and

erosion; a lower value of slope indicates less run-off (Dinakar, 2005; Pareta, 2004). The watershed of pontè river is characterized by a slope equal to 46 %.

Relief (m.a.s.l.)	Relief Ratio	Slope (m/m)
2010	0.5	0.46

Table 4. Relief Aspects of Pontè river watershed.

2.2. CLIMATOLOGIC CHARACTERIZATION OF WATERSHED

The climate of Piedmont can be classified as continental, while the mountainous areas above 1500 m have typical characteristics of the Alpine climate.

The climatological data were obtained from the meteorological database of *ARPA PIEMONTE* at the rain gauge station No. 150, *SALBERTRAND*, located at UTM coordinates 334301 X, 4993216 Y. The station is located at 1010 meters above sea level, data was analyzed considering a period of 19 years from 2000 to 2019.

An automatic validation criterion is applied to the daily rainfall data, shared by Arpa Piemonte as part of the National Environmental Protection System, which crosses the rainfall data with the air temperature value and the operation of the rain gauge heater. If this criterion is not met, the daily rainfall data are invalidated and temporarily not published; subsequently, with the manual control it is evaluated whether to recover them or not, this explains the missing data in Table 5 and Table 6.

2.2.1. PRECIPITATION

Monthly rainfall values were obtained in a period from 2000 to 2019, average monthly and annual precipitation values were calculated by adding the values of the various months. (Table 5).

Salbertrand is located 1032 meters above sea level. Salbertrand's climate is classified as humid and warm continental climate, the presence of reliefs in the study area favors convection, intensifying rainfall, and acting as a trigger factor. Salbertrand is a city with significant rainfall throughout the year, with an average total precipitation of 722 mm approximately.

Year	JAN	FEB	MAR	APR	MAY	JUN	JUL	AGO	SEP	OCT	NOV	DEC	Total/ year
2000	2.4	8.4	31.6	151.6	70.8	124	43.2	51	160	-	112.2	24.2	779.4
2001	-	39.8	130.6	26.6	199.2	43	43.8	17.2	42.8	44	41.8	2.4	631.2
2002	9.6	84	-	31	210.4	109.2	88.2	102.4	67.2	62	124.4	29.8	918.2
2003	15	15.2	5.6	63.8	38.8	88.4	11.8	46.8	45.4	101.8	61.4	99	593
2004	-	-	8.8	70.2	33	7.8	19.2	92.6	2.8	89.2	100.6	-	424.2
2005	8.4	1.2	29.8	160.2	25.8	63.2	50	44.2	78.2	62.4	24.2	20	567.6
2006	30.8	29.8	38.2	55	80.8	14	65.4	38	138	59.8	23.2	55	628
2007	17.4	7.6	77.6	72.2	121.4	99.4	18.2	29.6	26.8	36.8	25	30.4	562.4
2008	41.2	6.8	16.2	98	292.2	90.6	80.2	23.4	72.4	32.2	163	251.6	1167.8
2009	43.4	18.8	37.8	270.2	34.4	55.4	11.8	38.4	57	14	39.4	77	697.6
2010	38.8	49.8	41.2	48.4	126.6	116.8	33.6	36	31.8	58.2	81.8	30.6	693.6
2011	25.6	14	111	16.4	40	196.8	60.6	33	69.2	14.6	211.2	38.4	830.8
2012	36.6	0.2	10.8	132.4	65.6	21.4	30.6	24.6	82.6	50	170.6	30	655.4
2013	4.2	22.2	47.2	150	109.6	26.6	33.4	23.8	11.4	107.6	128.4	38.6	703
2014	57	58.4	27.6	26.8	32.4	70.4	106	48.4	48.2	40.8	107.6	-	623.6
2015	26	79.4	77.2	43.2	66.2	104.2	20.2	97.8	75	105.6	7.4	0	702.2
2016	36.2	96.2	59.6	57.4	64.6	58	48.4	7.2	54.2	46.6	356.6	-	885
2017	10.2	33.6	102.2	70.4	93	22.6	59.2	22.6	8.6	1.2	36.6	101.6	561.8
2018	219.4	38.4	63.2	136.8	160.4	34.4	54.4	62.2	29	175.6	177.8	-	1151.6
2019	4.4	38.6	19.4	82.2	64	-	95.6	-	-	-	252.4	102.2	658.8
Average	**34.81**	**33.81**	**49.24**	**88.14**	**96.46**	**70.85**	**48.69**	**44.17**	**57.93**	**61.24**	**112.28**	**58.18**	**721.76**

Table 5. Precipitation data (mm) from 2000 to 2019 at SALBERTRAND rain gauge station

The least amount of rain occurs in January – February with an average rainfall of approximately 34 mm. Most of the precipitation in the zone falls in November, averaging 112 mm (Figure 13).

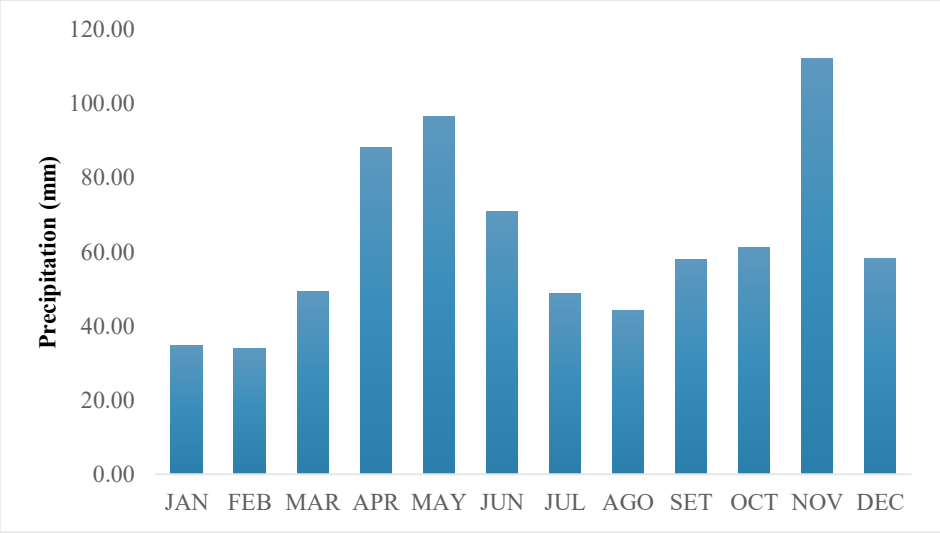

Figure 13. Average monthly Rainfall at SALBERTRAND rain gauge station

Data relating to intense rainfall was also obtained from the ARPA PIEMONTE database measured by the same station in the period between 1992 and 2015. In particular, the maximum annual values were used in the hydrologic analysis (see Chapter 3) for different precipitation durations available: 10, 20, and 30 minutes, and 1, 3, 6, 12, and 24 hours, shown in Table 6.

Year	10min	20min	30min	1h	3h	6h	12h	24h
1992	11.8	12.6	13	13.2	25.4	36.3	60.1	87.2
1993	10.6	11.8	11.8	11.8	15.4	27.2	48.9	66.5
1994	6.5	8.7	9.5	11.2	22.9	39.5	73.2	85.2
1995	11.8	13.8	14.6	15.4	20.6	38.2	64.1	100.6
1996	-	-	-	11.4	14.8	23	36	44.1
1997	3.6	6	8.2	13.2	17	26	39.8	43.9
1998	8.3	9.9	9.9	9.9	18	27.6	41.8	58.5
1999	5.8	6.6	7.4	10.8	23.4	35	57.3	84.6
2000	8.5	10.1	11.3	15.1	35.7	60.1	99.3	175.5
2001	6.3	8.1	9.1	11.1	19.8	32.4	51.7	60.3
2002	8	12.5	13.5	13.7	17.1	26.8	47.9	63.9
2003	12.1	15.7	17.5	18.5	24.3	31.2	46.9	49.3
2004	16	19.7	19.9	20.6	23.3	25.6	26.5	44.5
2005	11.1	17	17.2	17.2	24.9	43.3	68.6	80.4
2006	6.6	11	13.4	14.8	20.8	32.5	47.3	50.3
2007	7.4	13.6	18.2	22.9	26.9	27.3	37.7	47.1
2008	7	10	13	19.9	30.7	44	80.7	122.7
2009	5.2	5.4	5.9	10.4	21.2	31.1	55.7	93.2
2010	6.6	7.6	8	9.2	16.4	23.5	35.9	62
2011	9.8	12.6	14.6	16.4	25.7	47.5	83.6	132.5
2012	9	9.4	9.4	9.8	18.6	30.1	54.1	71
2013	5.1	6.3	6.9	9	15.6	26.5	38.1	45.3
2014	6.2	8.8	10.4	13.6	20.6	29.1	38.3	38.3
2015	5.6	6.4	7.6	10.2	21	33.3	38.1	50.1

Table 6. Maximum precipitation values for the various precipitation durations measured at SALBERTRAND rain gauge station

2.2.2. TEMPERATURE

The summers are comfortable, the winters are freezing and snowy, and it is partly cloudy year-round. Over the year, the temperature typically varies from -10 ºC to 28 °C.

The warm season lasts for almost three months, from June to September, with an average daily high temperature above 23 ºC. The cold season lasts almost three and a half months from November to March, with an average daily high temperature below 15.8 ºC (Figure 14).

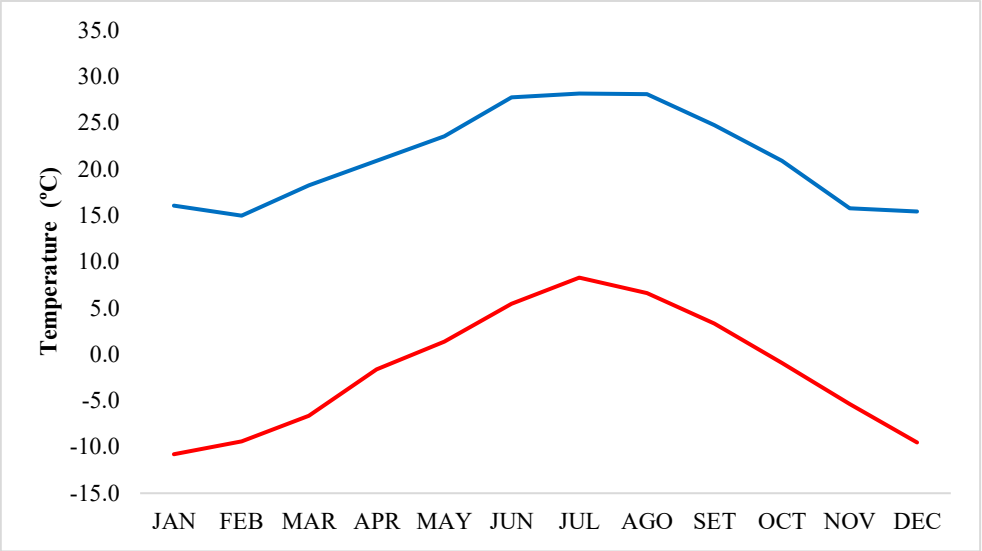

Figure 14. High (blue), and low (red) temperature at SALBERTRAND station.

2.2.3. HUMIDITY

Explained as relative humidity, which is the amount of water vapor actually in the air, expressed as a percentage of the maximum amount of water vapor the air can hold at the same temperature.

The humidity level in Salbertrand does not vary significantly over the year, which goes from a minimum of 62% during March to a maximum of 79.4% during October.

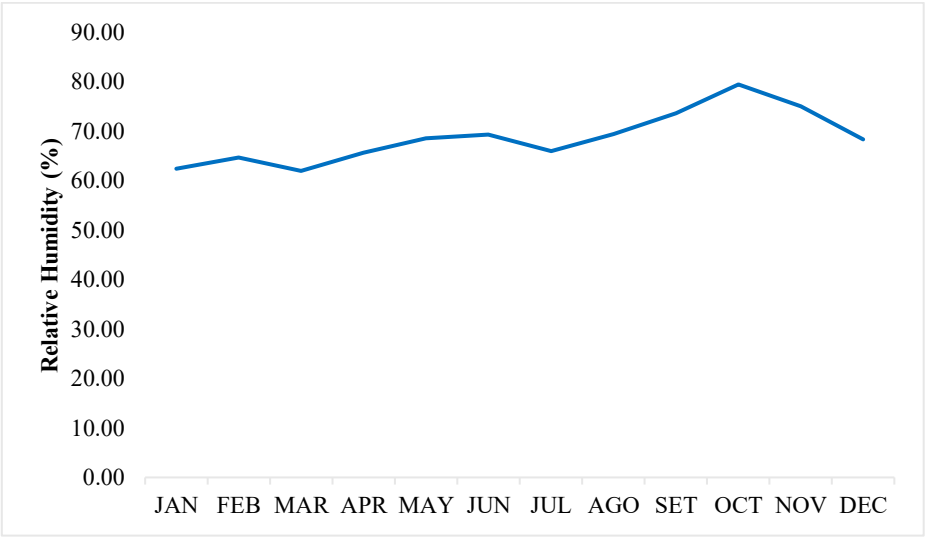

Figure 15. Average monthly Humidity at SALBERTRAND station

2.2.4. GEOLOGY

The investigated area is located in correspondence with the boundaries belonging to the Ambin Complex, near the contact area between the aforementioned unit and those of the Clarea Complex, both of which are part of the Ambin's tectonostratigraphic unit.

It is also known that throughout the area in question there is a wide distribution of Quaternary formations, almost always of significant importance, deriving mostly from the shaping of the valley in an alpine environment of glacial origin and subsequent evolution. There are also local gravitational accumulations and areas with debris layers, although of smaller thickness.

The Geological - Geotechnical Internal Report of Rio Pontè watershed area at Salbertrand (TO) contains the results and analysis of the geological survey carried out under the instructions of the correlator of this thesis made with the purpose of the Geological characterization of the study area, the conclusions, and summarized results are presented in this section of the thesis.

2.2.4.1. GEOLOGICAL FRAMEWORK

The characterization of the municipal territory of concern was made based on the results of the geological survey[1] carried out previously for this project, and on the available information reported on Sheet no. 153 “Bardonecchia” of the Geological Map of Italy at a 1:50,000 scale, as well as previous studies related to the adjacent Serre la Voute and Cassas landslides by Citiemme, Polithema, and Oboni (2000).

On the Geological Map of Italy concerning the basin in question, quaternary deposits are mainly identified, which dominate the terms of the substrate attributed to the “Ambin Complex” which is mainly constituted by Augen-gneiss containing albite + chlorite, showing a great compositional and textural homogeneity and of leucocratic gneiss (GAY, 1970).

The present facies are distributed on a continuum as follows:

- landslide, debris fan, and non-cohesive debris flow deposits;

[1] A. Valente Arnaldi (2020) Geological - Geotechnical Internal Report of Rio Pontè watershed area at Salbertrand (TO) unpublished.

- current gravelly-pebbly fluvial-torrential deposits with blocks;
- glacial and fluvioglacial deposits;
- eluvius-colluvial blanket
- lithoid substrate in rare outcrops.

In particular, based on the survey carried out, following what is indicated on the mentioned geological map, it can be said that in the intervention area they emerge, naturally or following anthropic interventions (road cuts, and earthworks), exclusively the following lithological terms: pretriassic crystalline basement, such as conglomerate metaconglomerates and quartzites (AZA) and gneiss of lens patterns with albite and chlorite (AZD), in addition to quaternary formations, represented by undifferentiated glacial deposits, Recent fluvial-torrential deposits, gravity deposits, and eluvial-colluvial blanket.

2.2.4.2. HYDROGEOLOGICAL CHARACTERISTICS

From the hydrogeological point of view, the survey carried out did not reveal the presence of groundwater collection points (wells) in the area as a whole and the surrounding area. Furthermore, the presence of natural water emergencies (sources) directly within the valley in question was not detected.

The area in question reveals overall characteristics of permeability strictly linked to the nature of the soils present on site, which show a lithoid substrate characterized by a medium-low primary permeability and by a secondary one, in the presence of partially altered and fractured levels. The loose cover deposits (glacial deposits, colluvium - eluvial layer, detrital layer) are affected by a permeability for porosity of varying degrees, from low to medium-high, as the glacial deposits and the colluvium - eluvial layer are formed in good it starts from relatively fine material, while the debris layer and gravitational deposits are made up of material with coarser grain size.

Deepwater circulation is made possible according to the extent and level of fracturing of the lithoid substrate.

2.2.4.3. LOCAL GEOLOGICAL MODEL

This study, aimed at defining the geological model of the site subject to intervention, follows the subsequent work phases, which have helped to determine the local geological structure:

- Preliminary bibliographic research;
- Geological-structural and geomorphological survey of the study area;
- Execution of the seismic survey campaign.

The preliminary bibliographic research allowed finding three simplified stratigraphies available from ARPA PIEMONTE carried out in correspondence with the highway pillars in question. The continuous coring boreholes carried out in the years 1980 and 1981 were taken to a variable depth between 23.0 and 28.0 m from the ground level.

The geological survey of the surface made it possible to define the lithostratigraphic and general geomorphological structure of the hydrological basin of the Pontè River, as well as the more detailed one of the study areas, as represented in the geological and geomorphological map presented in Figure 16.

In order to define the trend of the stratigraphy along the slope subject to intervention, the precise data deriving from the stratigraphic information of the surveys were integrated with a series of seismic tomography configurations, as well as point measurements.

The survey carried out in June 2020, provided for the realization of:

- n. 5 single-station microtremor measurements (HVSR).
- n. 3 MASW seismic prospecting;
- n. 1 seismic refraction prospecting;

The local geological model obtained, in accordance with the results of the surface and depth survey campaign carried out, as well as the information obtained from the stratigraphies available at *ARPA PIEMONTE*, is defined by the following units: Eluvial-colluvial hill, Quaternary cover deposits of mixed genesis and Lithoid substrate which are described below.

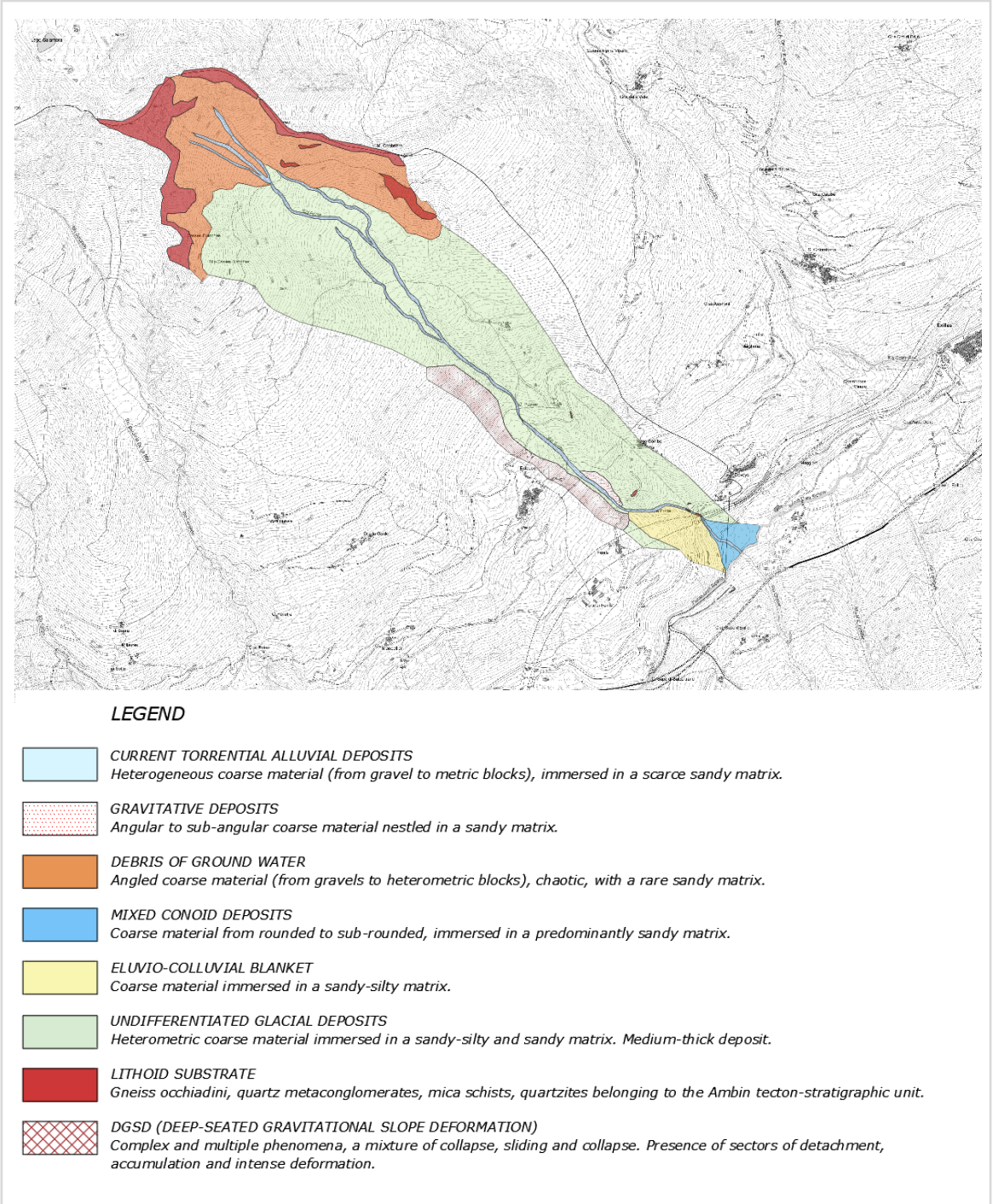

Figure 16. Geologic Map of the study area

Coltre eluvial – colluvial (0,0 – 0,50 m): Surface layer consisting of coarse material immersed in a sandy-silty matrix, mixed with vegetable soil rich in frustules and root systems, characterized by poor geotechnical parameters. Local presence of backfill.

Quaternary cover deposits of mixed genesis (0,50 – 18,0 / 20,0 m): Deposits characterized by a medium-low degree of densification, consisting of rounded to angular

clasts, immersed in a sandy and sandy-silty matrix. The clasts are generally slightly altered and with a differentiated petrographic composition according to the tributary basin to which they belong.

Lithoid substrate (>18,0/20,0 m): Calcescists with metabasite levels, fractured and altered in the upper portion, on average intact and compact at greater depths. The geotechnical characteristics improve with increasing depth.

2.3. GEOTECHNICS

Geotechnical characterization presented in this thesis is based on *The Geological - Geotechnical Internal Report of Pontè River watershed area at Salbertrand (TO)* as well as the geological characterization presented in the section above.

2.3.1. GEOMORPHOLOGICAL FRAMEWORK

From the geomorphological point of view, the area of concern is characterized by forming an alpine-like environment; it is located in a valley intersected by the Rio Pontè; the aforementioned watercourse appears to be a tributary of the Dora Riparia river and is located on its hydrographic left. The valley in question appears to be a sparsely built area, including some small villages inside.

The valley is characterized by slopes with variable steepness, interrupted by local slope breaks from upstream to downstream. The head of the hydrological basin under examination is characterized by the presence of high acclivity, with sub-vertical outcropping cliffs, which decrease at lower altitudes. The sector immediately upstream of the area near the highway viaduct is characterized by a greater steepness in correspondence with the sectors most affected by the waterway.

In the lower portion of the valley in question, in the adjacent areas to the inhabited zone, there are widespread old terraces, which locally are in a poor state of conservation.

The area under examination is therefore characterized by the rare presence of outcrop rocky substrate, represented by terms belonging to the pre-Triassic basement of the "Ambin Complex". In particular, the greater density of outcrop of the substrate is

observed at the road cuts and along the river channel, while in the remaining area the presence of Quaternary cover deposits is observed, as illustrated in the previous section.

From the detailed surveys carried out at the survey site, the presence of different disruptive phenomena related to natural and anthropogenic materials, distributed in different sectors of the slopes, emerged; in particular, the following problems are noted:

Active landslides or punctual reactivable landslides in natural material, in various sectors of the hydrographic basin under examination there are phenomena of instability of the quaternary coverings, highlighted by denuded areas and accumulation areas at the base. These areas are located mainly in the vicinity of the river course of the Rio Pontè. It is possible to identify highly critical sectors through the presence of natural elements that define situations of precarious stability. The landslides identified can be traced back to the type of surface slippage, depending on the textural composition and topography of the area (steepness and morphology).

*Sectors affected by old terraces characterized by punctual landslides, s*ectors located mainly in the areas adjacent to the built-up areas, in which wooded and grassy areas affected by a series of terraces are observed. They generally have a good state of conservation, but local situations of instability of the building and the upstream surface cover occur locally. The forms of surface instability in progress are generally linked to the state of abandonment of the water management works with the surface flow. However, it is noted that they are specific and minimal critical issues.

Accumulations of natural inert material in a precarious state of equilibrium, potentially movable during intense and/or prolonged meteoric events, Numerous portions of the riverbed of the Pontè river, with particular reference to the sectors characterized by greater steepness, but not only, are affected by accumulations of heterometric natural inert material in a precarious state of equilibrium, potentially movable during intense and/or prolonged meteoric events. This material is of detrital and/or vegetational nature (branches and trunks).

Potentially unstable sectors where movement and sliding of the surface blanket are possible, in the steepest sectors of the valley, the presence of a blanket of coverage has been identified, mainly in the vicinity of the most engraved sections of the Rio Pontè, with evidence of instability given by local stripped portions and accumulations of small debris.

Sectors characterized by linear erosion phenomena that can be reactivated during particularly intense and/or prolonged meteoric events, some traces of linear runoff have been observed located on the right bank of the Rio Pontè, in the sector closest to the viaduct pillars. This phenomenon is determined by the malfunctioning and/or absence of water regulation works, which are conveyed to a localized sector, and then flow, in an uncontrolled manner, towards the Rio Pontè, the main receptor of the valley in question.

Erosion phenomena along the torrential channel, on the site subjected to interventions, local problems related to the erosion due to the river can be encountered on the banks, especially in conjunction with intense and/or prolonged meteoric events that cause the occurrence of torrential events. The basal erosion of the banks of the river bed causes a strong instability of the bank itself which can evolve into local landslides.

Based on the above mentioned, it is possible to highlight the presence of various phenomena of current and/or potential instability, mainly attributable to the river dynamics of the Rio Pontè, to the morphology of the area in question, as well as to the presence of unstable and mobilizable material (surface blanket and torrential loose deposits).

2.3.2. GEOTECHNICAL MODEL

The investigations carried out showed the presence on site of a layer of natural blanket locally mixed with backfill material (average thickness between 0.5 and 1 m) above the quaternary deposits of mixed origin consisting, of course, heterometric material immersed in a finer sandy and sandy-silty. This layer rests on the stone substrate, which is altered, degraded, and fractured in the top portion and on average intact and compact in depth.

In order to reconstruct the geotechnical model of the intervention area, aimed at providing all the geotechnical data necessary for the design of the consolidation interventions and the stability checks, as well as for the setting of the subsequent stability analysis activities, the geotechnical parameters, possibly to be verified in the executive phase, to be attributed to the various soils, derived from surveys and tests carried out by the writer in similar soils in neighboring areas and from the literature, confirmed by table values.

It was possible to identify, three lithological units having homogeneous geotechnical characteristics. The geotechnical scheme valid for the area of concern deduced from the investigations carried out is characterized as follows:

- local reference campaign plan: inclined;
- depth of the water table: -
- significant volume: Lithological unit 1 + 2 + 3;
- average values of parameters: see Table 7.

					AVERAGE VALUES		
Lithological unit	**Lithology**	**Depth**	**Type**	**A.G.I. Classification**	**γ_m**	**φ'_m**	**C_m**
		m from g.l.			***t/m³***	°	***kg/cm²***
1	Natural blanket and landfill material.	0,0 – 0,5	Inconsistent	Loose	1,9	27	0,0
2	Quaternary deposits consisting of coarse material immersed in a sandy and sandy-silty matrix.	0,5 – 18,0/20,0	Inconsistent	Moderately thickened	1,8	35	0,1
3	An altered lithoid substrate, degraded and fractured on the surface, more intact and compact in depth.	> 18,0/20,0	Cohesive	Thickened	2,5	40	2,5

Where:

Table 7. Lithologic units of the study area

γ_m: volume weight;

φ'_m: effective internal friction angle;

C_m: drained cohesion.

2.4. LAND COVER AND USE

Land cover, in general, refers to the physical land type, for instance, how much of a region is covered by forests, impervious surfaces, agricultural lands, wetlands, and open water, whereas land use documents how people are using the land for development, conservation or mixed uses (NOAA, 2015). Certain kinds of land use can influence the hydrological characteristics of the Watershed, altering the way water and pollutants move through the drainage basin. The status of LULC of a particular region reflects the natural and socio-economic factors of that region and their utilization in terms of time and space (Rawat and Kumar, 2015).

It was used the information from the *PRGC (Piano Regolatore Generale Comunale)* of the province of Turin as well as GIS data of the study area available at *GEOPORTALE PIEMONTE*. The PRG is the main tool of urban planning at the municipal level, based

on the assessment of the state of affairs and the development forecasts of the Municipality in the period of validity of the plan, it provides *Law n.1150 of 17/8/1942 Art. 7* for the intended use of the areas, the possibility of building exploitation, the feasible interventions on the existing building stock and the areas to be allocated to public services.

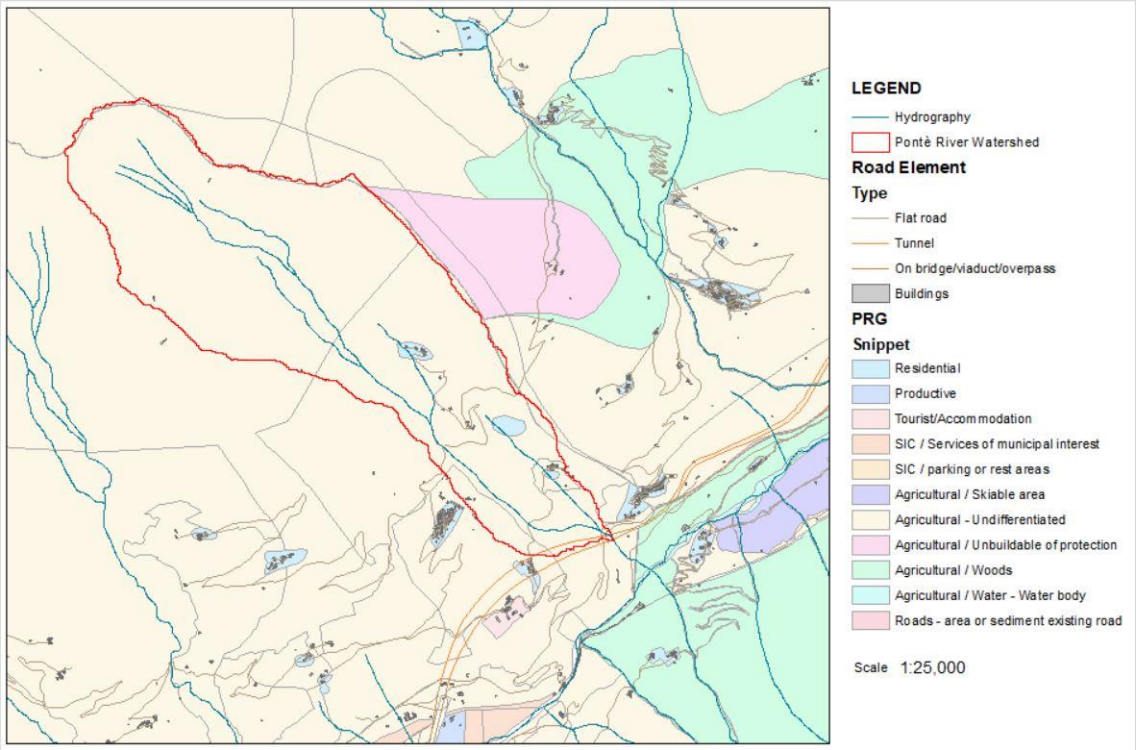

Figure 17. Piano Regolatore Generale Torino

As observed in Figure 17 from the Province of Turin PRG, the Agricultural – Undifferentiated activity is predominating in the drainage basin area under study (99%) the 1% remaining corresponds to Residential areas.

From Figure 18, it is possible to conclude that the watershed area is mostly covered with Woodland (43%). Characteristically, green vegetation plays an important role in the hydrological characteristics of a watershed by infiltrating most of the falling rain in the monsoon and minimizing both surface runoff and soil erosion. The second dominant land cover in the watershed was Pasture and green spaces (33%). The residential area (1%) and the Agricultural area (0.1%) are the less dominant land cover. The remaining land cover was classified as open spaces with grass (23%).

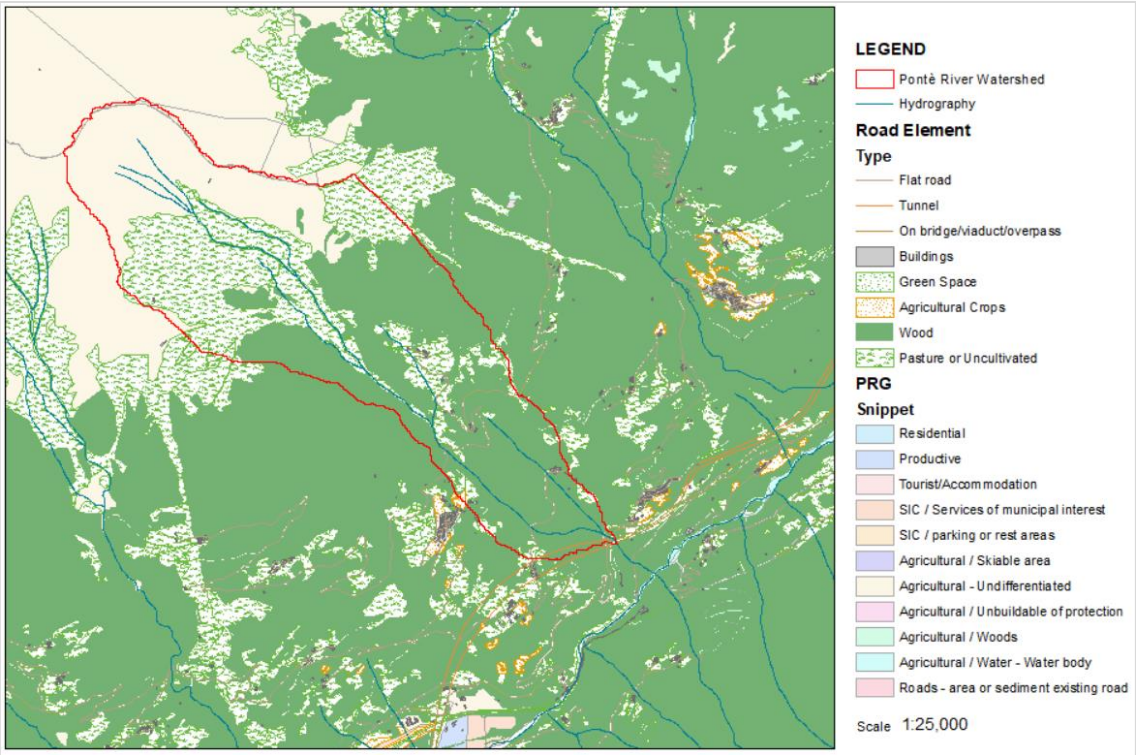

Figure 18. Land Cover of the Study Area.

2.5. TOPOGRAPHIC SURVEY

The modeling was based on the digital model of the terrain acquired by an aerial photogrammetric survey, of which Figure 19 shows a representative excerpt on an aerial photo.

The topographical survey of the area in question was performed with the use of a "topo-photogrammetric" type operating method, which integrates and enriches a "classic" GPS-TPS survey, of a "discrete" type, with a photogrammetric from SAPR (Remotely Piloted Aircraft System), of the "extensive" type (point cloud 3d model). This operating methodology makes use of the calculation algorithms developed by the theory of "Multi-image processing and bundle adjustment", where the photographic shots, which were carried out from "above" and "below", allowed the three-dimensional rendering of the surveying areas.

Figure 19. Aerial view of acquisition with the drone.

The point cloud 3d model, thus defined, was elaborated thanks to the execution of a "double grid image acquisition plan" photogrammetric flight (Figure 20), which allowed the acquisition of high-resolution georeferenced photographic shots.

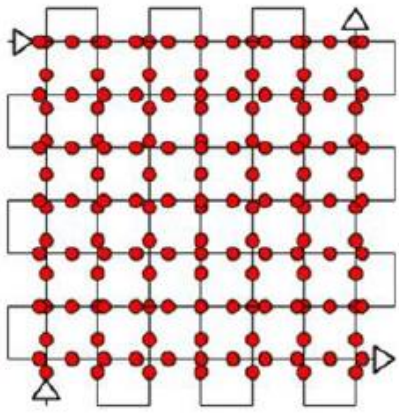

Figure 20. "Double grid image acquisition plan" type scheme.

The images were subsequently implemented and processed by the specialized software, which made it possible to define a geometrically congruent and georeferenced model according to the DATUM UTM32N-WGS84 with the use of gratings.

The georeferencing of the photographic takes was defined thanks to the identification of an adequate number of "control points" on the ground, which were first surveyed

topographically, with GNSS methodology, and subsequently identified on the corresponding photographic takes.

2.6. STABILITY ASSESSMENT

A stability test along the possible sliding surfaces between the interface and the interlayer was performed also under the instructions of the correlator of this thesis, results are reported in the *Geological - Geotechnical Internal Report of Rio Pontè watershed area at Salbertrand (TO)* from which it was extracted the information presented in this section of the Thesis.

The safety analysis of the section of the slope in question was carried out according to *Approach 1 - Combination 2: (A2 + M2 + R2)* of the *D.M. 17.01.2018*, with the geotechnical partial safety factors in *Table 6.2.II – Coefficienti parziali per i parametri geotecnici del terreno,* available in the aforementioned *D.M. 17.01.2018*, using the most precautionary limit state of prevention of collapse (*SLC Stato limite di prevenzione del collasso*).

Based on the results of stability tests performed along the possible sliding surfaces between the interface and the interlayer, in analogy with what has occurred in the modeling reported in previous studies, it can be stated as follows:

- the calculation method used is that of Morgenstern and Price, as it is one of the most accurate and reliable methods, as it becomes possible to define a totally balanced solution, which respects all the equilibrium equations of the problem;
- the most critical sectors, i.e. those characterized by the minimum safety factor, which therefore determines greater instability (FS = 0.75 in correspondence with the upstream Pillar and FS = 0.63 in correspondence with the downstream Pillar) are, as can be expected, those in current failure;
- in both cases, there are possible critical sliding surfaces, or characterized by FS <1 (limit equilibrium), affecting the entire right bank of the Rio Pontè;
- the critical sliding surfaces concern only the loose and moderately thickened surface deposits (eluvium-colluvial blanket and quaternary covering deposits), while the stone substrate can be considered stable.

The stability assessment results are reported as follows for the Upstream pillar (Pillar A) and Downstream pillar (Pillar B).

Calculation method	UPSTREAM PILLAR FS minimum	DOWNSTREAM PILLAR FS minimum
Morgenstern e Price	0.75	0.63
Jambu	0.67	0.59
Bishop	0.76	0.62
Fellenius	0.66	0.61
Spencer	0.75	0.63
Bell	0.76	0.63
Sarma	1.07	1.04

Table 8. Stability Assessment.

Table 8 defines the minimum safety factors calculated according to different methods. It is observed that although the FS may have variable values, the results of the stability assessment do not change, as in any case either instability conditions or limit equilibrium conditions occur.

CHAPTER 3: HYDROLOGIC ANALYSIS

3.1. RAINFALL PROBABILITY CURVES

The quantitative prediction of heavy rainfall at a given point is carried out through the use of a pluviometric probability curve, according to the PAI (2001) this refers to the relationship between the precipitation height to its duration, for an assigned return period, following to the law:

$$h_{(t)} = a \cdot t^n$$

where:

h (t), is the height of precipitation, measured in mm, which expresses the height of water that fell to the ground on a horizontal and impermeable surface, in a certain time interval t; *a* and *n,* are dimensionless coefficients relating to the pluviometric probability curve.

The historical data of maximum intense precipitation (Table 6) provided the basis of the probabilistic analysis aimed at determining the pluviometric probability signal curves for different return times. The elaborations were carried out by regularizing the maximum annual rainfall heights for each duration using Gumbel's probabilistic law.

3.1.1. FREQUENCY DISTRIBUTION

These data referring to a certain duration *d*, are considered as a sample of size *N* (number of years of observation) of a random variable *h*; therefore, it was chosen to adopt the Gumbel model as a probabilistic model. By estimating the parameters with the method of moments, it is possible to directly express the generic quantile h_T (of the variable *h* for a fixed return time T_R), as a function of mean and deviation through the equation:

$$h_T = h\left\{1 - CV_h\left[0.45 + \frac{\sqrt{6}}{\pi}\ln\ln\frac{T}{T-1}\right]\right\}$$

Where CV_h represents the coefficient of variation of the data, which in the case of a Gumbel distribution is assumed to be constant over the duration and equal to the average value of the CV calculated for the different durations. The expression of Gumbel's law thus ends up being the product of the mean by a quantity that represents the growth rate of the mean as a function of the return period, a quantity which is called the growth factor with the return period (K_T), and which allows representing the precipitation frequency relationship according to the product:

$$h_T = \bar{h} \cdot K_T$$

This corresponds to the Index method for representing the quantile of a random variable, since the quantity $\bar{h}$ is called the "Index quantity". This representation is particularly useful in writing in compact form the Pluviometric Probability Curves, as it is assumed that K_T does not vary between extreme rainfall of different duration.

The law of dependence of the mean of the maximum precipitation with the duration can be expressed as:

$$\overline{h_d} = a \cdot d^n$$

With the coefficients *a* and *n* to be estimated using a regression model on the available data. One of the characteristics of this type of expressions is that they are represented by lines in a bi-logarithmic plane in which the aforementioned relationship in fact assumes the expression of an equation of a line:

$$\ln \overline{h_d} = \ln a + n \cdot \ln d$$

In which $\overline{h_d}$ is the average height relating to each duration of the meteorological events considered expressed in millimeters, *d* is the corresponding duration expressed in hours, *a* and *n* are the characteristic parameters of the curve. In particular, *a* is the hourly pluviometric coefficient that represents the height of rainfall for a unitary duration of the rainy event (1 hour); *n*, called scale exponent, is a parameter that assumes values between 0 and 1 and confers the concavity downwards to the pluviometric probability curve. These two parameters can be evaluated by identifying, in the logarithmic biplane [$ln(d)$; $ln(h_d)$], the straight line that best interpolates the rainfall heights (obtained from the averages of the measurements of the maximum available values) of equal duration. As can be seen from the graph, shown in Figure 21, parameter *a* can be obtained starting from the value of the intercept (applying the exponential), while *n* is directly derived from the value of

the angular coefficient of the line. The parameters *a* and *n* assume the values of 16.03 and 0.4417 respectively.

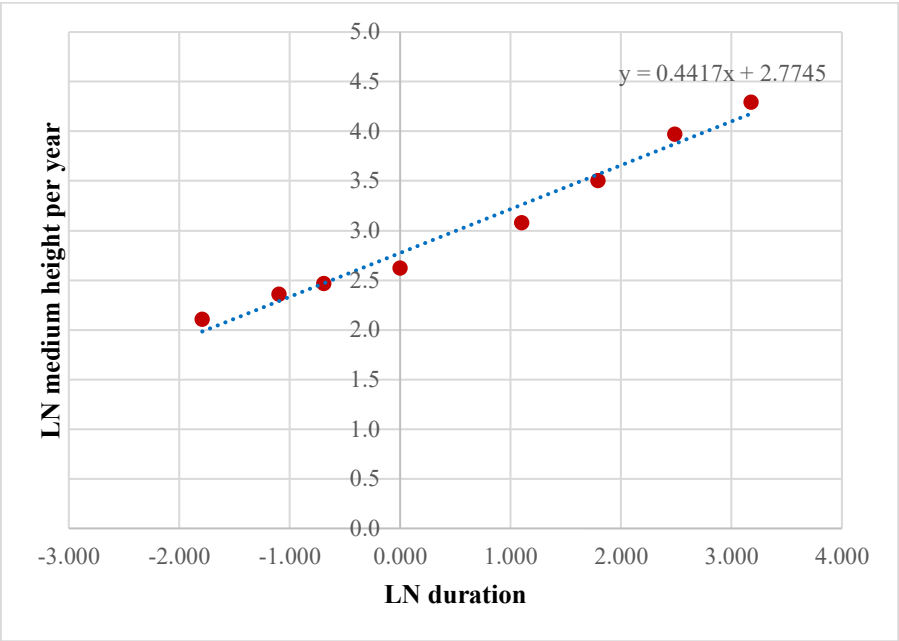

Figure 21. Linear regression on bilogarithmic graph

3.1.2. VALUES ACCORDING TO PAI

The Plan for the Hydrogeological Asset (*PAI Piano per l'Assetto Idrogeologico*) is the legal instrument for the hydrogeological defense of the territory from landslides and floods. The main objective is the reduction of hydrogeological risk within values compatible with the land uses in place, in such a way as to safeguard the safety of people and minimize damage to exposed assets. (REGIONE PIEMONTE)

The Extract Plan for the Hydrogeological Asset (PAI), in Article 10 of the Implementation Rules, provides:

"The Basin Authority defines, with its own directive:

- the values of the flood flows and intense precipitation to be taken as the basis of the project and related assessment methods and procedures for the different areas of the basin;

- the criteria and methods for calculating flood profiles in watercourses;

[...] "

The Po River Basin Authority provides a spatial interpolation with the kriging method of the parameters *a* and *n* of the signaling lines for return times of 20, 100, 200, and 500 years, discretized on the basis of a grid of 2 km per side, as a tool for the frequency analysis of heavy rains where there are no direct measurements.

The extract Plan for the Hydrogeological Asset contains the so mentioned tool in the Chapter *"Interventi sulla rete idrografica e sui versanti – 7. Norme di attuazione – Direttiva sulla piena di progetto da assumere per le progettazioni e le verifiche di compatibilità idraulica, in data 26 aprile 2001 – Allegato 3 Distribuzione spaziale delle precipitazioni intense"*;

The parameters *a* and *n* were taken from the tables included in the aforementioned document from the identification of the cell corresponding to the study area (Table 9).

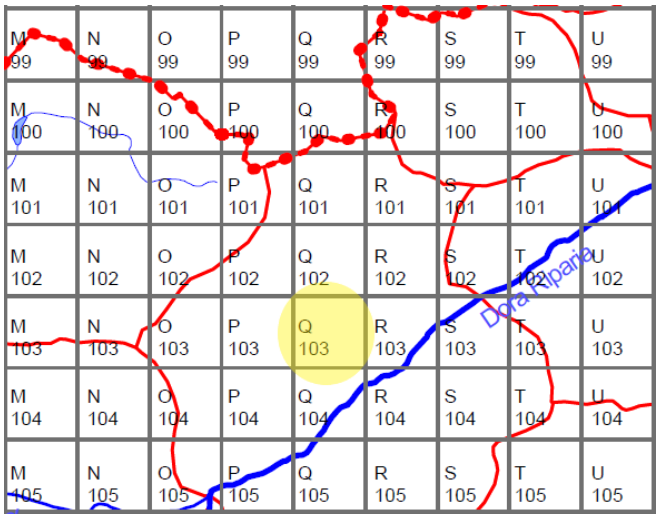

Figure 22. Location of cell Q103 relating to Pontè river from table 8 (Annex 3 - PAI)

In the case of study, the point located on the cartography corresponds to cell Q103, highlighted in Figure 22, and identified in the Basin underlying the Pontè river at the closing section downstream of the A32 Turin-Bardonecchia highway viaduct, contained in Table 08 of the so mentioned document.

Return Period (yrs)	*a*	*n*
20	22,06	0,525
100	28,22	0,524
200	30,85	0,523
500	34,32	0,523

Table 9. Parameters "a" and "n" from "Annex 3 of PAI"

3.1.3. RESULTS

Precipitation values were obtained for both methods, results are shown in Table 10 for the method using PAI values and Table 11 for the one using the Frequency Distribution of the historical data.

The PAI provides coefficients *a* and *n* to be used for Return Periods of 20, 100, 200, and 500 years, therefore, precipitation values for this method correspond only to these data available.

T (years)	20	100	200	500
h (mm) =	16.92	21.56	23.55	26.18
Q (m3/s) =	11.86	15.11	16.51	18.35

Table 10. Precipitation values obtained using PAI values of "a" and "n"

In the method using the frequency distribution (Section 3.1.1), precipitation data were calculated using six Return Periods of 10, 20, 30, 100, 200, and 500 years. All the parameters required to develop this method were obtained using the historical data of precipitation available in Table 6. *Maximum precipitation values for the various precipitation durations measured at SALBERTRAND rain gauge station.* Coefficient of Variation (*CV)* of the so mentioned data is equal to 0.327, used to calculate the growth factor (K_T) and eventually the precipitation value (h_T) for the various Return Periods.

T (years)	20	100	200	500
h (mm) =	16.92	21.56	23.55	26.18
Q (m3/s) =	11.86	15.11	16.51	18.35

Table 11. Precipitation values obtained using the Frequency Distribution of the historical data.

From the comparison between the two methods, it was decided to use the method that provides the most severe precipitation values, ie. The one using the frequency distribution of the historical data. Using the calculated parameters with this method, the pluviometric possibility curves for the various return times, shown in Figure 23, were reconstructed.

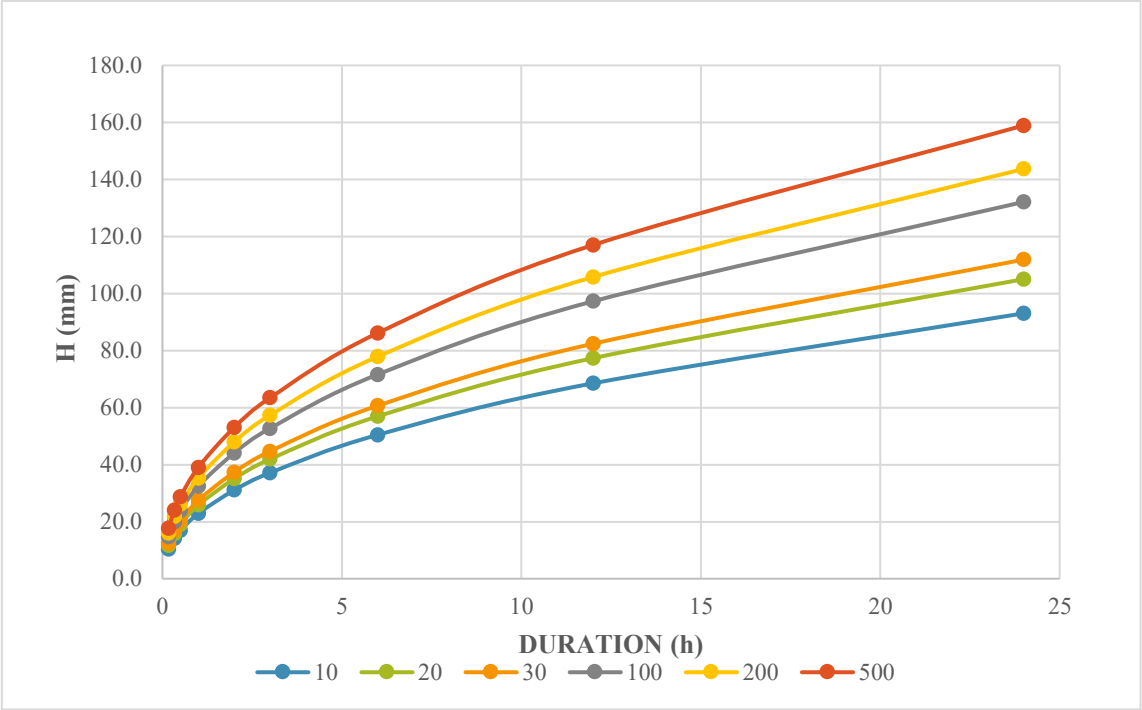

Figure 23. Pluviometric possibility curves for the various return times with Gumbel distribution.

3.2. DESIGN FLOW

3.2.1. RATIONAL METHOD

The rational method was developed by Kuichling (1889), is one of the most popular runoff estimation methods used for estimating peak flow from small catchments (with a surface of fewer than 20 hectares).

Cleveland et al. (2011), suggests some assumptions to be made when employing the rational method:

- The rainfall has a uniform time distribution for at least a duration equal to the time of concentration of the catchment
- The maximum runoff occurs when the rainfall intensity lasts at least as long as the time of concentration
- The value of φ is constant during a storm
- The contributing area is kept constant during the rainfall

Based on these assumptions, the formula of the rational method is expressed by the following relationship:

$$Q_c = 0.28 \cdot c \cdot i \cdot A$$

Where *Qc* is the flow rate at the top expressed in m3/s, c the runoff coefficient, *i* the intensity of rainfall in mm/h and *A* represents the surface underlying the basin at the section of interest in Km2.

3.2.2. TIME OF CONCENTRATION

There are different definitions of Time of concentration available in literature, the definition that reflects the hydraulic and physical characteristics of this parameter in a better way is the one that states that it is the time that a drop of rainwater takes to arrive at the basin outlet section starting from the most hydraulically distant point of the basin.

The measure of streamflow or precipitation data for a particular point in a catchment for analysis is not always available, hence, since the 1920s many researchers have developed empirical equations in order to predict *Tc* for ungauged catchments of varying size and physiography.

With the exception of the NRCS, the following equations were developed using regression analysis, with input parameters as watershed and channel parameters, which include watershed drainage area, channel length, watershed or channel slope, and watershed shape parameters (Perdikaris, Gharabaghi & Rudra, 2018).

Depending on the overestimation or underestimation of *Tc*, there will be a reduction or increase in the value of the flow rate at the peak, while the outflow volume remains unchanged. The time of concentration used in the calculation of design flow was therefore calculated as the average of the following equation taken into consideration:

Giandotti (1934), developed an equation to define *Tc* considering the basin morphology:

$$T_c = \frac{(4\sqrt{A} + 1.5LAP)}{0.8\sqrt{H_m - H_0}}$$

Where *Tc* is calculated in hours, *A* is the area of the basin under the calculation section (km2), *LAP* the length of the rod of the watercourse (km), *Hm* the average height of the basin (m.a.s.l.), and *Ho* the height of the closing section (m.a.s.l). Compared to other relationships, Giandotti's formula has the advantage of including various characteristics of the basins analyzed in the parameters used for calculating concentration time. This guarantees a reconstruction of *Tc* based on the main parameters of the basins.

Kirpich (1940), developed an equation for small mountainous watersheds in Tennessee. The watersheds used in Kirpich's study ranged in size from 0.004 to 0.45 km2, with slopes from 3-12%.

$$T_c = 0.0078 LAP^{0.77} S^{-0.385}$$

Where *Tc* is calculated in minutes, *L* is the length of the main channel expressed in feet, and *S* the average slope of the basin (km/km).

Jhonston & Cross (1949), developed an equation for watersheds of large area:

$$T_c = 300 \sqrt{\frac{LDP}{S}}$$

California Culvert Practice (1995), developed an equation for small mountain basins in California:

$$\mathrm{Tc} = 60(11.9\mathrm{LDP}^3/\mathrm{H})^{0.385}$$

Where *Tc* is calculated in minutes, LDP (miles) is the longest drainage path length, H (feet) is the height difference.

NRCS-SCS (1997), developed for small rural basins:

$$T_c = 0.0526 \left[\left(\frac{1000}{CN}\right) - 9\right] LDP^{0.8} S^{0.5}$$

Where *Tc* is calculated in minutes, *LDP* expressed in feet, *S* the average slope of the basin expressed as a percentage and *CN* the curve number calculated using the values contained in the Tables in section 6.2 of the document contained in the PAI *"7. Norme di Attuazione - Direttiva sulla piena di progetto da assumere per le progettazioni e le verifiche di compatibilità idraulica",* and the area percentages obtained from the GIS software (Figure 18).

Considering the presence of several soil types and land uses in a watershed, it is calculated a composite CN as:

$$CN_{composite} = \frac{\sum A_i CN_i}{\sum A_i}$$

In which *CNcomposite* is used for runoff volume computations; *i*, is an index of watershed subdivisions of uniform land use and soil type; *CNi* is the corresponding Curve Number for subdivision *i*; *Ai*, will be the drainage area of subdivision *i.*

As described in Section 2.6 of this Thesis, the study area is mainly characterized by woodland and pastures, with a small portion of residential and cropland areas. Using the CN calculation method described above, it was possible to define a CN value of 82.3 for the watershed in question.

The results obtained are reported in Table 12, from which a time of concentration of about 36 minutes is obtained.

Method	***t_c (h)***	***t_c (min)***
Giandotti	0,387	23,235
Kirpich	0,266	15,978
Jhonston & Cross	1,215	72,888
California Culvert	0,278	16,708
NRCS-SCS	0,873	52,384
Average	**0,604**	**36,239**

Table 12. Calculation results of Tc

3.2.3. RUNOFF COEFFICIENT

The runoff coefficient is a coefficient with a value between 0 and 1 defining the proportion of rainfall that turns into runoff. This value is crucial to the correct implementation of the rational method equation. A runoff coefficient with a value of 0, means that all of the falling water on the surface gets infiltrated through it, while a value of 1 means that all of the falling water on the surface turns into runoff.

The selection of the runoff coefficient could lead to inaccurate results when using the rational method due to difficulties in selecting this parameter adequately. The value of runoff coefficient encompasses the effects of infiltration, interception, evapotranspiration, and retention by a certain type of surface and thus the selection of an

appropriate value for calculations requires sound judgment from an experienced engineer (UDFCD, 2016).

Normally, for small basins, the reservoir effect is neglected, while an indication of the values to be attributed to the soil retention factor is provided in the FAO guide (1976), described in Table 13.

	Land-use Type		
Soil Type	***Cropland***	***Pasturelands***	***Woodlands***
Very permeable sandy or gravelly soils	0.2	0.15	0.10
Medium permeable soils (without layers of clay) - Medium-textured soils or similar	0.5	0.35	0.3
Poorly permeable soils. heavily clayey or similar soils with layers of clay close to the surface. Shallow soils above impermeable rock.	0.5	0.45	0.4

Table 13. Runoff coefficient values - FAO (1976)

Through the GIS software, it was possible to identify the areas relating to each type of soil (Figure 18). In particular, the areas in question are mainly characterized by the presence of woods and pastures, evaluated in the most severe type of soil, or in the condition of poorly permeable soil. The runoff coefficient *c* thus calculated, is equal to 0.44.

3.2.4. RESULTS

The results of the design flow rates with the application of the rational method previously described are reported in Table 14.

Return period (years)	20	50	100	200	500
Discharge (m3/s)	15,52	17,81	19,52	21,23	23,49

Table 14. Design Flow values.

CHAPTER 4: HYDRAULIC ANALYSIS

4.1. HYDRAULIC MODEL

The hydraulic study is aimed at evaluating the hydraulic parameters that characterize the flow (medium velocity of the stream, water head, Froude number, total and kinetic load) of a generic discharge in one or more study sections. These values will be subsequently related to the erosion and deposit phenomena that characterize the watercourse

A good hydraulic model requires a good geometry and flow data input. However, the simulations are also influenced by model type, i.e., one dimensional (1D), two dimensional (2D), or combined (1D/2D) types. When simulating flow in the main river channel, the 1D model is generally used to simulate flow in the main river channel and in certain cases is also very effective in predicting flood extent. 1D modeling also shows computational efficiency and simple parameterization in dealing with flows in large and complex networks (Ahmad & Hassan, 2011). 1D model has limited application but is economical, robust, gives useful information on water profile properties, and is a widely preferred alternative as long as the flow paths can be identified.

Based on the results obtained from the hydrological study and the specially developed topography, a numerical model was built for the watercourse, following the steady flow analysis in the riverbed with a gradually varied section. The calculation procedure used is based on the solution of the one-dimensional energy balance equation (known in literature as the Standard Step Method).

The software used for the model is HEC-RAS 5.0.7, developed by the Hydrologic Engineering Center of the U.S. Army Corps of Engineers. HEC-RAS is a software that allows to perform one-dimensional steady flow hydraulics; one- and two-dimensional steady flow river hydraulics calculations; quasi unsteady and full unsteady flow sediment transport-mobile bed modeling; water temperature analysis; and generalized water quality modeling (HEC, 2016).

4.2. HEC-RAS CALCULATING METHODOLOGY

When studying gradually varying currents in natural riverbeds, the availability of information relating only to a rather limited number of cross-sections of the watercourse represents one of the greatest limitations for the analysis. Furthermore, it is not possible for these riverbeds to apply usual calculation procedures, consequently, in order to determine the course of the water surface profile along a section of the riverbed, it is necessary to proceed by attempts and subsequent approximations, assigned the appropriate boundary conditions (downstream or upstream) according to the type of regime characterizing the current. HEC-RAS computes it from one cross-section to the next by solving the following energy equation with the standard step method:

$$Z_2 + Y_2 + \frac{a_2 V_2^2}{2g} = Z_1 + Y_1 + \frac{a_1 V_1^2}{2g} + h_e$$

Where:

Z_1, Z_2 are elevations of the main channel inverts,

Y_1, Y_2, are the depth of water at cross-sections,

a_1, a_2, the velocity weighting coefficients,

g is the gravitational acceleration and

h_e, the energy head loss between two cross-sections, this one is compromised by friction losses and contraction or expansion losses, and is calculated as follows:

$$h_e = L\bar{S}_f + C\left|\frac{a_2 V_2^2}{2g} - \frac{a_1 V_1^2}{2g}\right|$$

Where:

S_f is the representative friction slope between two sections,

C is the expansion or contraction loss coefficient and

L is the discharge weighted reach length, calculated as:

$$L = \frac{L_{lob}\overline{Q}_{lob} + L_{ch}\overline{Q}_{ch} + L_{rob}\overline{Q}_{rob}}{\overline{Q}_{lob} + \overline{Q}_{ch} + \overline{Q}_{rob}}$$

Where:

L_{lob}, L_{ch}, L_{rob} are the cross-section reach lengths specified for flow in the left overbank, main channel, and right overbank, respectively.

Q_{lob}+ Q_{ch}+ Q_{rob}, are the arithmetic average of the flows between sections for the left overbank, main channel, and right overbank, respectively.

The diagram in Figure 24, shows the terms of the energy equation.

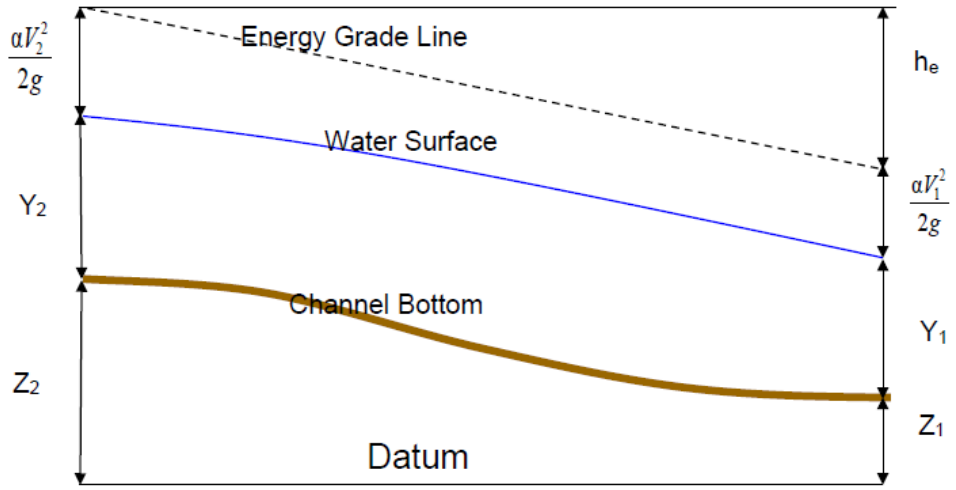

Figure 24. Representation of terms in the Energy Equation. From: HEC-RAS 5.0 Reference Manual.

The numerical calculation model sets the outflow into the riverbed and the boundary conditions apply the system described above to two adjacent sections starting from, and resolves it iteratively, to determine the height of the water surface in each of them as already said. The calculation process, therefore, continues similarly for pairs of successive sections, until it affects all the sections used to define the geometry. In this way, it is possible to determine the profile of the free surface for the section of the riverbed considered.

The calculation code allows the subdivision of the current into parallel branches, to be able to simulate the outflow, as well as in the riverbed, also in the lateral floodplain areas, which can be characterized with different roughness indices.

HEC-RAS subdivide cross-section area using the input cross-section n-value breakpoints (locations where n-values change) as the basis for subdivision as shown in Figure 25. Within each subdivision, it is calculated the conveyance using the following form of Manning's equation:

$$Q = KS_f^{1/2}$$

$$K = \frac{1.486}{n} AR^{2/3}$$

Where:

K is the conveyance for subdivision,

n is the Manning's roughness coefficient for subdivision

A is the flow area for subdivision

R is the hydraulic radius for subdivision (area/wetted perimeter)

S_f is the slope of the energy gradeline

The program sums up all the incremental conveyances in the overbanks to obtain a conveyance for the left overbank and the right overbank. The main channel conveyance is normally computed as a single conveyance element. The total conveyance for the cross-section is obtained by summing the three subdivision conveyances (left, channel, and right) (HEC-RAS, 2016).

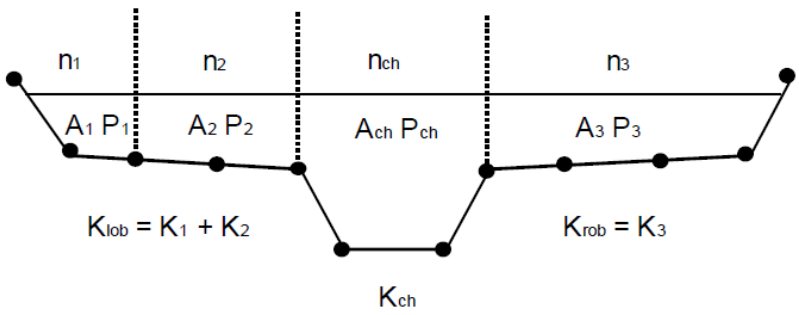

Figure 25. HEC RAS default conveyance subdivision method

The calculations can also consider the effects due to the presence of infrastructures, such as bridges, underpasses, and gates. In this case, the model evaluates the energy loss due to the presence of infrastructures, dividing it into three parts: the loss due to expansion of the flow, which is recorded in the section immediately downstream; the loss due to contraction of the flow, upstream of the structure; and that (determined with different possible approaches) that occurs at the infrastructure itself.

The bridge routines utilize four user-defined cross sections in the computations of energy losses due to the structure. During the hydraulic computations, the program automatically formulates two additional cross-sections inside of the bridge structure (Figure 26).

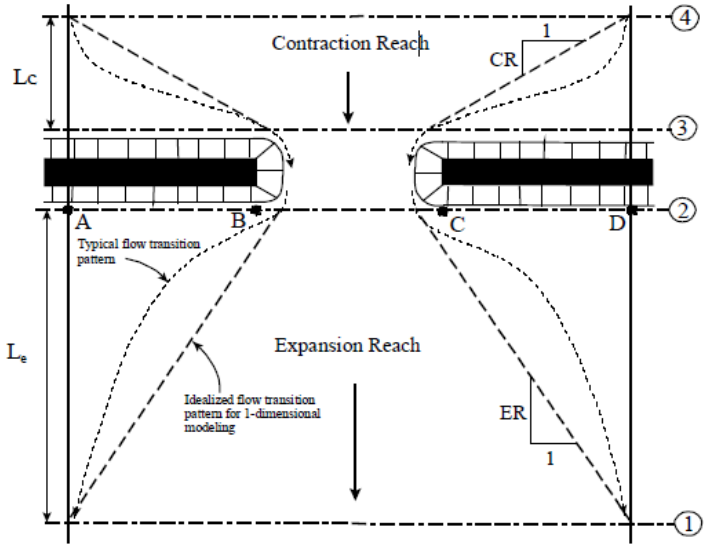

Figure 26. Cross-section locations at a bridge. From: HEC-RAS 5.0 Reference Manual

First cross-section is located downstream at a distance far enough from the structure so that the flow is not affected by the structure.

Second one is located also downstream at a shorter distance from the bridge. This cross-section should represent the natural ground of the main channel and flood plain just downstream of the bridge.

Third one is located upstream at a short distance from the bridge. the length required for the abrupt acceleration and contraction of the flow that occurs in the immediate area of the opening is reflected by the distance between this cross-section and the bridge.

Fourth one is located upstream as well, where the flow lines are almost parallel and the cross-section is fully effective. Essentially, flow contractions are more likely to occur over a shorter distance than flow expansions.

Summarizing, in addition to the knowledge of cross-sections, there’s some relevant information required for the process of calculation, such as the distance of the section considered from the one immediately downstream, measured along the axis of the ordinary riverbed; Indication of the banks in the cross-section; Possible presence of embankments, intended to identify the active part of the course of water; Manning's

roughness coefficient "*n*" which can be variable within the section; contraction and expansion coefficients for the calculation localized head loss.

When bridge structures are present, further information is considered: the geometric description of the bridge; reduction of the wet section due to the bridge abutments; the presence of any pillars, specifying for each one the distance between centers and thicknesses at the various heights under the deck.

4.3. MODEL GEOMETRY

The construction of the hydraulic numerical model requires first of all the knowledge of the morphological course of the watercourse and the topographical characterization of the area. In a one-dimensional model, the geometry of the area subject to water analysis is described through cross-sections of the watercourse.

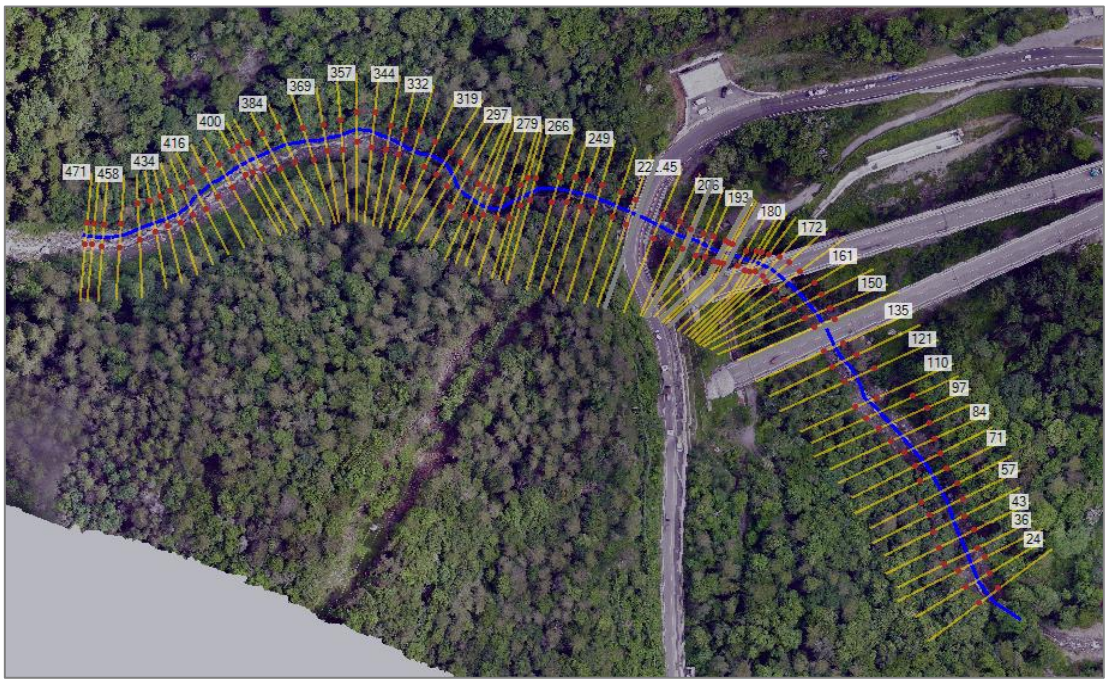

Figure 27. Cross sections defined in HEC-RAS

The cross-sections were defined for a 470 m long stretch in correspondence with the area of the viaduct, subject to refurbishment as shown in Figure 27. A topographic survey made it possible to define the contour lines with a 2 m pitch; from these, it was possible through GIS software to obtain a Digital Terrain Model (DTM), from which 79 cross-

sections were extrapolated directly in HEC-RAS. The reference system used is WGS84 zone 32N (EPSG 32632).

The identified sections have an average pitch of 5 m but are denser where the morphology of the ground and the riverbed require a greater degree of detail, for the purposes of the simulation in HEC-RAS. The average longitudinal slope of the section under analysis is approximately 32%.

Along the segment in question there are, from upstream to downstream, the following four bridges:

a) Bridge of the SS24 Highway of Monginevro;
b) Bridge adjacent to the Highway, connected to the road that passes through the boxes of the abutments of the viaduct.
c) Viaduct of the A32 Turin-Bardonecchia highway, direction Bardonecchia;
d) Viaduct of the A32 Turin-Bardonecchia highway, direction Turin.

The geometry of the bridges was defined starting from the topographic survey specifically carried out in order to detect the geometric characteristics of the area, from the inspections, and from the data that can be deduced from the project drawings of the highway viaduct.

In correspondence with the abutments and the segment immediately downstream of the bridge adjacent to the highway viaduct, there is, on both banks of the Pontè River, a stone wall, probably having the function of bank protection and stabilization of the slope on which the viaduct abutment is set of.

Along the section in question, downstream of the bridge of the SS24 Highway, there is a concrete threshold of reduced dimensions, with the function of stabilizing the riverbed.

The threshold was modeled as a weir, with the characteristics deduced from the observation made during the inspection, as there is no information regarding the actual dimensions of it. It was considered an elevation of 988.38 m.a.s.l., which means the height of the structure equal to 0.5 m with respect to the point of the riverbed at a lower level. The thickness was considered equal to 0.5 m (Figure 28).

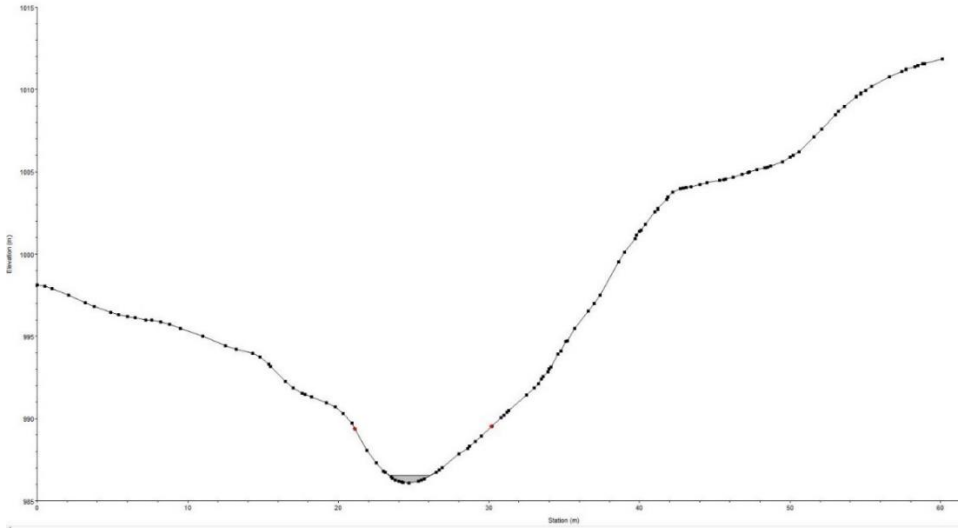

Figure 28. modeling of the concrete threshold

The structures present in the section under study are modeled as described below.

A) BRIDGE OF THE SS24

The bridge, shown in Figure 29 is located upstream under the SS24 Highway at a distance of approximately 40 meters from the A32 Viaduct at Salbertrand. The elevation of the structure is about 998 m.a.s.l.; the opening is about 12,3 m wide. Figure 30 shows the bridged as it was modeled in HEC-RAS.

Figure 29. bridge of the SS24 Highway

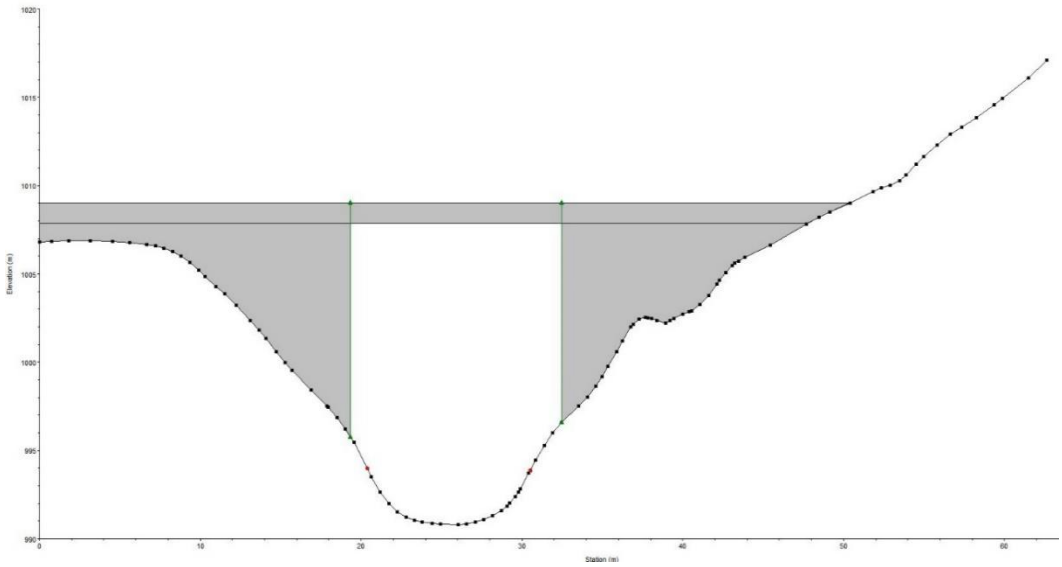

Figure 30. modeling of the bridge of the SS24 Highway in HEC-RAS

B) BRIDGE ADJACENT TO VIADUCT

The bridge is located upstream passing under through the abutments of the A32 Viaduct at Salbertrand, with an altitude of approximately 988.4 m.a.s.l., the structure has a width of about 8 meters. Figure 32 shows the cross-section of the modeling of the bridge in HEC-RAS.

Figure 31. Bridge adjacent to the Highway viaduct

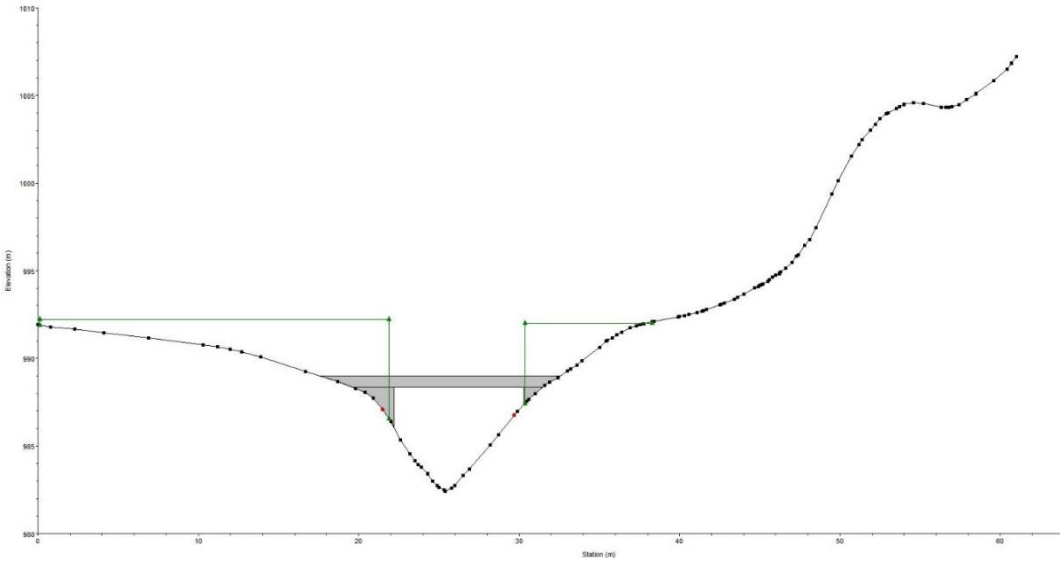

Figure 32. modeling of Bridge adjacent to the Highway viaduct in HEC-RAS

C) UPSTREAM VIADUCT TOWARDS BARDONECCHIA

The abutment of the viaduct towards Bardonecchia (Abutment A) is located on the hydrographic right, and is characterized by a box-like structure, which allows passage through itself; it is founded on four piles immersed in the compact base formation with micropiles. The elevation of the abutment's foundation is approximately 989 m a.s.l.

Figure 33. Abutment of the viaduct towards Bardonecchia (Abutment A)

The pillar of the viaduct towards Bardonecchia (Pillar A) is located on the hydrographic left at a distance from the riverbed greater than 20 m and at a much higher altitude. Consequently, the Pillar is not affected by the passage of current and by the phenomena of erosion and deposition of solid material (See Figure 33 and Figure 34).

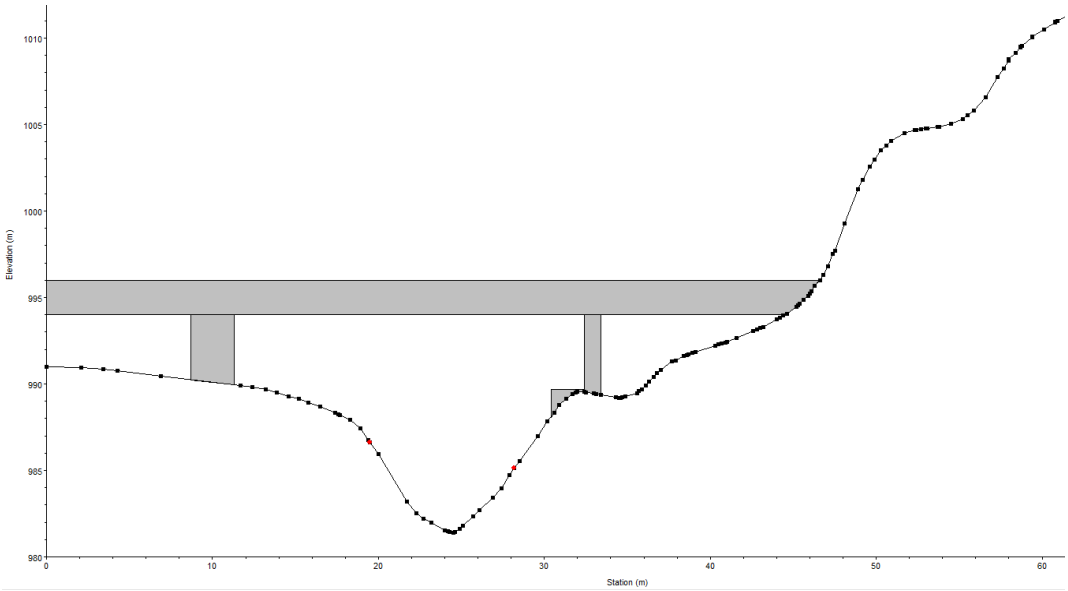

Figure 34. Modeling of the Viaduct Abutment towards Bardonecchia in HEC-RAS

D) DOWNSTREAM VIADUCT TOWARDS TURIN

The abutment of the viaduct towards Turin (Abutment B) is located on the hydrographic right, and is characterized by a box-like structure as well; it is founded on four poles immersed in the compact base formation with micropiles. The altitude of the foundation is about 988 m.a.s.l., which suggests that it does not come into contact with the current even for rare flood events, as the thalweg is located at an altitude of 960 m.a.s.l. at the same section (Figure 36).

The downstream Pillar (Pillar B), on the hydrographic left, has a composite shape, is based on 8 piles, also immersed in the compact base formation with micropiles. The pillar has a length of 7 m in the direction of the current, and a width of 2.60 m. The position of Pillar B near the bed of the watercourse suggests an interaction of the current with the pillar itself, which will be verified through the hydraulic simulation object of this thesis. During the inspections, the presence of blocks and plant material was found in correspondence with the pillar as a sign of a possible deposit phenomenon in this area of material coming from upstream and carried by the current as shown in Figure 35.

Figure 35. Pillar of the downstream viaduct towards Turin (Pillar B)

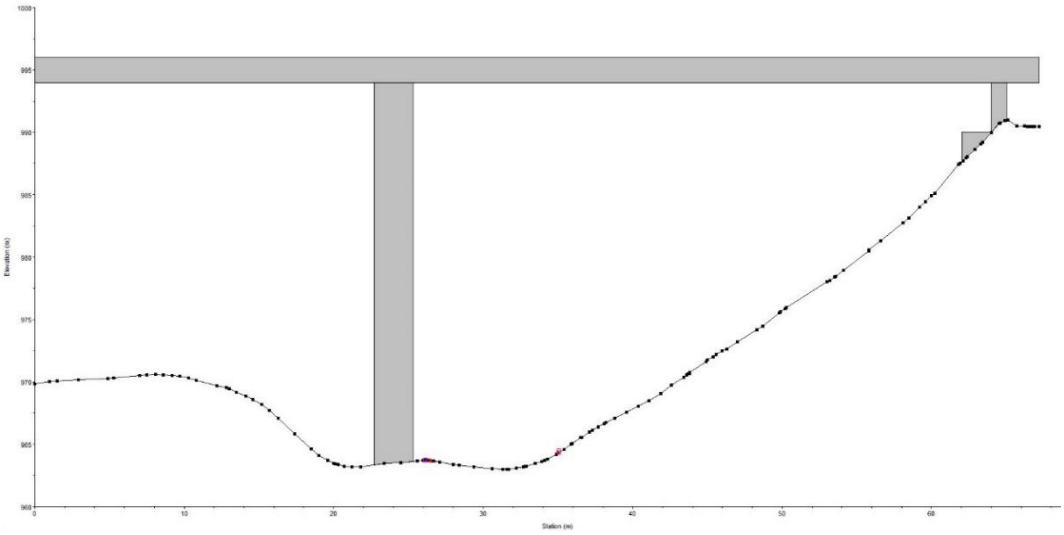

Figure 36. modeling of the downstream viaduct towards Turin in HEC-RAS

4.4. MANNING'S ROUGHNESS COEFFICIENT

The resistance to flow in channels and floodplains is represented by manning's roughness coefficient. This value depends on different factors including surface roughness, vegetation, irregularities in the channel, degree of meander, obstructions, and size and shape of the channel. In order to evaluate the resistance to motion offered by the roughness, the riverbed and the floodplains were analyzed separately.

The granulometric characteristics of the Pontè River, which influence the roughness parameter, are variable along the section under analysis. The bed of the riverbed is mainly made up of abundant coarse material mobilized and deposited by the stream itself during its evolution, while outcrops of the lithoid substrate, shaped and eroded by the waters of the river, are rarely observed.

The definition of the roughness values was performed on the basis of the observations and measurements carried out during the inspections, and the results were compared with the values provided by literature.

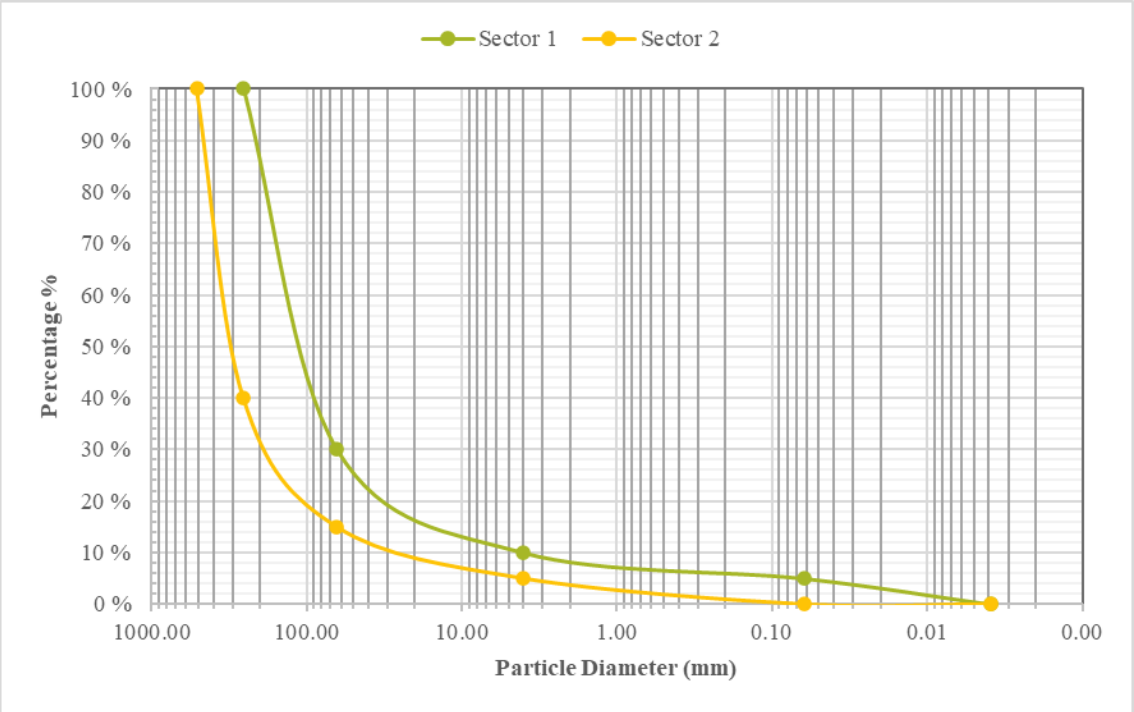

Figure 37. granulometric curve of sector 1, sector 2.

It was performed a granulometric analysis which made possible the estimation of the Manning roughness coefficient in the riverbed of Pontè River. The section in question was divided into four sectors characterized by presenting constant roughness in the riverbed. Starting from upstream, the first section is characterized by the presence of sand and gravel, with the presence of small pebbles (sector 1); the second one has coarser gravel and medium-sized pebbles (sector 2); in the following sector, the slope of the watercourse increases significantly, where it can be seen outcropping rock smoothed by the passage of the current (sector 3); finally, there's a section with granulometric

characteristics similar to the first one (sector 4). Figure 37 shows the granulometric curves obtained for the first two sections that have been identified.

From the granulometric curve, the values of D90 and D50 were obtained, which were then introduced in the Strickler and Müller formulas, for the evaluation of the roughness coefficients. The presence of vegetation has not been taken into account, as it is present only at such altitudes that it does not come into contact with the current and does not interfere with the flow; The basic values of the roughness within the riverbed were therefore considered, influenced only by the granulometric characteristics of the bottom material.

$$K_{Strickler} = \frac{21.1}{D_{50}{}^{\frac{1}{6}}}$$

$$K_{Müller} = \frac{26}{D_{90}{}^{\frac{1}{6}}}$$

Table 15 shows the roughness values obtained for the different sections of the stretch in question and included in the model to take into account the resistance to motion offered by the material of the riverbed.

Initial section	***Final section***	***Riverbed type***	***D_{90} (m)***	***D_{50} (m)***	***$K_{Strickler}$***	***K_{Muller}***	***n***
471	234.81	gravel, sand and small pebbles	0.22	0.11	30.5	33.5	0.03
222.45	202	gravel, medium-large pebbles, boulders	0.46	0.3	25.8	29.6	0.035
196	180	outcropping rock	-	-	-	-	0.025
178	17	gravel, sand and small pebbles	0.22	0.11	30.5	33.5	0.03

Table 15. roughness coefficient to be used in the model

The Manning roughness coefficients were obtained starting from those of Strickler and Müller, through the simple relationship n = 1 / K, and compared with the literature values reported in Table 16 to identify the value that best describes the roughness of the riverbed.

Type of Channel and Description	Minimum	Normal	Maximum
A. *Natural Streams*			
1. **Main Channels**			
a. Clean, straight, full, no rifts or deep pools	0.025	0.030	0.033
b. Same as above, but more stones and weeds	0.030	0.035	0.040
c. Clean, winding, some pools and shoals	0.033	0.040	0.045
d. Same as above, but some weeds and stones	0.035	0.045	0.050
e. Same as above, lower stages, more ineffective slopes and sections	0.040	0.048	0.055
f. Same as "d" but more stones	0.045	0.050	0.060
g. Sluggish reaches, weedy. deep pools	0.050	0.070	0.080
h. Very weedy reaches, deep pools, or floodways with heavy stands of timber and brush	0.070	0.100	0.150
2. **Flood Plains**			
a. Pasture no brush			
1. Short grass	0.025	0.030	0.035
2. High grass	0.030	0.035	0.050
b. Cultivated areas			
1. No crop	0.020	0.030	0.040
2. Mature row crops	0.025	0.035	0.045
3. Mature field crops	0.030	0.040	0.050
c. Brush			
1. Scattered brush, heavy weeds	0.035	0.050	0.070
2. Light brush and trees, in winter	0.035	0.050	0.060
3. Light brush and trees, in summer	0.040	0.060	0.080
4. Medium to dense brush, in winter	0.045	0.070	0.110
5. Medium to dense brush, in summer	0.070	0.100	0.160
d. Trees			
1. Cleared land with tree stumps, no sprouts	0.030	0.040	0.050
2. Same as above, but heavy sprouts	0.050	0.060	0.080
3. Heavy stand of timber, few down trees, little undergrowth, flow below branches	0.080	0.100	0.120
4. Same as above, but with flow into branches	0.100	0.120	0.160
5. Dense willows, summer, straight	0.110	0.150	0.200
3. **Mountain Streams, no vegetation in channel, banks usually steep, with trees and brush on banks submerged**			
a. Bottom: gravels, cobbles, and few boulders	0.030	0.040	0.050
b. Bottom: cobbles with large boulders	0.040	0.050	0.070

Table 16. roughness coefficient for riverbed and flood plains. From: Chow, V.T., 1959, Open-channel hydraulics.

Regarding the areas outside the banks of the watercourse, or the riverbanks, the roughness coefficients were estimated on the basis of the observations made during the inspections and the literature on river hydraulics, and are shown in the following Table 17:

		n	
Initial sec.	***Final sec.***	***LOB***	***ROB***
1	15	0.06	0.06
16	20	0.06	0.035
21	32	0.035	0.035
33	36	0.04	0.04
37	78	0.06	0.06

Table 17 .roughness coefficients for the overbanks

4.5. BOUNDARY CONDITIONS

4.5.1. UPSTREAM BOUNDARY CONDITIONS

The upstream boundary conditions of the hydraulic model are constituted by the Design Flow rates, evaluated in correspondence with the Pontè river watershed, and reported in Chapter 3 of this thesis.

4.5.2. DOWNSTREAM BOUNDARY CONDITIONS

Under the hypothesis of uniform motion at the valley boundary of the model, it is defined a slope of the energy gradeline, assumed to be equal to the slope of the bed, and the software automatically calculates the height of uniform motion using the Manning equation. A line has been drawn along the final section of the river, and the slope obtained from a slope is equal to 0.16.

4.6. RESULTS

The current profiles determined for the Rio Pontè, relating to the return times of 20, 50, 100, 200, 500 years are shown in the Figures below (Figure 38 - Figure 44).

From the analysis of the results, it can be seen that the water depths, even for a return time of 500 years, are contained, and the velocity values are high. The current is supercritical for the entire section object of the simulation, as can be seen from the observation of the Froude numbers calculated for the sections and reported in Table 21 in the Appendix.

The energy of the watercourse is high, as expected given the morphological and altimetric characteristics of the Rio Pontè in this section. The maximum velocity reached by the flow for a return time of 200 years is higher than 14 m/s.

There is a decrease in velocity and energy at the highway viaduct towards Turin, in relation to the decrease in the slope and the minor incision of the watercourse in this section, with a consequent increase in the flow section.

The high velocity and energy values suggest that the current is capable of transporting sediments of even considerable size, as it was possible to observe during the inspections in relation to past flood events.

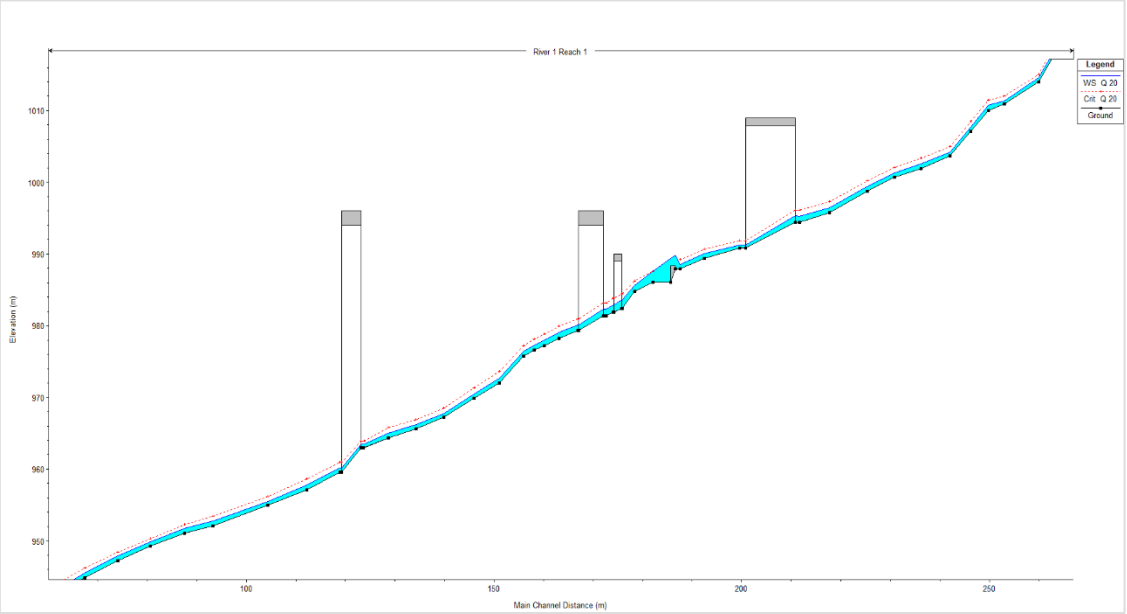

Figure 38. Water Stream Profile for TR 20 years

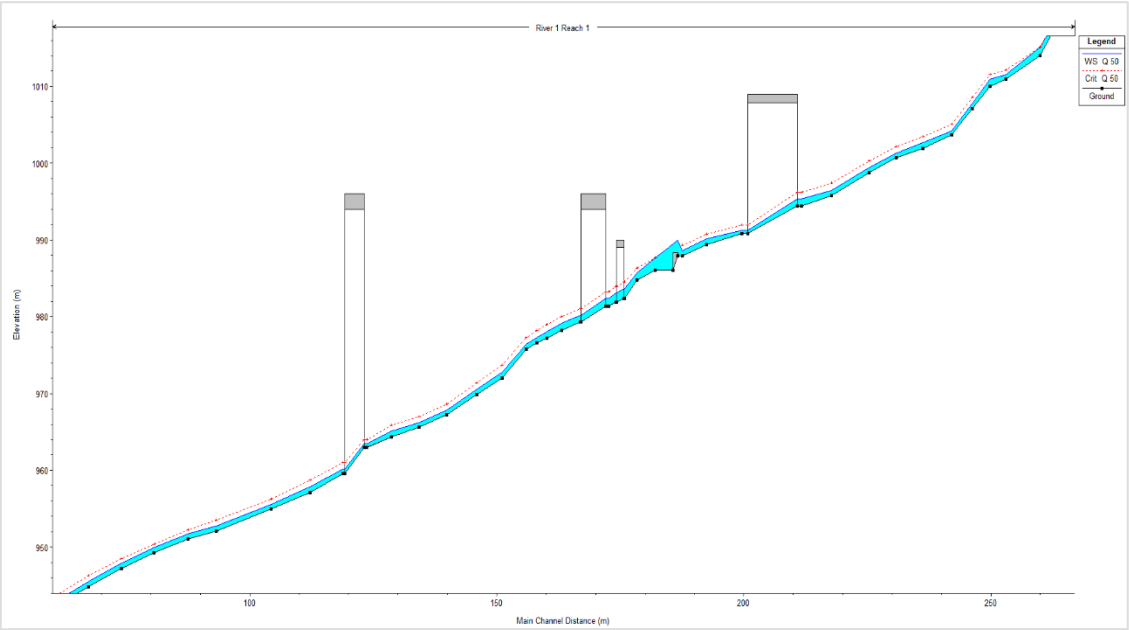

Figure 39. Water Stream Profile for TR 50 years

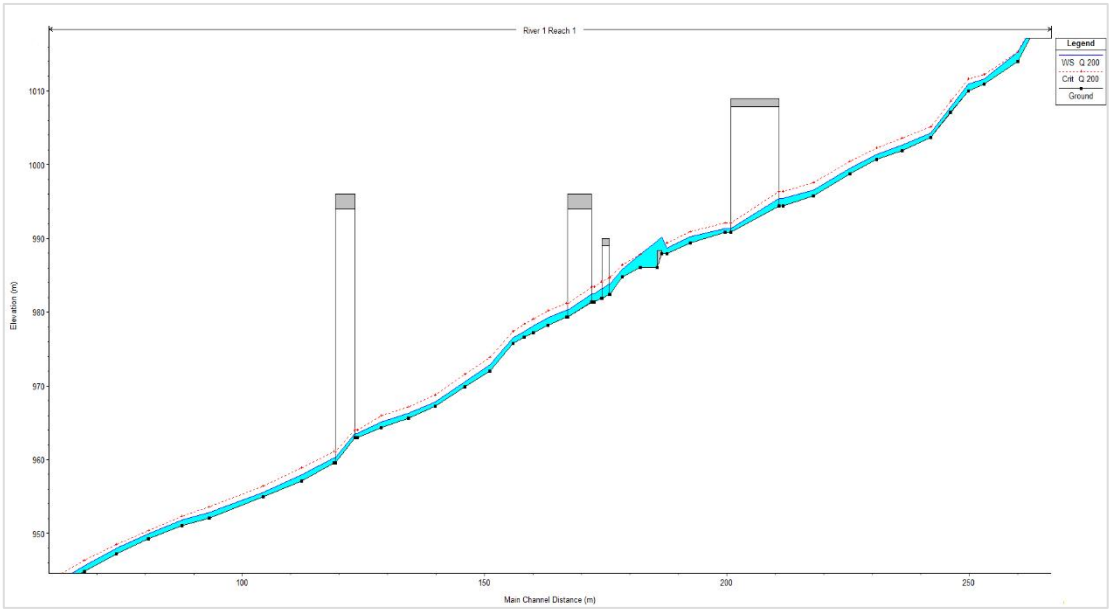

Figure 40. Water Stream Profile for TR 100 years

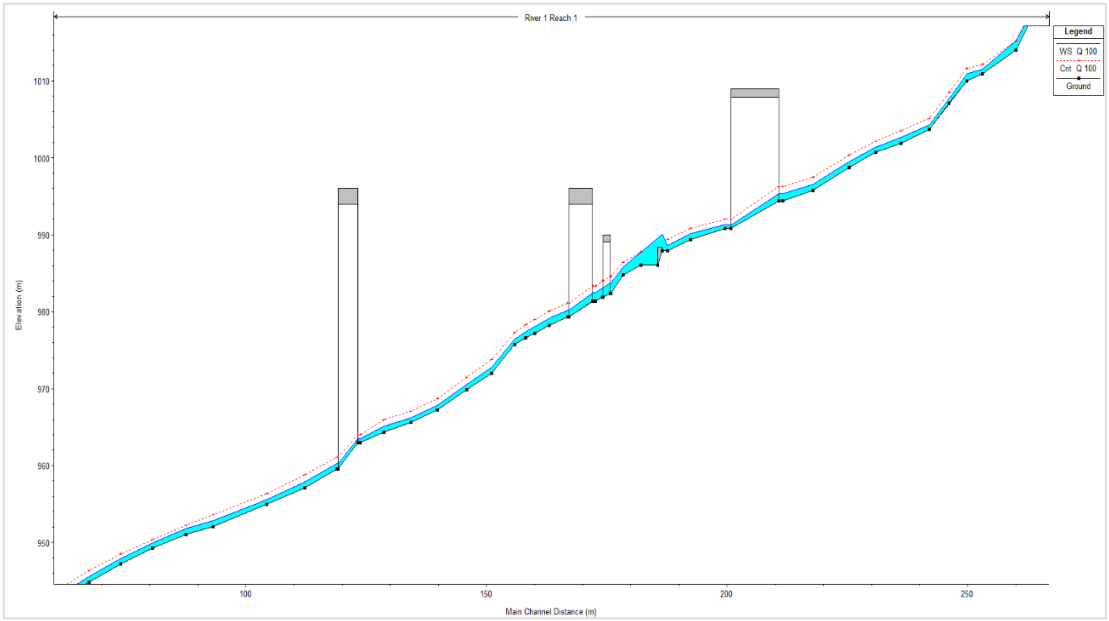

Figure 41. Water Stream Profile for TR 200 years

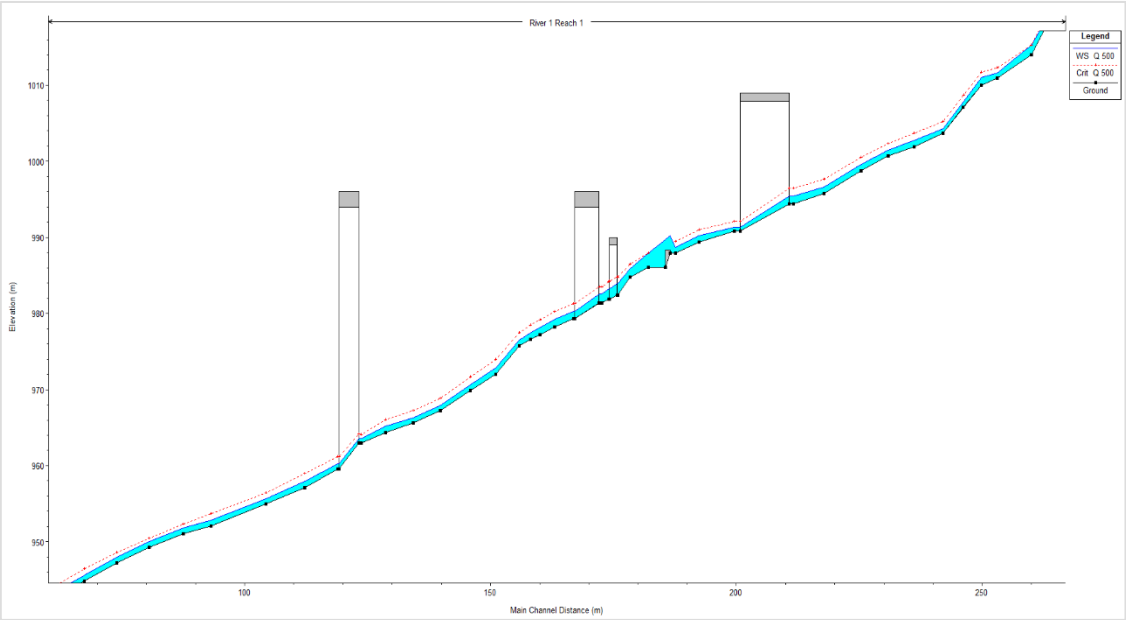

Figure 42. Water Stream Profile for TR 500 years

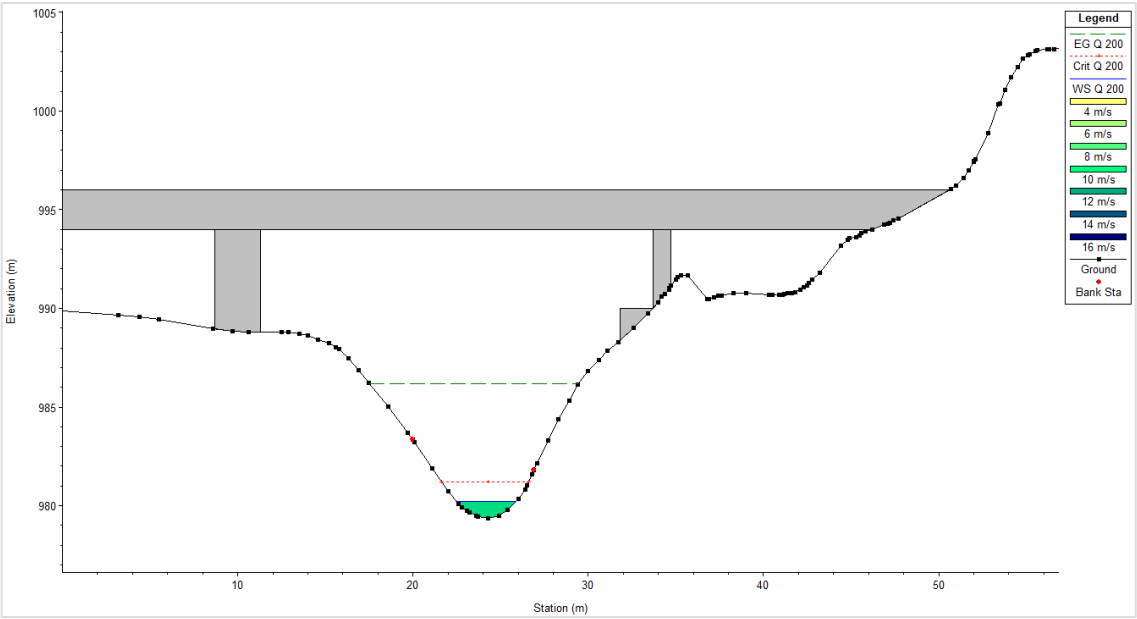

Figure 43. Cross section at the Upstream Viaduct towards Bardonecchia (Pillar A)

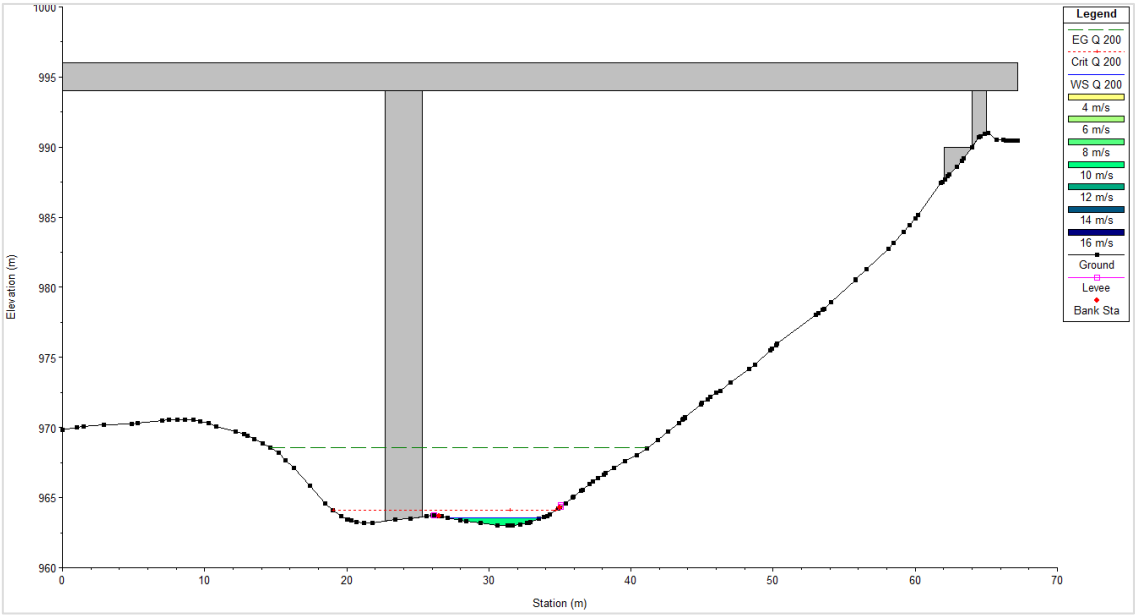

Figure 44. Cross-section at the Downstream Viaduct towards Torino (Pillar B)

CHAPTER 5: SEDIMENT TRANSPORT ANALYSIS

5.1. HEC-RAS CALCULATING METHODOLOGY

The characteristic parameters of a river are not constant, which implies some difficulties when dealing with river hydraulic problems. The calculations may not be entirely accurate as the flow varies according to the hydrological regime of the basin, the plan, and the section of the channel is fixed neither in space nor in time, and roughness is a difficult parameter to define. However, there are enough tools available to predict, in general terms, the behavior of a river.

5.1.1. QUASY-UNSTEADY FLOW

The river hydraulics must be determined before the HEC-RAS can calculate sediment transport, for this purpose the program uses a simplification very common in many sediment transport models.

The quasi-unsteady flow approximates a continuous hydrograph with a series of discrete steady flow profiles. For each record of the flow series, the flow rate remains constant for a specified period of time for transport. These permanent flow profiles are easier to develop than a full unsteady flow model, and the program will run faster.

Each discrete steady flow is divided and subsequently subdivided into smaller times for sediment transport calculations. The HEC-RAS uses three different types of subdivisions, each one being a subdivision of the previous one. The three-time steps are the *Flow Duration*, the *Computational Increment*, and the *Bed Mixing Time Steps*.

FLOW DURATION

The duration of the flow is the longest time interval. This represents the time interval during which the flow, its characteristics, the temperature, and the sediment load are assumed to be constant. If the flow rate is gauged daily the duration of the flow would be twenty-four hours unless a shorter time is interpolated. To specify a constant flow,

temperature, or sediment increment stage, it must be assigned a long enough time value, and if it is long enough it will be the reference parameter for the entire run.

COMPUTATIONAL INCREMENT

The duration of the flow is then subdivided into a calculation increment (Figure 45). Although the flow remains the same for the duration of the flow, the bed geometry and the hydrodynamics of the river are updated after each computational increment. The stability of the model can be very sensitive to this subdivision of time. When the calculation increment is too long, the bed geometry is not updated correctly and the results may vary.

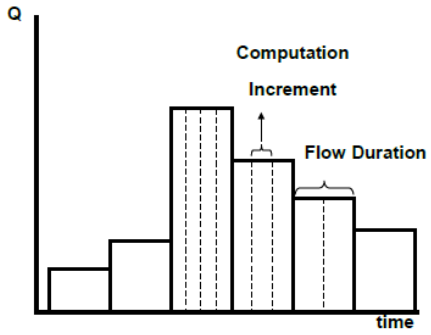

Figure 45. Quasi-Unsteady Flow series with time step. (HEC-RAS,2016)

BED MIXING TIME STEP

Finally, the calculation increment is subdivided into the bed mixing time. During each mixing time in a computational increment the bathymetry, the hydraulic parameters, and transport potential for each particle size remain constant. However, erosion and sedimentation calculations occur in this period of time and can cause changes in the composition of the mixed layers in the bed. The vertical gradation profile is rearranged due to the addition or removal of material. Since changes in the gradation layer are activated during the mixing time, the sediment transport capacity changes even though the hydrodynamics, consequently, the transport potential remains constant.

SEDIMENT CONTINUITY

The HEC-RAS program solves the Sediment Continuity equation known as the Exner equation:

$$(1-\lambda_p)B\frac{\partial \eta}{\partial t} = -\frac{\partial Q_s}{\partial x}$$

Where:

B, the channel width;

η, channel elevation;

λ_p, active layer porosity;

t, time;

x, distance;

Q_s, transported sediment load.

The sediment continuity equation is solved by calculating the sediment transport capacity through the control volume associated with each cross-section. This capacity is compared to the entire sediment supply entered for the control volume. If this capacity is greater than the supply, there is a sediment deficiency which is satisfied by eroding the bed. If the supply is greater than the capacity there is a surplus of sediment causing the transported material to deposit in the riverbed.

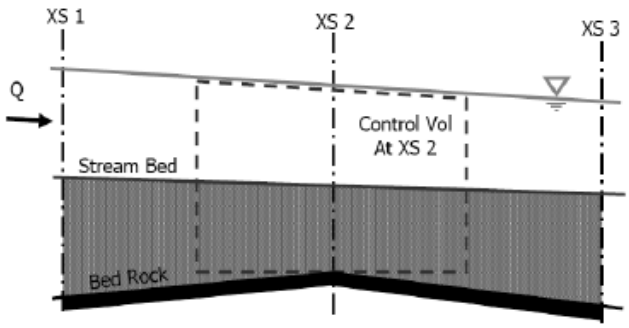

Figure 46. Sediment transport capacity between sections. (HEC-RAS, 2010)

5.1.2. EROSION, TRANSPORT AND SEDIMENTATION PROCESSES

When fluid in motion comes into contact with the channel that contains it, there is a mutual relationship, whose result depends on the characteristics of the movement of the fluid itself, which cause different pressure losses due to friction with the contour, and the type of particle size, slope, and geometry of the channel, thus always appearing for each of the cases, a range of forces, whether destabilizing and dragging or stabilizing and deposition of solid particles.

For a particle in the river bed to be dragged, it is necessary for the bottom shear, or bottom stress, to exceed a certain characteristic value or resistive force, (τ_o-τ_c > 0), which generally depend on the size of the sediment, its shape, its confinement in the bed, and the cohesion in the case of cohesive sediments.

Once the movement has started, the particles can be in suspension, or be dragged in the vicinity of the sill, there is a possibility of intermediate in which the particle initially located at the bottom, is lifted by the flow and temporarily transported, until the forces acting on it decrease, and then it is deposited again at the bottom. The finest particles and susceptible to the slightest movement will always remain in suspension, originating the so-called washload.

With regards to the particles of greater diameter and specific weight, if they cannot reach the core of the fluid, they are doomed to bottom transport, in the form of rolling or small jumps.

COMPUTING TRANSPORT CAPACITY

One of the main parts of the continuity equation is the sediment gradient through the control volume, comparing the increase with the sediment losses. Sediment increment is sediment that enters the control volume upstream and/or from local sources (lateral sediment increments). The maximum amount of sediment that can get out of the control volume, however, is a function of the amount of sediment that the water can move. This is what is called Transport Capacity, and it is calculated for each control volume at each mixing time.

GRAIN CLASSES

The HEC-RAS divides the sediment material into multiple types of particles. The range of transportable material, between 0.002 mm and 2048 mm is divided into 20 types of particles. The program's classification is presented in Table 18.

Grain Classes		Lower Bound	Upper Bound	Mean Diameter	Geometric Mean
Clay	Clay	0.002	0.004	0.003	0.00283
Very Fine Silt	VFM	0.004	0.008	0.006	0.00566
Fine Silt	FM	0.008	0.016	0.011	0.0113
Medium Silt	MM	0.016	0.032	0.023	0.0226
Coarse Silt	CM	0.032	0.0625	0.045	0.0447
Very Fine Sand	VFS	0.0625	0.125	0.088	0.0884
Fine Sand	FS	0.125	0.25	0.177	0.177
Medium Sand	MS	0.25	0.5	0.354	0.354
Course Sand	CS	0.5	1	0.707	0.707
Very Course Sand	VCS	1	2	1.41	1.41
Very Fine Gravel	VFG	2	4	2.83	2.83
Fine Gravel	FG	4	8	5.66	5.66
Medium Gravel	MG	8	16	11.3	11.3
Coarse Gravel	CG	16	32	22.6	22.6
Very Coarse Gravel	VCG	32	64	45.3	45.3
Small Cobbles	SC	64	128	90.5	90.5
Large Cobbles	LC	128	256	181	181
Small Boulders	SB	256	512	362	362
Medium Boulders	MB	512	1024	724	724
Large Boulders	LB	1024	2048	1448	1450

Table 18. Grain classes according to HEC-RAS

SEDIMENT TRANSPORT CAPACITY

The determination of sediment transport in a channel can be done in two ways, first one is by direct measurement and second one by means of equations proposed by different researchers. Sediment measurements are unusual due to the difficulties of working in rivers, so it is necessary to use equations that show a high degree of uncertainty.

The Sediment Transport Potential is the measure of how much material of a certain class of particle can transport certain hydrodynamic conditions. In the HEC-RAS model, the Transport Potential is calculated with a sediment transport equation. Since most of these equations were developed to be used with single particle size or at most two particle sizes, each equation is applied independently for each particle size considered in the system. There are seven sediment transport functions in the HEC-RAS model, the range of each input parameter for any function is shown in Table 19, these ranges are presented only as a guide.

Function	d	d_m	s	V	D	S	W	T
Ackers-White (*flume*)	0.04 - 7.0	NA	1.0 - 2.7	0.07 - 7.1	0.01 - 1.4	0.00006 - 0.037	0.23 - 4.0	46 - 89
Englund-Hansen (*flume*)	NA	0.19 - 0.93	NA	0.65 – 6.34	0.19 – 1.33	0.000055 – 0.019	NA	45 - 93
Laursen (*field*)	NA	0.08– 0.7	NA	0.068 – 7.8	0.67 – 54	0.0000021 – 0.0018	63 – 3640	32 - 93
Laursen (*flume*)	NA	0.011 - 29	NA	0.7 - 9.4	0.03 – 3.6	0.00025 – 0.025	0.25 – 6.6	46 - 83
Meyer-Peter Muller (*flume*)	0.4 – 29	NA	1.25 – 4.0	1.2 – 9.4	0.03 – 3.9	0.0004 – 0.02	0.5 – 6.6	NA
Tofaletti (*field*)	0.062 – 4.0	0.095 – 0.76	NA	0.7 - 7.8	0.07 – 56.7 (R)	0.000002 – 0.0011	63 - 3640	32 – 93
Tofaletti (*flume*)	0.062 – 4.0	0.45 – 0.91	NA	0.7 - 6.3	0.07 – 1.1 (R)	0.00014 – 0.019	0.8 – 8	40 - 93
Yang (*field-sand*)	0.15 – 1.7	NA	NA	0.8 - 6.4	0.04 – 50	0.000043 – 0.028	0.44 – 1750	32 - 94
Yang (*field-gravel*)	2.5 – 7.0	NA	NA	1.4 - 5.1	0.08 – 0.72	0.0012 – 0.029	0.44 – 1750	32 - 94

Table 19. Range of input values for sediment transport functions (HEC, 2016)

Where:

d, Overall particle diameter in mm

d_m, Median particle diameter in mm

s, Sediment specific gravity

V, Average channel velocity in fps

D, Channel depth in ft

S, Energy gradient

W, Channel width in ft

T, water temperature in ºF

(*R*), Hydraulic radius in ft

NA, Data not available.

The empirical equations which describe the movement of the particles within a fluid, and which are used by HEC-RAS in channel modeling are described as follows:

- ***Ackers and White (1973***

Is a total load function that was developed with data from a gauge for gradations ranging from sand to fine gravel. Hydrodynamics was selected to cover a range of bed configurations including ripples, dunes, and plane bed conditions. Suspended sediment is a function of shear velocity while bed loading is a function of shear stress.

The transport equation for Ackers-White function for a single grain size is described by the following equations:

$$X = \frac{G_{gr} s d_s}{D\left(\frac{u_*}{V}\right)^n} \qquad G_{gr} = C\left(\frac{F_{gr}}{A} - 1\right)$$

Where:

X, Sediment concentration, in parts per part

G_{gr}, Sediment transport parameter

S, Specific gravity of sediments;

dsd_s, Mean particle diameter;

D, Effective depth

$u*$, Shear velocity

V, Average channel velocity

n, Transition exponent, depending on sediment size

C, Coefficient

F_{gr}, Sediment mobility parameter

A, Critical sediment mobility parameter.

- ***Engelund and Hansen (1967)***

It is an equation of total transport load that was developed from gauged data. Sands of relatively uniform size between 0.19 mm and 0.03 mm were used. Although it is a relatively simple function of the channel velocity, the shear force in the bed, and the d50 type material. The application of this equation should be only for sandy systems.

$$g_s = 0.05\gamma_s V^2 \sqrt{\frac{d_{50}}{g\left(\frac{\gamma_s}{\gamma} - 1\right)}} \left[\frac{\tau_o}{(\gamma_s - \gamma) d_{50}}\right]^{3/2}$$

Where:

g_s, Unit sediment transport

γ, Unit weight of water

γ_s, Unit weight of solid particles

V, Average channel velocity

τ_o, Bed level shear stress

d_{50}, Particle size of which 50% is smaller.

- ***Copeland´s from Laursen (1968,1989)***

It is also a total head function that was initially based on gauge equations and was later extended by Madden to include data from the Arkansas River. It is a basic function of excess shear stress and the relationship between shear rate and rate of fall. Years later, Copeland (1989) generalized the equation for gravel transport, so the equation can be used for graded beds.

Laursen's contribution is that the function was developed for a large number of fine silts. No other functions included in the HEC-RAS were developed for silt. Any potential sedimentation calculated by the other functions would be an extrapolation, taking into account that extrapolation errors may exist in addition to the standard uncertainty due to the calculation of the transport capacity. Recent studies in the State of Colorado have shown that the Laursen equation outperforms other transport functions in the silt field.

$$C_m = 0.01\gamma\left(\frac{d_s}{D}\right)^{7/6}\left(\frac{\tau_o^{'}}{\tau_c}-1\right)f\left(\frac{u_*}{\omega}\right)$$

C_m, Sediment discharge concentration, in weight7volume

G, Unit weight of water

d_s, Mean particle diameter

D, Effective depth of flow

$\tau_o{}'$, Bed shear stress due to grain resistance

τ_c, Critical bed shear stress

$f\left(\frac{u_*}{\omega}\right)$, Function of the ratio of shear velocity to fall velocity.

- ***Meyer, Peter, and Müller (1948)***

This equation was one of the first equations developed and is still one of the most widely used. It is a simple excess shear stress ratio. It is strictly a bedload equation developed with gauging experiments for sand and gravel under plane bed conditions. Most of the data was developed using uniform gravel substrates. This function is mostly successful in the gravel range and tends to underestimate the transport of fine materials.

$$\left(\frac{k_r}{k_r'}\right)^{3/2}\gamma RS = 0.047(\gamma_s - \gamma)d_m + 0.25\left(\frac{\gamma}{g}\right)^{1/3}\left(\frac{\gamma_s - \gamma}{\gamma_s}\right)^{2/3} g_s^{2/3}$$

g_s, Unit sediment transport rate in weight/time/unit width

k_r, A roughness coefficient

k_r', A roughness coefficient based on grains

γ, Unit weight of water

γ_s, Unit weight of solid particles

g, acceleration of gravity

d_m, Mean particle diameter

S, Energy gradient

R, Hydraulic radius.

- ***Toffaleti (1968)***

It is a total charge function developed primarily for sand-size particles. It is generally considered a function for large rivers. This function is not seriously influenced by the shear speed or the shear stress in the bed. Instead, the equation was formulated based on temperature regressions and an empirical exponent that describes the relationship between sediment and hydraulic characteristics.

Additionally, the Toffaleti equation is used for two different particle sizes, in an attempt to quantify the dependence of transport on the mean gradation deviation. This made more sense when the equation was used to calculate the transport of graded bulk material. When this is applied to individual classes of particles, the program will use the d50 and d65 for the classes of particles entered, narrowing the original parameter d65.

Toffaleti defined a function for a single grain size, represented by the following transport equations:

Lower zone:
$$g_{ssL} = M\frac{\left(\frac{R}{11.24}\right)^{1+n_v-0.756z} - (2d_m)^{1+n_v-0.756z}}{1+n_v-0.756z}$$

Middle zone:
$$g_{ssM} = M\frac{\left(\frac{R}{11.24}\right)^{0.244z}\left[\left(\frac{R}{2.5}\right)^{1+n_v-z} - \left(\frac{R}{11.24}\right)^{1+n_v-z}\right]}{1+n_v-z}$$

Upper zone:
$$g_{ssU} = M\frac{\left(\frac{R}{11.24}\right)^{0.244z}\left(\frac{R}{2.5}\right)^{0.5z}\left[R^{1+n_v-1.5z} - \left(\frac{R}{2.5}\right)^{1+n_v-1.5z}\right]}{1+n_v-1.5z}$$

Bed zone:
$$g_{sb} = M(2d_m)^{1+n_v-0.756z} \qquad M = 43.2C_L(1+n_v)VR^{0.756z-n_v}$$

$$g_s = g_{ssL} + g_{ssM} + g_{ssU} + g_{sb}$$

g_{ssL}, Suspended sediment transport in the lower zone, in tons/day/ft

g_{ssM}, Suspended sediment transport in the middle zone, in tons7day7ft

g_{ssU}, Suspended sediment transport in the upper zone, in tons/day7ft

g_{sb}, Bedload sediment transport in tons/day/ft

g_s, Total sediment transport in tons/day/ft

M, Sediment concentration parameter

C_L, Sediment concentration in the lower zone

R, Hydraulic radius

Median particle diameter

z, Exponent describing the relationship between the sediment and hydraulic characteristics

n_v, Temperature exponent

- ***Yang (1973,1984)***

Is a total transport load equation that bases transport on the product of velocity and shear stress. The function was developed and tested on a variety of gauges and field data.

The equation is made up of two separate transport ratios for sand and gravel. The transition between sand and gravel is smoothed in order to avoid large discontinuities. Yang tends to be very sensitive to the speed of the current and is more sensitive to the speed of fall than all the other equations.

For sand $d_m < 2mm$

$$\log C_t = 5.435 - 0.286\log\frac{\omega d_m}{\nu} - 0.457\log\frac{u_*}{\omega} + \left(1.799 - 0.409\log\frac{\omega d_m}{\nu} - 0.314\log\frac{u_*}{\omega}\right)\log\left(\frac{VS}{\omega} - \frac{V_{cr}S}{\omega}\right)$$

For gravel $d_m \geq 2mm$

$$\log C_t = 6.681 - 0.633\log\frac{\omega d_m}{\nu} - 4.816\log\frac{u_*}{\omega} + \left(2.784 - 0.305\log\frac{\omega d_m}{\nu} - 0.282\log\frac{u_*}{\omega}\right)\log\left(\frac{VS}{\omega} - \frac{V_{cr}S}{\omega}\right)$$

Where:

C_t, Total sediment concentration;

ω, Particle fall velocity;

d_m, Mean particle diameter;

v, Kinematic viscosity;

$u*$, Shear velocity;

V, Average channel velocity;

S, Energy gradient;

- ***Wilcock (2001)***

It is a bed loading equation designed for graded beds containing both sand and gravel. This is a surface transport method based on the theory that transport depends mainly on the material in direct contact with the flow. This equation was developed based on the grading of the surfaces of the gauges and rivers. Therefore, the bed grading should reflect the properties of the bed surface. Wilcock, additionally, has a hidden function that reduces the potential for particle transport based on the premise that particles can be deposited between large gravel deposits and not fully experience the force of the flow field (at the boundary of the turbulent layer).

Finally, the central theory of the Wilcock equation is that the transport potential of gravel increases as it increases in sand content. Dimensionless referential shear stress is calculated for the substrate which is a function of the sand content at the surface of the bed.

As the sand content increases, the referential shear stress decreases, if the excess shear in the bed increases and the total transport increases. Wilcock's equation is very sensitive to the sand content parameter. This tends to be better for bimodal systems and diverges from the other unimodal equations.

$$\tau_{rm}^{*} = 0.021 + 0.15e^{-20FS}$$

Where:

$\tau_{rm}*$, The reference shear stress

FS, Percentage of Sand content.

5.1.3. SUSPENSION LOAD MOVEMENT

FALL VELOCITY

This refers to the maximum velocity that the particle reaches when it falls freely in water. The rate of fall takes into account the weight, shape, particle size, temperature, and density of the water. Suspension of a sediment particle begins once the shear or tangential velocity at the bottom level approaches the magnitude of the particle's fall velocity. The

particle will remain in suspension as long as the vertical components at the bottom level exceed the rate of fall. Therefore, the determination of suspended sediment transport is highly dependent on the rate of fall of the particles.

Within HEC-RAS, there are three methods to calculate the rate of fall: Toffaleti (1968), Van Rijn (1993), and Rubey (1933). Furthermore, the default value can be chosen, in case the fall velocity used in the development of the corresponding sediment transport function will be used. In general, the fall velocity method should be used to be consistent with the development of the sediment transport function, however, if the user has specific information on the validity of one method over another for a particular combination of sediment and hydraulic properties, the calculation with this method is valid. The form factor (sf) is the most important for medium and large arenas. Toffaleti uses a 0.9 sf, while Van Rijn develops his equations for a 0.7 sf. Natural sand usually has a size of around 0.7.

- ***Toffaleti (1968)***

Suggests a table of fall velocity with a shape factor of 0.9 and a specific gravity of 2.65. Different rates of fall are given for a range of temperatures and particle sizes classified as very fine sands (Very Fine Sand, VFS) and medium gravel (Medium Gravel, MG). The falling speeds of Toffaleti are given in Table 20:

Sand Grain Settling Velocity Versus Temperature, SP.G. 2.65, Shape Factor 0.9

TEMP °F	SETTLING VELOCITY IN FT/SEC							
	VFS	FS	MS	CS	VCS	VFG	FG	MG
35	.013	.045	.130	.305	.590	1.00	1.41	1.95
36	.013	.045	.131	.307	.592	1.00	1.41	1.95
37	.013	.046	.132	.310	.594	1.00	1.41	1.95
38	.014	.047	.133	.312	.596	1.00	1.41	1.95
39	.014	.047	.135	.314	.598	1.00	1.41	1.95
40	.014	.048	.136	.316	.600	1.00	1.41	1.95
41	.015	.049	.137	.318	.602	1.00	1.41	1.95
42	.015	.050	.138	.320	.604	1.00	1.41	1.95
43	.015	.051	.140	.321	.606	1.00	1.41	1.95
44	.016	.051	.141	.322	.608	1.00	1.41	1.95
45	.016	.052	.142	.323	.609	1.00	1.41	1.95
46	.016	.053	.143	.325	.610	1.00	1.41	1.95
47	.016	.053	.144	.326	.612	1.00	1.41	1.95
48	.017	.054	.145	.328	.614	1.00	1.41	1.95
49	.017	.055	.146	.330	.616	1.00	1.41	1.95
50	.017	.055	.147	.331	.618	1.00	1.41	1.95
51	.018	.056	.148	.333	.620	1.00	1.41	1.95
52	.018	.057	.150	.334	.621	1.00	1.41	1.95
53	.018	.057	.151	.336	.623	1.00	1.41	1.95
54	.018	.058	.152	.338	.624	1.00	1.41	1.95
55	.018	.059	.153	.340	.626	1.00	1.41	1.95
56	.019	.059	.154	.341	.627	1.00	1.41	1.95
57	.019	.060	.155	.343	.629	1.00	1.41	1.95
58	.019	.061	.156	.344	.630	1.00	1.41	1.95
59	.019	.061	.157	.346	.632	1.00	1.41	1.95
60	.020	.062	.158	.347	.633	1.00	1.41	1.95
61	.020	.063	.160	.349	.635	1.00	1.41	1.95
62	.020	.063	.161	.350	.636	1.00	1.41	1.95
63	.020	.064	.162	.351	.638	1.00	1.41	1.95
64	.021	.065	.163	.353	.639	1.00	1.41	1.95

TEMP °F	SETTLING VELOCITY IN FT/SEC							
	VFS	FS	MS	CS	VCS	VFG	FG	MG
65	.021	.065	.165	.354	.640	1.00	1.41	1.95
66	.021	.066	.166	.356	.641	1.00	1.41	1.95
67	.021	.067	.167	.357	.643	1.00	1.41	1.95
68	.022	.067	.168	.359	.644	1.00	1.41	1.95
69	.022	.068	.170	.360	.646	1.00	1.41	1.95
70	.022	.069	.171	.361	.647	1.00	1.41	1.95
71	.022	.070	.172	.362	.649	1.00	1.41	1.95
72	.023	.071	.173	.363	.650	1.00	1.41	1.95
73	.023	.071	.175	.364	.652	1.00	1.41	1.95
74	.023	.072	.176	.365	.653	1.00	1.41	1.95
75	.024	.072	.177	.366	.655	1.00	1.41	1.95
76	.024	.073	.178	.367	.656	1.00	1.41	1.95
77	.024	.073	.180	.368	.657	1.00	1.41	1.95
78	.024	.074	.181	.370	.658	1.00	1.41	1.95
79	.025	.074	.182	.371	.659	1.00	1.41	1.95
80	.025	.075	.183	.373	.660	1.00	1.41	1.95
81	.025	.075	.184	.375	.661	1.00	1.41	1.95
82	.025	.076	.185	.376	.662	1.00	1.41	1.95
83	.025	.077	.186	.378	.663	1.00	1.41	1.95
84	.026	.077	.187	.380	.664	1.00	1.41	1.95
85	.026	.078	.188	.381	.665	1.00	1.41	1.95
86	.026	.078	.190	.383	.666	1.00	1.41	1.95
87	.026	.079	.192	.385	.667	1.00	1.41	1.95
88	.027	.079	.194	.386	.668	1.00	1.41	1.95
89	.027	.080	.195	.388	.669	1.00	1.41	1.95
90	.027	.080	.196	.390	.670	1.00	1.41	1.95
91	.028	.081	.197	.391	.671	1.00	1.41	1.95
92	.028	.081	.198	.392	.672	1.00	1.41	1.95
93	.028	.082	.199	.393	.673	1.00	1.41	1.95
94	.028	.082	.200	.394	.674	1.00	1.41	1.95

Table 20. Fall Velocity by Toffaleti (HEC, 2016)

- ***Rubey (1933)***

Established an analytical relationship between fluid, sediment properties, and fall velocity based on the combination of Stokes' law and an impact formula including both fine particles subject only to viscous resistance and particles outside the region of Stokes. This equation has been modified to be applied to silts, sands, and gravels, although Rubey mentions that particles with a specific gravity of approximately 2.65 are the most appropriate since the other particles tend to fall earlier than that equation predicts:

$$\omega = F_1\sqrt{(s-1)gd_s}$$

In which:

$$F_1 = \sqrt{\frac{2}{3} + \frac{36\nu^2}{gd^3(s-1)}} - \sqrt{\frac{36\nu^2}{gd^3(s-1)}}$$

- ***Van Rijin (1993)***

Approximates the fall velocity curves from the US Interagency Committee on Water Resources for non-spherical particles with a shape factor of 0.7 and a water temperature of 20ºC. Depending on the size of the particle, there are three equations to be used:

For $0.001 < d < 0.1$ mm

$$\omega = \frac{(s-1)gd}{18\nu}$$

For $0.1 < d \leq 1$ mm

$$\omega = \frac{10\nu}{d}\left[\left(1 + \frac{0.01(s-1)gd^3}{\nu^2}\right)^{0.5} - 1\right]$$

For $d \geq 1$

$$\omega = 1.1\left[(s-1)gd\right]^{0.5}$$

Where:

ω, Particle fall velocity

ν, cinematic viscosity

s, specific gravity of the particle

d, particle diameter

5.2. BOUNDARY CONDITIONS

For the analysis of solid transport, the quasi-permanent motion was considered: this motion regime allows to simulate the time series of the flow rates as a sequence of constant flow rates defined for time steps so that the HEC-RAS code calculates for each time step the solid transport model in conditions of permanent motion.

For the Transport Capacity calculations, it was used the Yang transport function, the sorting method was set as "Active Layer" and the fall velocity method used was the one of Van Rijin.

5.2.1. UPSTREAM BOUNDARY CONDITIONS

In the case in question, a flood event with a total duration of 36 minutes was considered, and a time step of 6 minutes was defined for the time discretization required by the quasi-permanent motion regime. The value of the flow rate considered is the one relating to a return time of 200 years, corresponding to 21.23 m3/s.

5.2.2. DOWNSTREAM BOUNDARY CONDITIONS

Downstream, a bottom slope of 0.16 was defined at the end section of the section in question. The slope is used by the program to calculate the height of uniform motion (Normal Depth) using the Chezy formula, which constitutes the downstream boundary condition.

5.3. GRAIN SIZE OF THE RIVERBED

In order to evaluate the erosion and deposit phenomena that occur due to the mobility of the riverbed bottom, it is necessary to define the grain size of the riverbed for each section of the model. It is possible to create a database of grain size curves to be assigned to each section along the river. For sections with intermediate characteristics between two granulometric curves, it is possible to interpolate the available data.

The data entered for the definition of the two grain size curves are presented in Figure 47 and Figure 48.

	Class	diam (mm)	% Finer
1	Clay	0.004	0
2	VFM	0.008	0
3	FM	0.016	0
4	MM	0.032	0
5	CM	0.0625	5
6	VFS	0.125	5.83
7	FS	0.25	6.67
8	MS	0.5	7.5
9	CS	1	8.33
10	VCS	2	9.17
11	VFG	4	10
12	FG	8	15
13	MG	16	20
14	CG	32	25
15	VCG	64	30
16	SC	128	65
17	LC	256	100
18	SB	512	
19	MB	1024	
20	LB	2048	

% Finer Grain Class % Convert: %finer<-->%

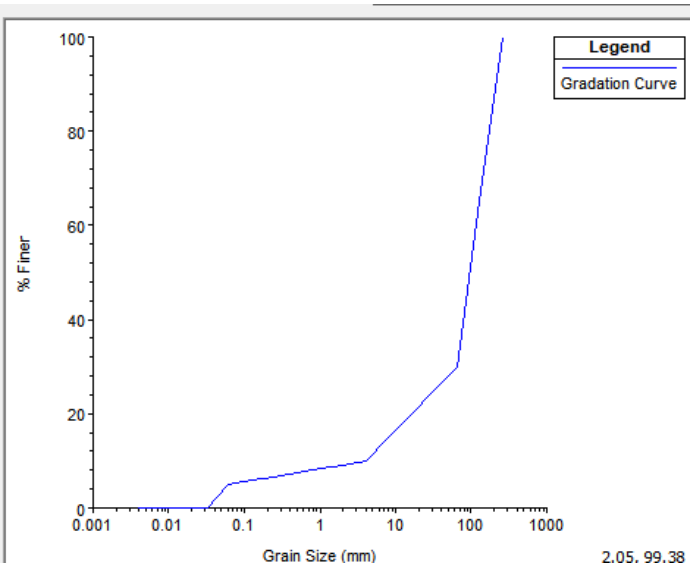

Figure 47. Granulometric curve 1 used for solid transport simulation.

	Class	diam (mm)	% Finer
1	Clay	0.004	0
2	VFM	0.008	0
3	FM	0.016	0
4	MM	0.032	0
5	CM	0.0625	0
6	VFS	0.125	0
7	FS	0.25	0
8	MS	0.5	0
9	CS	1	0
10	VCS	2	0
11	VFG	4	5
12	FG	8	7.5
13	MG	16	10
14	CG	32	12.5
15	VCG	64	15
16	SC	128	27.5
17	LC	256	40
18	SB	512	100
19	MB	1024	
20	LB	2048	

% Finer Grain Class % Convert: %finer<-->%

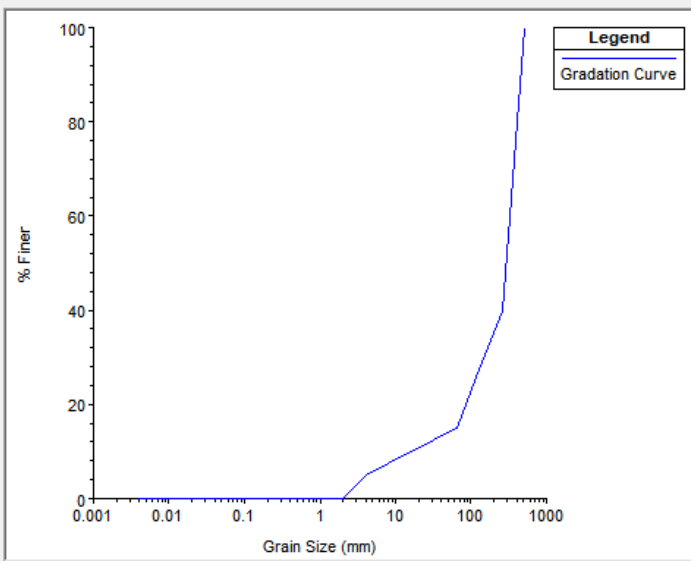

Figure 48. Granulometric curve 2 used for solid transport simulation.

In the case in question, two "typical" granulometric curves were defined on the basis of the observations and measurements that were conducted during the inspection, these curves were assigned to some of the sections, while for other sections the granulometry was defined by interpolation.

5.4. RESULTS

The results obtained evidence the presence of solid transport along the section of the watercourse under study. Along the steepest sections, where the velocity and energy of the current are greater, erosion of the bottom and overbanks occurs, while where the

slopes are less, for example in correspondence with the Viaduct Pillar B located downstream on the hydrographic left there are phenomena of deposit of material, for thicknesses of the order of 15 cm for a return period of two hundred years as reported in Figure 50.

The solid transport phenomenon is however contained for all the sections taken into consideration and is not such as to cause particular problems, in particular at Pillar A of the Highway Viaduct.

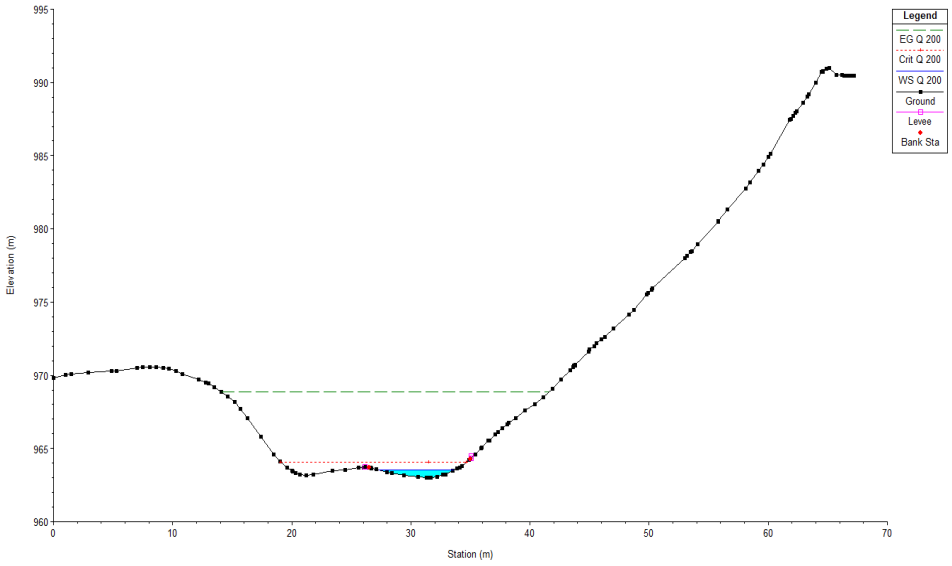

Figure 49. Cross-section viaduct towards Torino

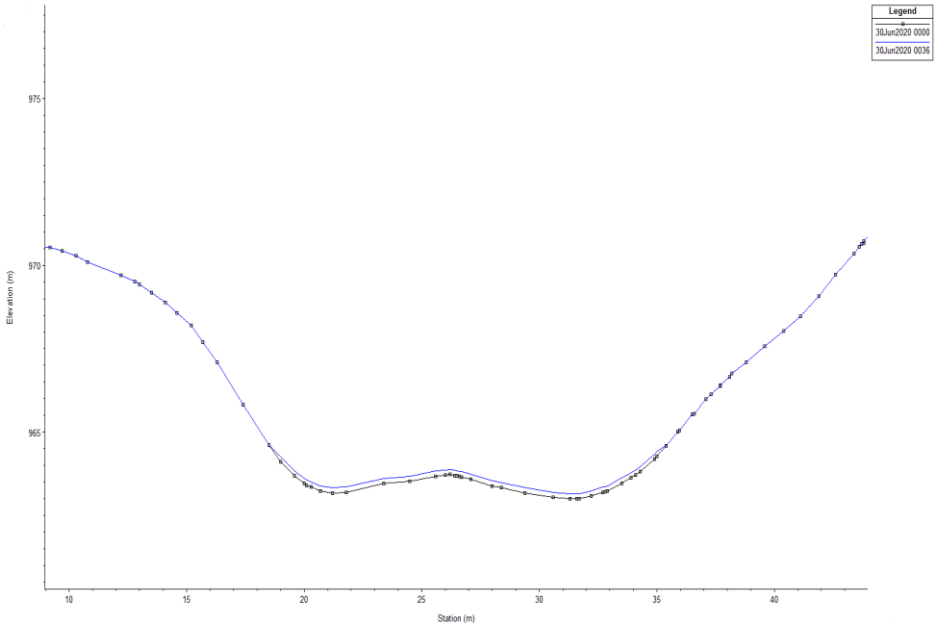

Figure 50. Solid Transport simulation at Section viaduct towards Torino

CHAPTER 6: DESIGN INDICATIONS OF THE POSSIBLE SOLUTION

6.1. EROSION CONTROL FOR ABUTMENTS

The phenomena of solid transport that occur along the river is explained by the high total energy of the watercourse. From the results of the simulation of solid transport, it emerges that the erosion and deposit phenomena affect all the sections of the stretch under examination, with the exception of the stretch characterized by the presence of outcropping rock, not subject to erosion and deposition in relation to the high slopes.

However, the simulations show that the extent of these phenomena is contained and there are no particular critical issues related to erosion at the piles and abutments of the Highway viaduct.

Given the presence of a modest instability at the base of Abutments, caused by the sliding of surface material, it was considered the protection of the banks implementing an anti-erosion system with geosynthetics.

6.1.1. GEOSYNTHETICS

As reported in the UNI EN ISO 10318 standard "Geosynthetics - Terms and definitions", the term "geosynthetic" describes an industrial product of which at least one of the components is made up of a synthetic or natural polymer, in the form of a sheet, strip or a three-dimensional structure, used in contact with soil and/or other materials in many geotechnical and civil engineering applications. These are mainly polymeric, organic, or textile materials, marketed in rolls that can be classified according to the manufacturing method. Their use is constantly growing thanks to their low costs and their simplicity of installation, as well as an ever-wider choice. Today geosynthetics are classified according to the UNI EN ISO 10318 standard on the basis of their structure, their use, and their function.

GEOMATS (GMA)

The geomats have a three-dimensional structure made with filaments of polymers or other tangled synthetic or natural elements or by sewing extruded nets. In the case of tangled filaments, there will be high deformability as a result of crushing by the ground. In the case of extruded nets, the geomats will be composed of two layers of flat nets with a third net inside which will, however, be folded and will have the purpose of making the structure non-deformable and increasing the thickness.

Geomats are characterized by a high void index, usually greater than 90%. They can be coated with a geogrid to increase longitudinal strength. The geomats are used on slopes or escarpments to counteract erosive phenomena due to rainwater. In fact, they constitute a surface protection during the growth period of the vegetation. They can also be used on the banks of waterways and canals but limited to areas not wet by water and only subjected to runoff and rainwater actions.

Figure 51. Three-dimensional geomat in polyamide monofilaments. Obtained from Harpo Seic

The anti-erosion geomat is widely used in landscape design for the construction of complex landscape figures and is also often used to strengthen the lines of river banks, waterways, and reservoirs.

It is important to note that although many polypropylene and polyethylene geomatics manufacturers claim protection, this material can be quickly destroyed under the influence of ultraviolet light and chemically active media. The term of anti-corrosion geomats made of polypropylene and polyethylene shall not exceed 3 years and 1 year respectively. If the estimated life of the anti-corrosion geometric mat is more than 3 years, it is recommended to consider the use of polyamide geomat.

Often these materials are coupled with polymeric or metal reinforcements to combine the need for mechanical resistance with anti-erosive ones; this is typical in the application for stabilization of layers of backfill on inclined surfaces with low adhesion or for covering very friable rock walls.

Figure 52. Three-dimensional PP Geomat used as superficial erosion control bonded during the production process to a double twisted metal mesh. Obtained from Temacorporation.com

6.1.2. DESIGN INDICATIONS

The choice of the geomat model most suitable for the situation in question must be carried out according to the procedures described below in the case of dry banks and wet banks. On dry embankments, three-dimensional anti-erosion open-bottom geomats are used. On wet banks, on the other hand, three-dimensional anti-erosion geomats of the flat bottom type are used. The flat bottom has the function of preventing the establishment of micro-turbulence due to the current at the bottom which would end up removing the gravel used as clogging material.

Coating the bank of a watercourse with a geomat is a process of rapid execution and an immediate and lasting surface anti-erosion effect; how it is performed can be summarized in the following 9 steps:

1. Regularization of the bank or embankment by removing any root systems and eliminating bumps and depressions (surface irregularities);
2. Creation of a groove at least 30 cm deep upstream of the bank;

3. Positioning of one end of the geomat inside the groove, fixing the latter with iron pegs or metal brackets with a minimum diameter of 8 mm and covering the groove with suitable fill material;
4. Sowing;
5. Unrolling of the geomat along the bank or embankment and overlapping of the contiguous sheets (overlaps of at least 10 cm), making sure that it is in contact with the ground below and is not too tight. The installation must be carried out in the opposite direction to the current (the fabric upstream must overcome the one downstream) to avoid water infiltration between one mat and another;
6. Fixing the mat with brackets or U-shaped pegs in correspondence with the overlapping of the various sheets used and in the center of the same. The density of the stakes varies according to the slope of the bank or embankment and the consistency of the substrate: in general, it is possible to recommend the insertion of 1 stake / m2 for inclinations of less than 30 ° and 2 ÷ 3 stakes / m2 in the case of higher slopes;
7. Covering the edges and fixing the geomat to the foot of the bank or embankment;
8. Planting of cuttings by driving and shrubs by localized cutting of the mat;
9. Possible sowing, fertilization, and irrigation.

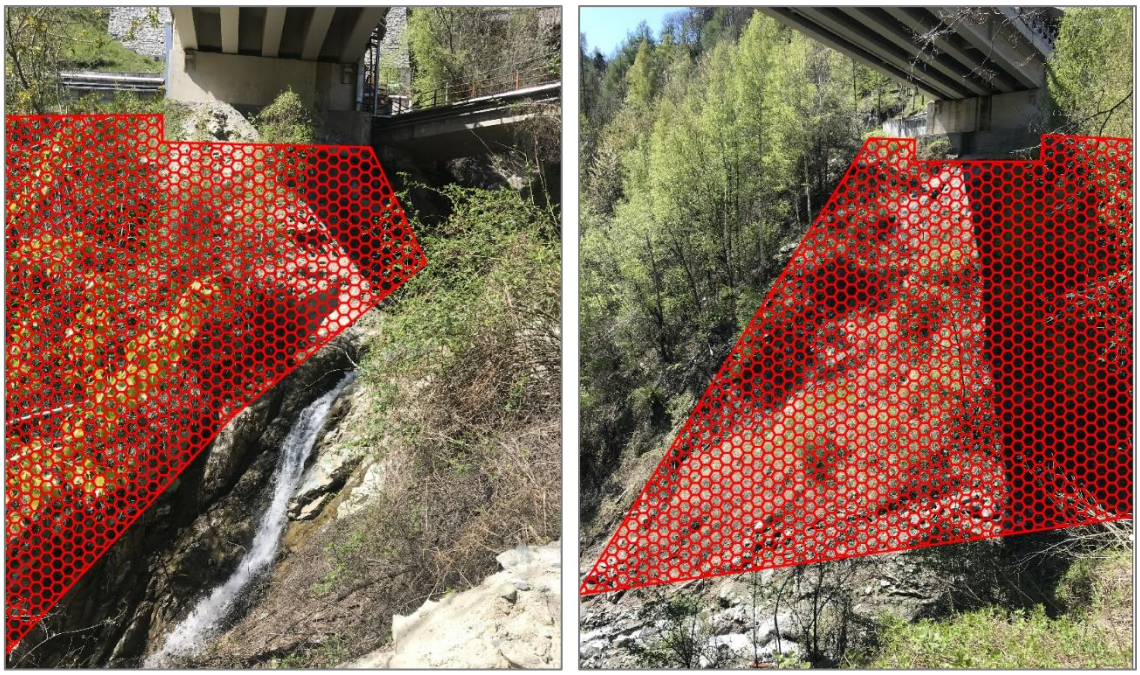

Figure 53. Areas of Intervention. Abutment A (left) and Abutment B (right)

The Geomat is projected to have an extension that covers the left riverbank area going from Abutment A to Abutment B. Intervention areas for both abutments are shown in Figure 53 where it is seen how the Geomat extends in an area presumed to be mostly dry as the water depth does not present very high values even during flood events.

Due to the possibility of erosion that has been ascertained for the banks in question, the most appropriate type of coating was chosen according to the general conditions. It was determined that it will be suitable the use of a Geomat Anti-erosion in Polyamide fiber Nylon type or Polypropylene (P.P), with overlapping metallic containment net with double twisted hexagonal mesh with strong galvanization, extended as shown in Figure 54.

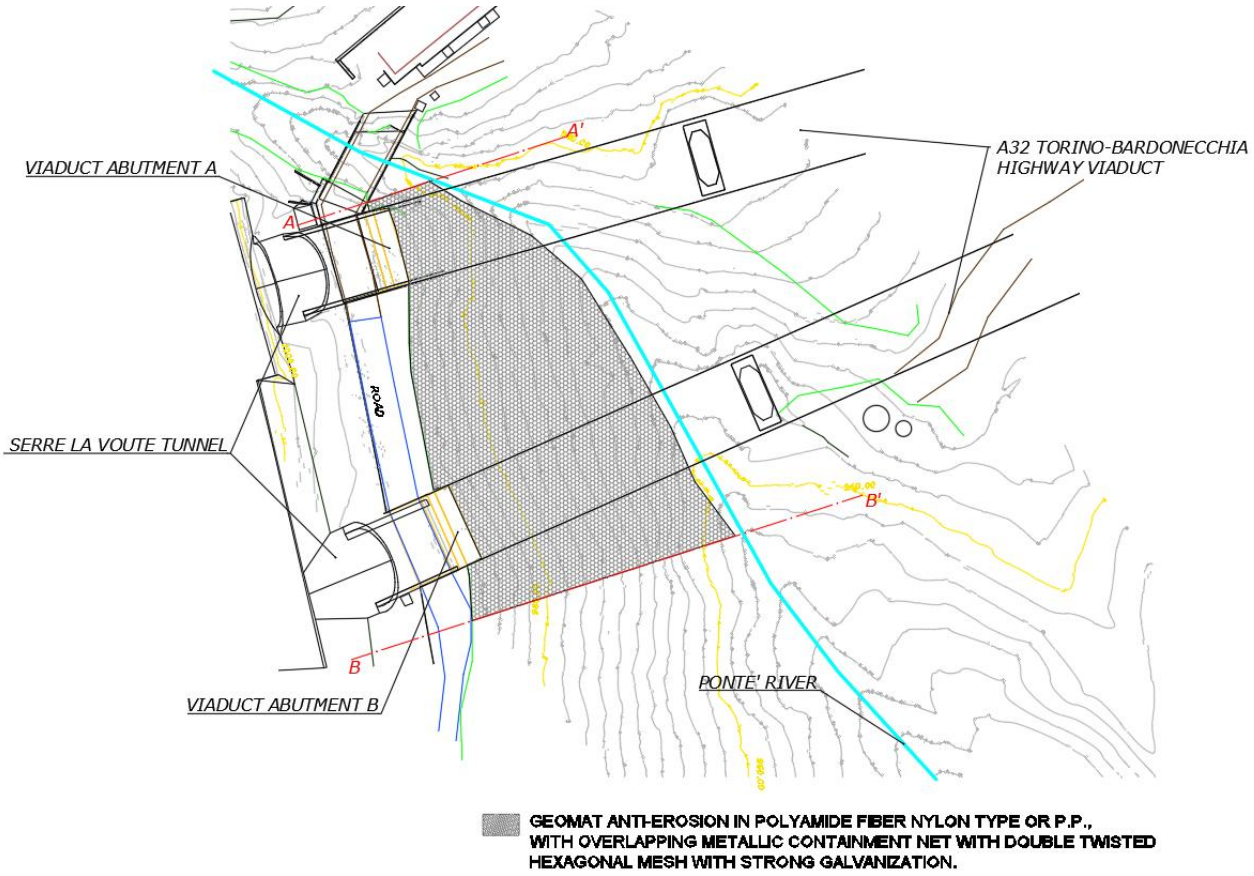

Figure 54. Plan view of the GEOMAT for erosion control of Abutments A and B.

It is projected an anchoring system based on the ground conditions. For the initial part, Corresponding to Abutment A, it is provided a total length of the geomat equal to 13.5 m, with the installation of anchor bars with lengths of 3 m, 6 m to 9 m distributed as shown in Figure 55.

The final part, corresponding to Abutment B, is projected to have a total length of the geomat equal to 50.8 m, with an anchoring system formed by Anchor bars whose length goes from 3m to 9m as shown in Figure 56.

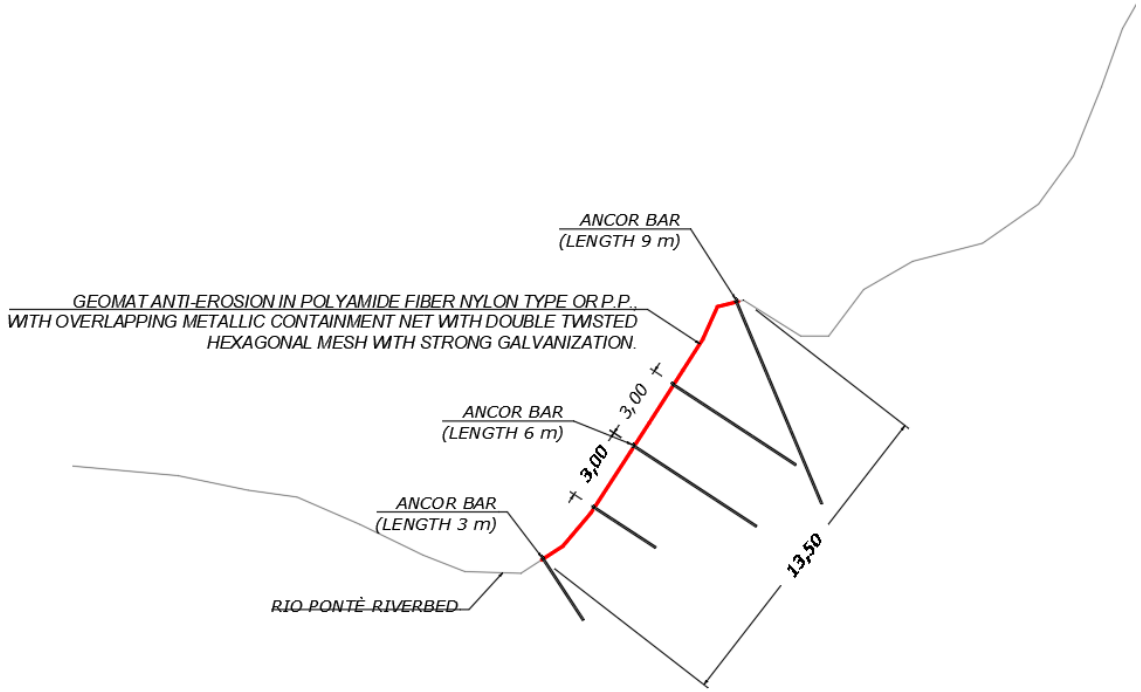

Figure 55. Profile view section A, A'. GEOMAT abutment A.

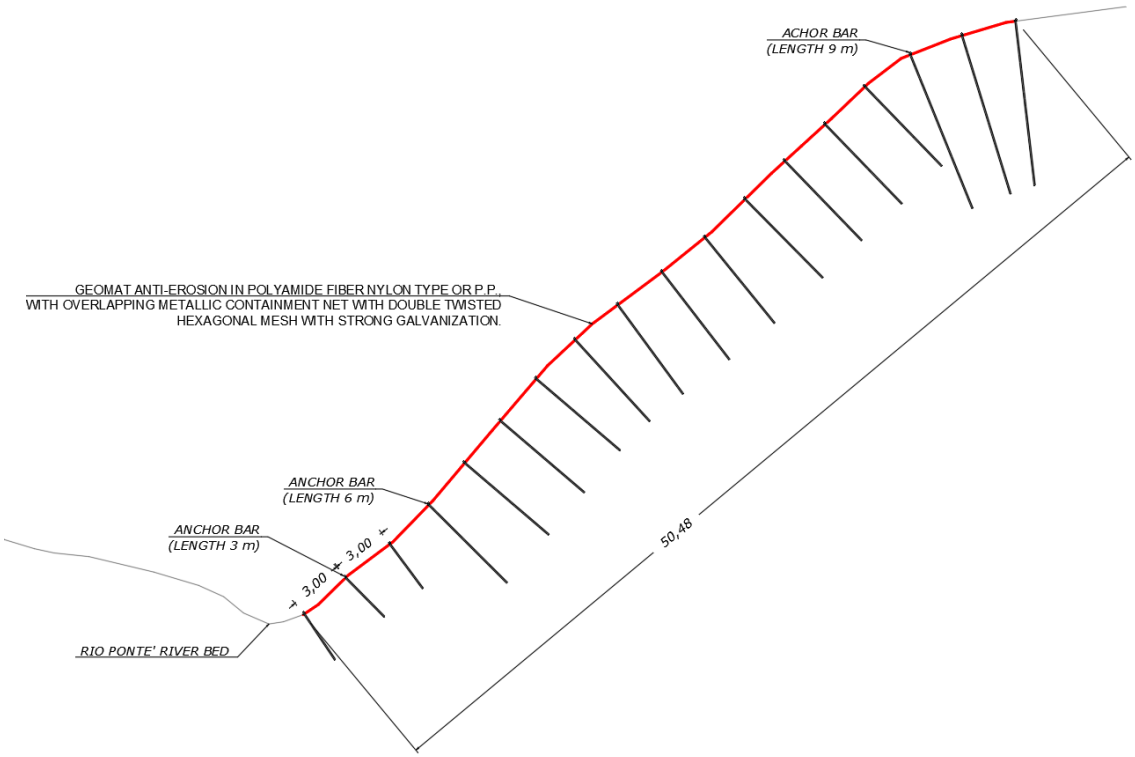

Figure 56. Profile view section B, B'. GEOMAT abutment B.

6.2. PROTECTION FOR PILLAR B

The main criticality on the left bank is linked to the solid transport and its deposition during flood events, in correspondence with the pillar B, located almost inside the riverbed. The morphology of the site is characterized by a decrease in the slope of the riverbed, by a smaller incision in the watercourse, and by the consequent increase in the runoff section causing an accumulation of transport material against the Pillar B and its immediate surroundings

It was not provided any protection structure against rockfall for Pillar B, because despite the presence of deposition phenomena of material of variable size due to the decrease in the slope of the riverbed, the criticality was not such as to require the installation of a protective barrier or similar structure; the installation of the barrier also presents many technical problems, also linked to the presence of the foundation of the pile which complicates the process of anchoring the barrier.

CONCLUSION

With this thesis, it was possible to verify the influence of the Rio Pontè, a tributary of the Dora Riparia river, on the current integrity of the structures constituting the Serre la Voute A32 viaduct, located in the municipality of Salbertrand (Torino) under the presumptions on instability and erosion phenomena due to the sediment transport and the fluvial dynamics of the river.

The behavior of the river was analyzed with particular attention to the hydraulic behavior and the dynamics of solid transport. Particularly, it was determined the erosion in the riverbed, specifically in correspondence with the structures of interest, whose integrity could be influenced by the fluvial dynamics, these structures correspond to two pillars, and two abutments built in reinforced concrete and footing on micro-piles of variable length, determined by the depth of the rigid and compact substrate.

A Hydraulic and Sediment Transport model was built and implemented with the HEC-RAS numerical software. From the simulations carried out, it is clear that the water velocities present in the watercourse for frequent, infrequent, and rare flood events are high, as expected given the slopes that characterize the Rio Pontè in the stretch covered by the hydraulic analysis carried out. The total energy of the watercourse is consequently high, and this explains the phenomena of transport of solid material that occur along the river. Where the energy of the watercourse decreases, in correspondence with the slope reductions and the minor incision of the watercourse, with a consequent increase in the runoff section, there is a deposit of solid material, as occurs in the surroundings of the viaduct pillar on the Turin side (Pillar B).

From the results of the simulation of solid transport, it emerges that the erosion and deposition phenomena affect all the sections of the section under examination, with the exception of the section characterized by the presence of outcropping rock, not subject to erosion and deposit in relation to the high slopes.

However, the simulations show that the extent of these phenomena is contained and there are no particular critical issues related to erosion at piles and abutments of Serra la Voute viaduct of the Rio Pontè.

From the surveys carried out during the inspections it was found the presence of blocks and plant material in correspondence with Pillar B, in all probability carried by the current on the occasion of past flood events; an analysis of the pillar, however, did not reveal any damage attributable to the possible impact of such materials on the pillar itself.

Due to the possibility of erosion phenomena that has been ascertained for the banks on the hydrographic right, where the viaduct abutments are located, it was provided the implementation of structures aimed at reducing hydrogeological risk and consolidation of slopes corresponding to critical areas, such as Geomat anti-erosion in Polyamide fiber Nylon type or Polypropylene (P.P), with overlapping metallic containment net with double twisted hexagonal mesh with strong galvanization.

BIBLIOGRAPHY

AHMAD B, HASSAN ZA (2011) Flood map of Tupai River using combined 1D and 2Dmodelling. In: *3rd international conference on managing rivers in the 21st century: sustainable solutions for global crisis of flooding, pollution and water scarcity*, Penang, Malaysia28. Vozinaki A-EK,

BIANCOTTI A., DESTEFANIS E., FRATIANNI S., & MASCIOCCO L. (2005). *OSSERVAZIONI SU PLUVIOETRIA E IDROLOGIA DELLA VALLE DI SUSA (Alpi Occidentali).* Retrieved from http://www.glaciologia.it/wp-content/uploads/Supplementi/FullText/SGFDQ_VII_FullText/08_SGFDQ_VII_Biancotti_51_58.pdf

CLEVELAND, T. G., THOMPSON, D. B. & FANG, X. 2011. Use of the Rational and Modified Rational Method
for Hydraulic Design. Lubbock, Texas: *Texas Tech University*

CLIMATE-DATA.ORG. (n.d.). Retrieved from OULX Clima (Italia): https://es.climate-data.org/europe/italia/piamonte/oulx-112690/

CUTILLAS, F. M. (2015). *Análisis y evaluación del transporte de sedimentos en la Rambla del Albujón.* Universidad Politécnica de Cartagena. Retrieved from https://docplayer.es/44437861-Analisis-y-evaluacion-del-transporte-de-sedimentos-en-la-rambla-del-albujon.html

GALLO E., GANORA D., LAIO F., MASOERO A., & CLAPS P. (2014, July 20). *ATLANTE DEI BACINI IMBRIFERI PIEMONTESI.* Retrieved from http://www.idrologia.polito.it/web2/open-data/Renerfor/atlante_bacini_piemontesi_LR.pdf

HADELY, R.F. & SCHUMM, S.A. (1961) Sediment sources and drainage basin characteristics in upper Cheyenne river basin. *United State Geological Survey water-supply paper.*

HARPO Seic. (2010). *Geostuoie tridimensionali antierosione Enkamat.* Tratto da https://www.termoplasticasas.com/sites/default/files/2018-06/ENKAMAT%20relazione%20tecnica.pdf

HORTON, R.E. (1945) Erosional development of streams and their drainage density: hydrophysical approach to quantitative geomorphology. *Geol. Soc. Amer. Bull., no.56*.

MAGISTRI A., LIPPOLIS G., & MINA N. (1983). *Relazione di Calcolo pile e spalle del viadotto Rio Pontè per il collegamento stradale tra il traforo del Frejus e Torino (Tangenziale Nord di Rivoli).* unpublished.

PERDIKARIS J., GHARABAGHI B., & RUDRA R. (2018). Reference Time of Concentration Estimation for Ungauged Catchments. *Canadian Center of Science and Education*.

PEROSINO G., & ZACCARA P. (2006). *ELEMENTI CLIMATICI DEL PIEMONTE.* Retrieved from http://www.crestsnc.it/divulgazione/media/clima-piemonte.pdf

REGIONE PIEMONTE. (n.d.). *Piano per l'assetto idrogeologico (PAI)*. Retrieved from https://www.regione.piemonte.it/web/temi/protezione-civile-difesa-suolo-opere-pubbliche/difesa-suolo/strumenti-per-difesa-suolo/piano-per-lassetto-idrogeologico-pai

REGIONE PIEMONTE, D. R. (1999). *Geologic map of Italy at a scale of 1:50.000, Sheet 132-152-153 BARDONECCHIA* .

SCHUMM, S.A. (1956) Evolution of drainage systems and slopes in Badlands at Perth Amboy, *New Jersey. Bull. Geol. Soc. Amer*., v.67, pp.597-646.

SMITH, K.G. (1950) Standards for grading texture of erosional topography. *American Jour. Science*, v.248, pp.655-668.

SREEDEVI P.D., OWAIS S., KHAN H.H., & AHMED S. (2009). Morphometric analysis of a watershed of South India using SRTM data and GIS. *Journal of the Geological Society of India*.

STRAHLER, A.N. (1964) Quantitative geomorphology of drainage basins and channel networks. *In:* V.T. Chow (Ed.), Handbook of Applied Hydrology. McGraw-Hill, New York.

UDFCD 2016. Chapter 6: Runoff Urban Storm Drainage Criteria Manual: Volume 1 Management, Hydrology, and Hydraulics. *Urban Drainage and Flood Control District*

WEATHER SPARK. (n.d.). *Average Weather in Sauze d'Oulx.* Retrieved from https://weatherspark.com/y/53220/Average-Weather-in-Sauze-d&%2339;Oulx-Italy-Year-Round

ANNEXES: HYDRAULIC MODEL RESULTS

In this section, the results of the Hydraulic Model are presented in detail. X-Y-Z perspective plot in Figure 57 allows getting a quick view of the entire reach.

The following figures show the cross-section water surface profile data of the river stations going from Upstream with station 471 to Downstream with station 24. The following variables are displayed in the figures:

- EG (Energy grade)
- Crit (Critical depth)
- WS (Water surface)
- Ground (Ground Level)
- Leeve
- Bank Station
- Manning n values

The Profile Table (Table 21) is used to display the data for all the river stations simultaneously. This table displays the water surface elevation and energy grade line elevation (among other values) for all the cross-sections. The following variables are contained in the table:

- Q Total (m3/s): Total flow in cross-section
- W.S. Elev (m): Calculated water surface from energy equation.
- Min Ch El (m): Minimum main channel elevation.
- Crit W.S. (m): Critical water surface elevation.
- E.G. Elev (m): Energy grade line for calculated WS Elev.
- E.G. Slope (m/m): Slope of the energy grade line.
- Vel Chnl (m/s): Average velocity of the flow in the main channel.
- Flow Area (m2): Total area of cross-section active flow.
- Top Width (m): Top width of the wetted cross-section.
- Froude # Chl: Froude number of the main channel.

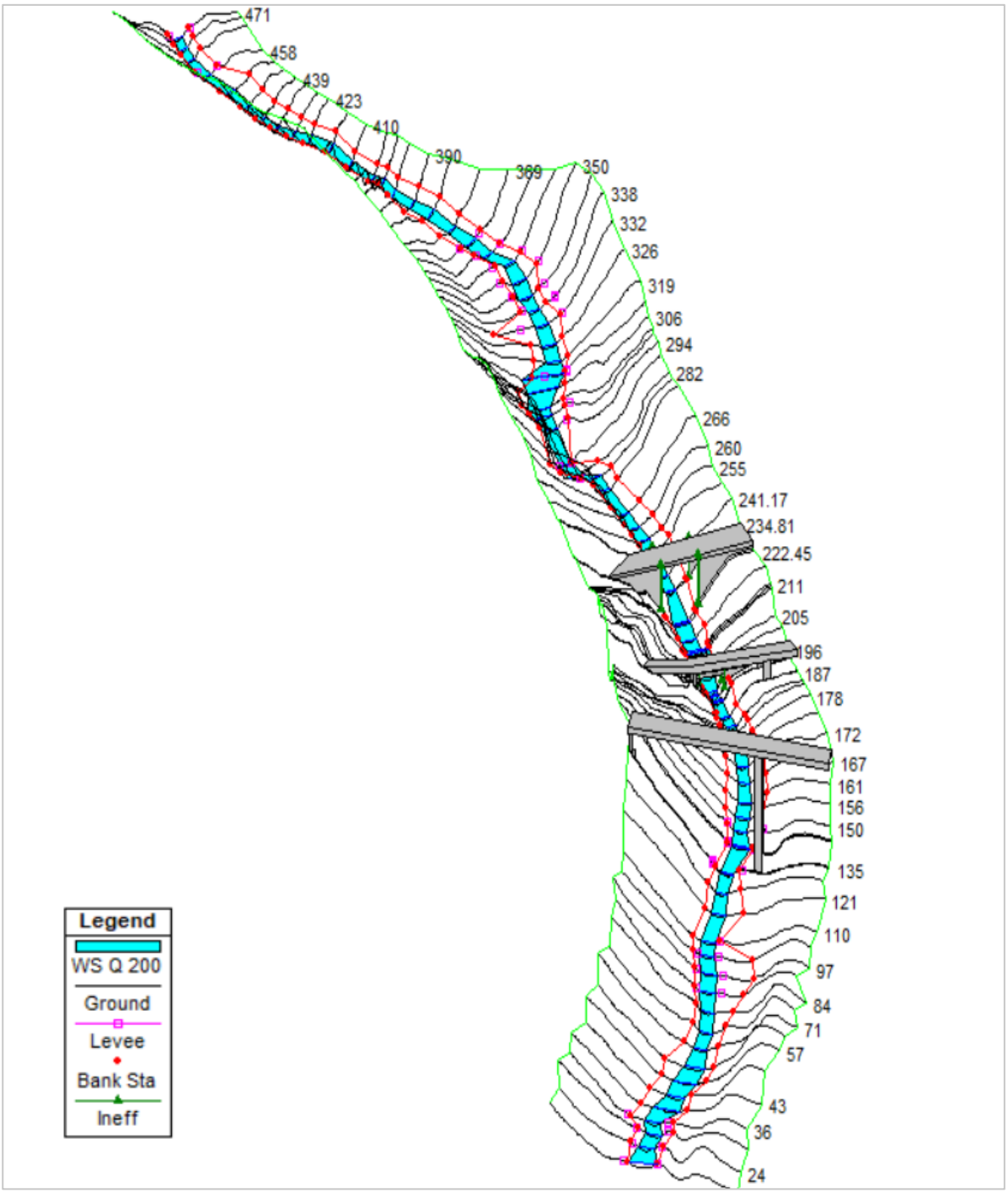

Figure 57. X-Y-Z Perspective plot of the model results

CROSS-SECTIONS WATER SURFACE PROFILE

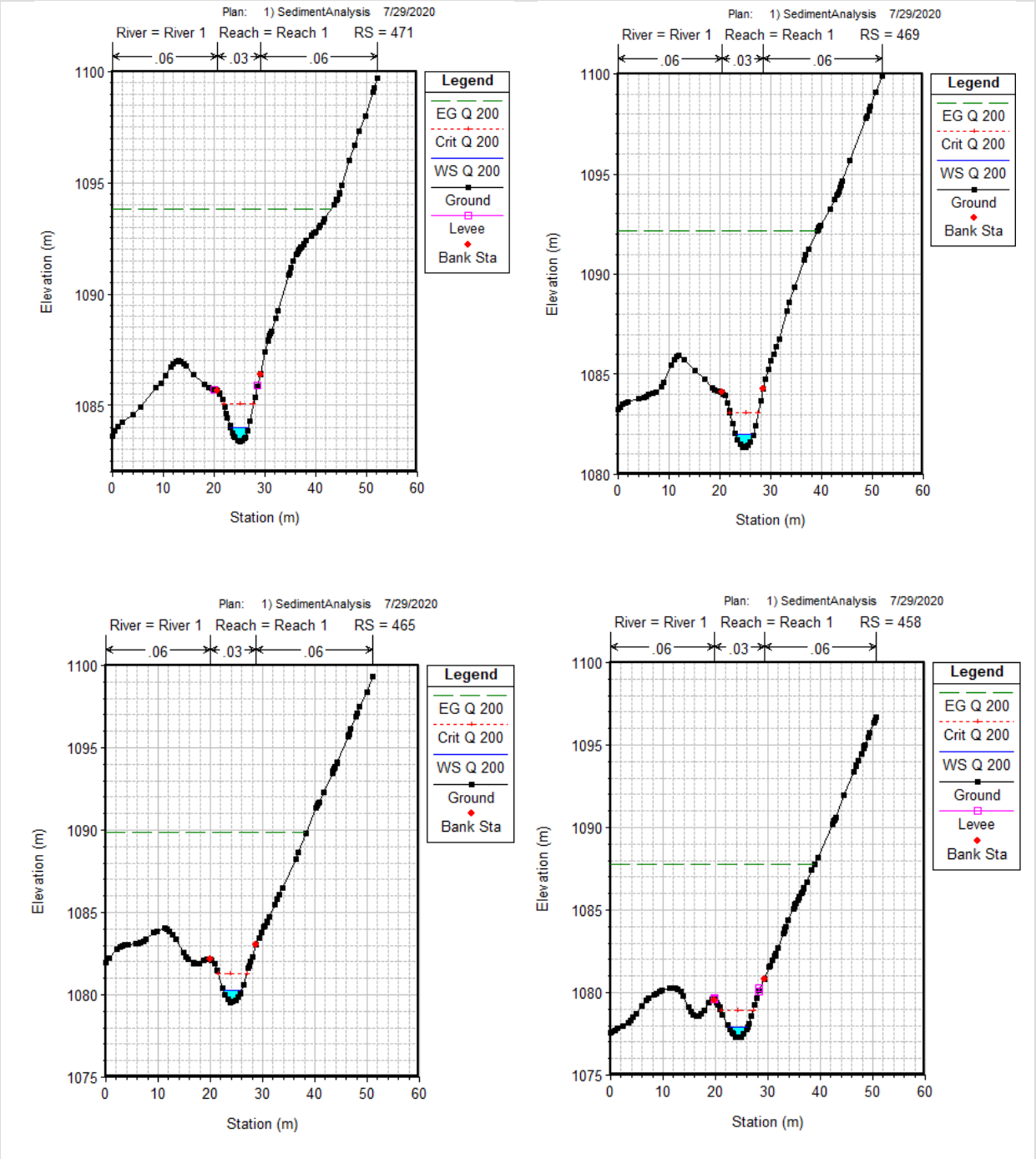

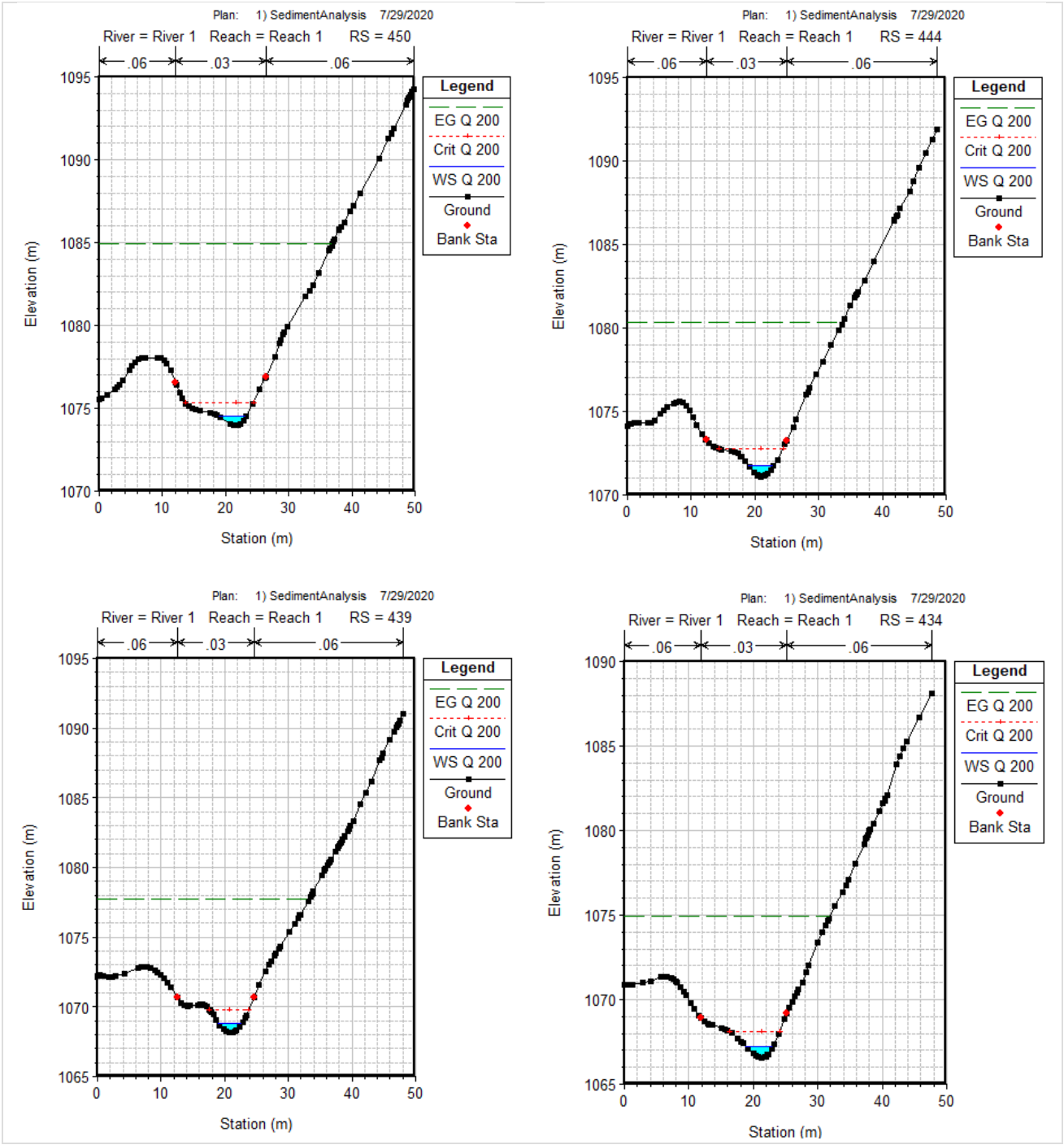
Plan: 1) SedimentAnalysis 7/29/2020
River = River 1 Reach = Reach 1 RS = 450
.06
.03
.06
Legend
EG Q 200
Crit Q 200
WS Q 200
Ground
Bank Sta
Elevation (m)
Station (m)
Plan: 1) SedimentAnalysis 7/29/2020
River = River 1 Reach = Reach 1 RS = 444
.06
.03
.06
Legend
EG Q 200
Crit Q 200
WS Q 200
Ground
Bank Sta
Elevation (m)
Station (m)
Plan: 1) SedimentAnalysis 7/29/2020
River = River 1 Reach = Reach 1 RS = 439
.06
.03
.06
Legend
EG Q 200
Crit Q 200
WS Q 200
Ground
Bank Sta
Elevation (m)
Station (m)
Plan: 1) SedimentAnalysis 7/29/2020
River = River 1 Reach = Reach 1 RS = 434
.06
.03
.06
Legend
EG Q 200
Crit Q 200
WS Q 200
Ground
Bank Sta
Elevation (m)
Station (m)

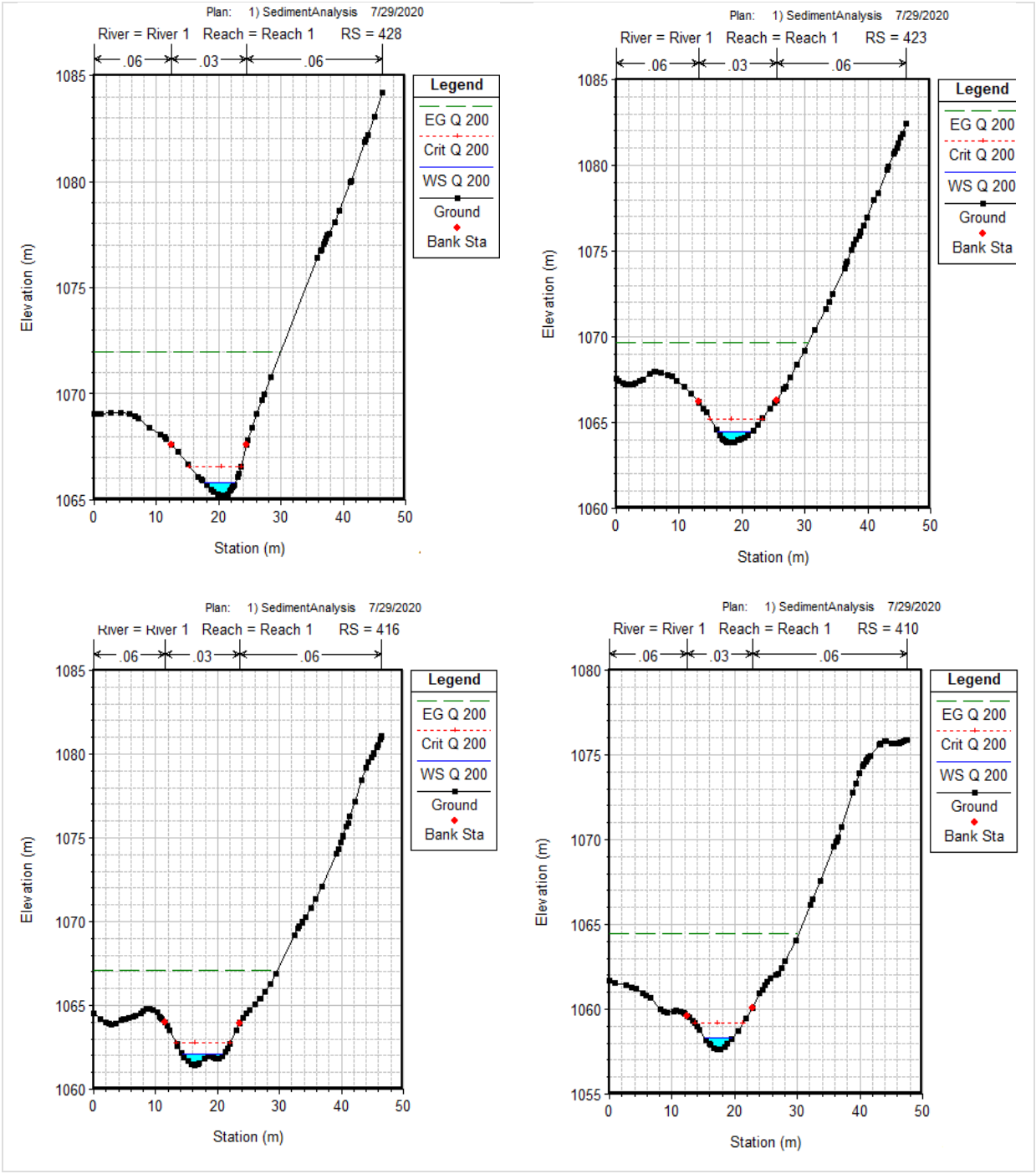
Plan: 1) SedimentAnalysis 7/29/2020
River = River 1 Reach = Reach 1 RS = 428
.06 .03 .06
Legend
EG Q 200
Crit Q 200
WS Q 200
Ground
Bank Sta
Elevation (m)
Station (m)
Plan: 1) SedimentAnalysis 7/29/2020
River = River 1 Reach = Reach 1 RS = 423
.06 .03 .06
Legend
EG Q 200
Crit Q 200
WS Q 200
Ground
Bank Sta
Elevation (m)
Station (m)
Plan: 1) SedimentAnalysis 7/29/2020
River = River 1 Reach = Reach 1 RS = 416
.06 .03 .06
Legend
EG Q 200
Crit Q 200
WS Q 200
Ground
Bank Sta
Elevation (m)
Station (m)
Plan: 1) SedimentAnalysis 7/29/2020
River = River 1 Reach = Reach 1 RS = 410
.06 .03 .06
Legend
EG Q 200
Crit Q 200
WS Q 200
Ground
Bank Sta
Elevation (m)
Station (m)

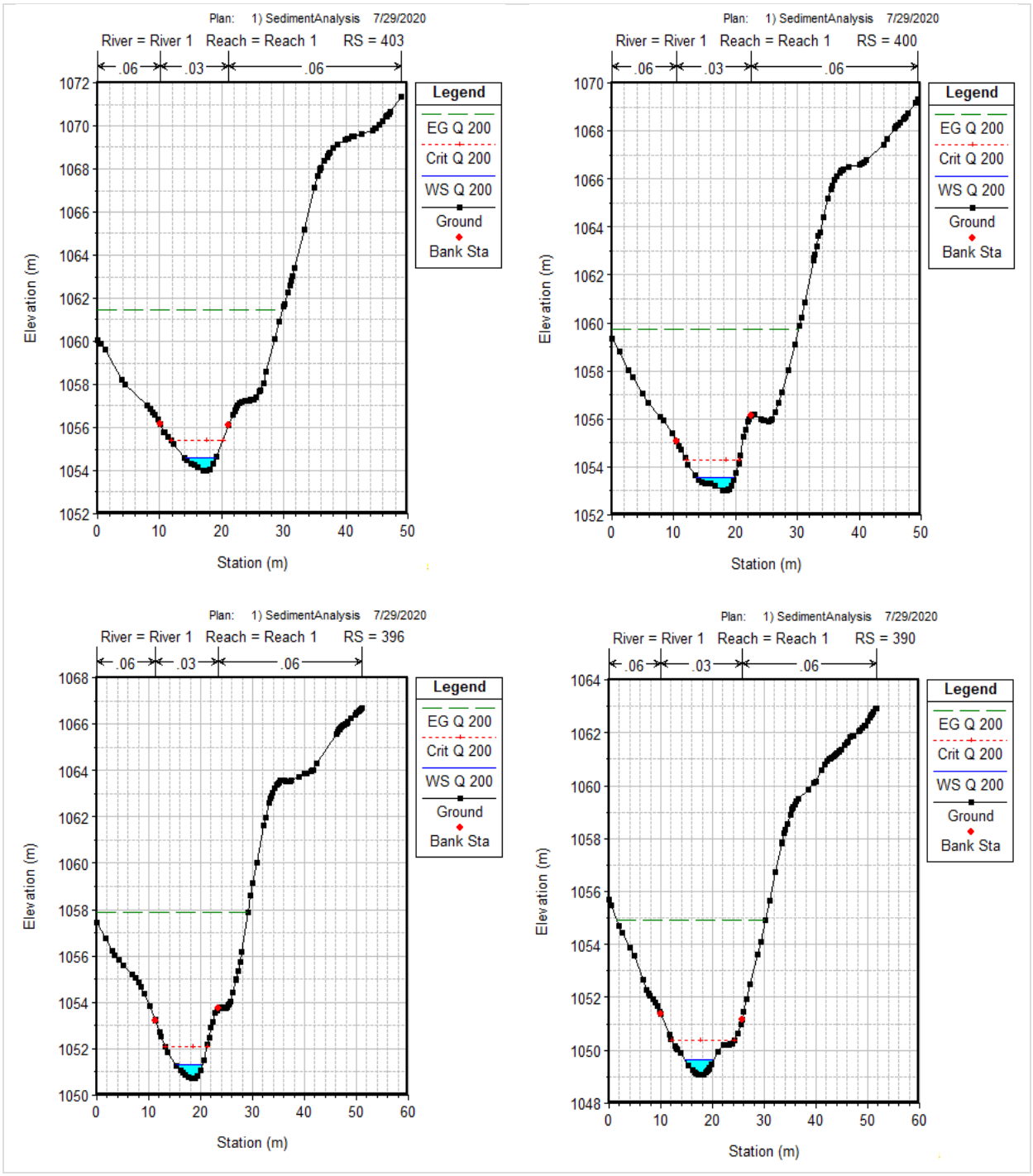
Plan: 1) SedimentAnalysis 7/29/2020
River = River 1 Reach = Reach 1 RS = 403
.06 .03 .06
Legend
EG Q 200
Crit Q 200
WS Q 200
Ground
Bank Sta
Elevation (m)
Station (m)
Plan: 1) SedimentAnalysis 7/29/2020
River = River 1 Reach = Reach 1 RS = 400
.06 .03 .06
Legend
EG Q 200
Crit Q 200
WS Q 200
Ground
Bank Sta
Elevation (m)
Station (m)
Plan: 1) SedimentAnalysis 7/29/2020
River = River 1 Reach = Reach 1 RS = 396
.06 .03 .06
Legend
EG Q 200
Crit Q 200
WS Q 200
Ground
Bank Sta
Elevation (m)
Station (m)
Plan: 1) SedimentAnalysis 7/29/2020
River = River 1 Reach = Reach 1 RS = 390
.06 .03 .06
Legend
EG Q 200
Crit Q 200
WS Q 200
Ground
Bank Sta
Elevation (m)
Station (m)

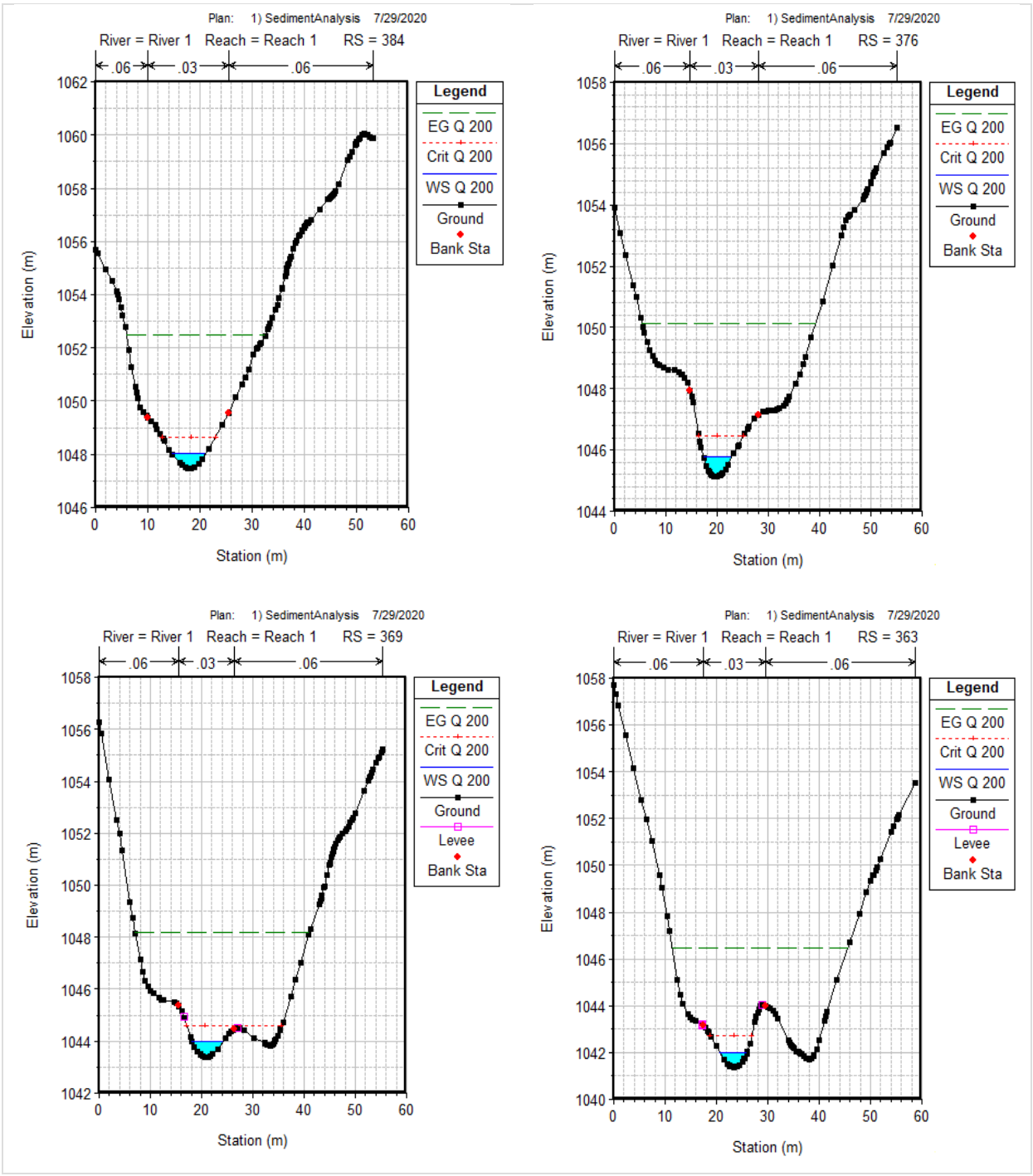
Plan: 1) SedimentAnalysis 7/29/2020
River = River 1 Reach = Reach 1 RS = 384
.06 .03 .06
Legend
EG Q 200
Crit Q 200
WS Q 200
Ground
Bank Sta
Elevation (m)
Station (m)
Plan: 1) SedimentAnalysis 7/29/2020
River = River 1 Reach = Reach 1 RS = 376
.06 .03 .06
Legend
EG Q 200
Crit Q 200
WS Q 200
Ground
Bank Sta
Elevation (m)
Station (m)
Plan: 1) SedimentAnalysis 7/29/2020
River = River 1 Reach = Reach 1 RS = 369
.06 .03 .06
Legend
EG Q 200
Crit Q 200
WS Q 200
Ground
Levee
Bank Sta
Elevation (m)
Station (m)
Plan: 1) SedimentAnalysis 7/29/2020
River = River 1 Reach = Reach 1 RS = 363
.06 .03 .06
Legend
EG Q 200
Crit Q 200
WS Q 200
Ground
Levee
Bank Sta
Elevation (m)
Station (m)

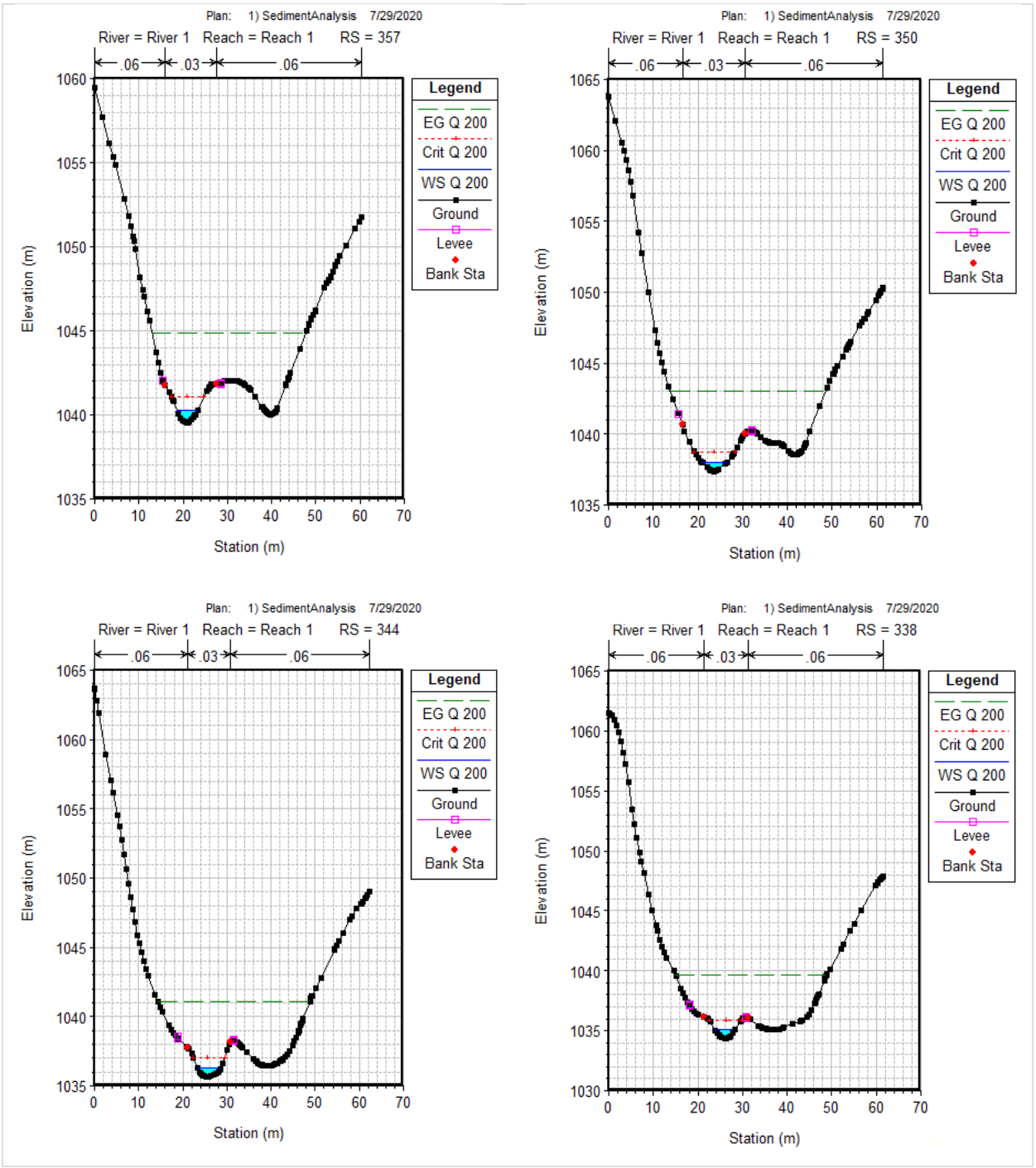
Plan: 1) SedimentAnalysis 7/29/2020
River = River 1 Reach = Reach 1 RS = 357
.06 .03 .06
Legend
EG Q 200
Crit Q 200
WS Q 200
Ground
Levee
Bank Sta
Elevation (m)
Station (m)
Plan: 1) SedimentAnalysis 7/29/2020
River = River 1 Reach = Reach 1 RS = 350
.06 .03 .06
Legend
EG Q 200
Crit Q 200
WS Q 200
Ground
Levee
Bank Sta
Elevation (m)
Station (m)
Plan: 1) SedimentAnalysis 7/29/2020
River = River 1 Reach = Reach 1 RS = 344
.06 .03 .06
Legend
EG Q 200
Crit Q 200
WS Q 200
Ground
Levee
Bank Sta
Elevation (m)
Station (m)
Plan: 1) SedimentAnalysis 7/29/2020
River = River 1 Reach = Reach 1 RS = 338
.06 .03 .06
Legend
EG Q 200
Crit Q 200
WS Q 200
Ground
Levee
Bank Sta
Elevation (m)
Station (m)

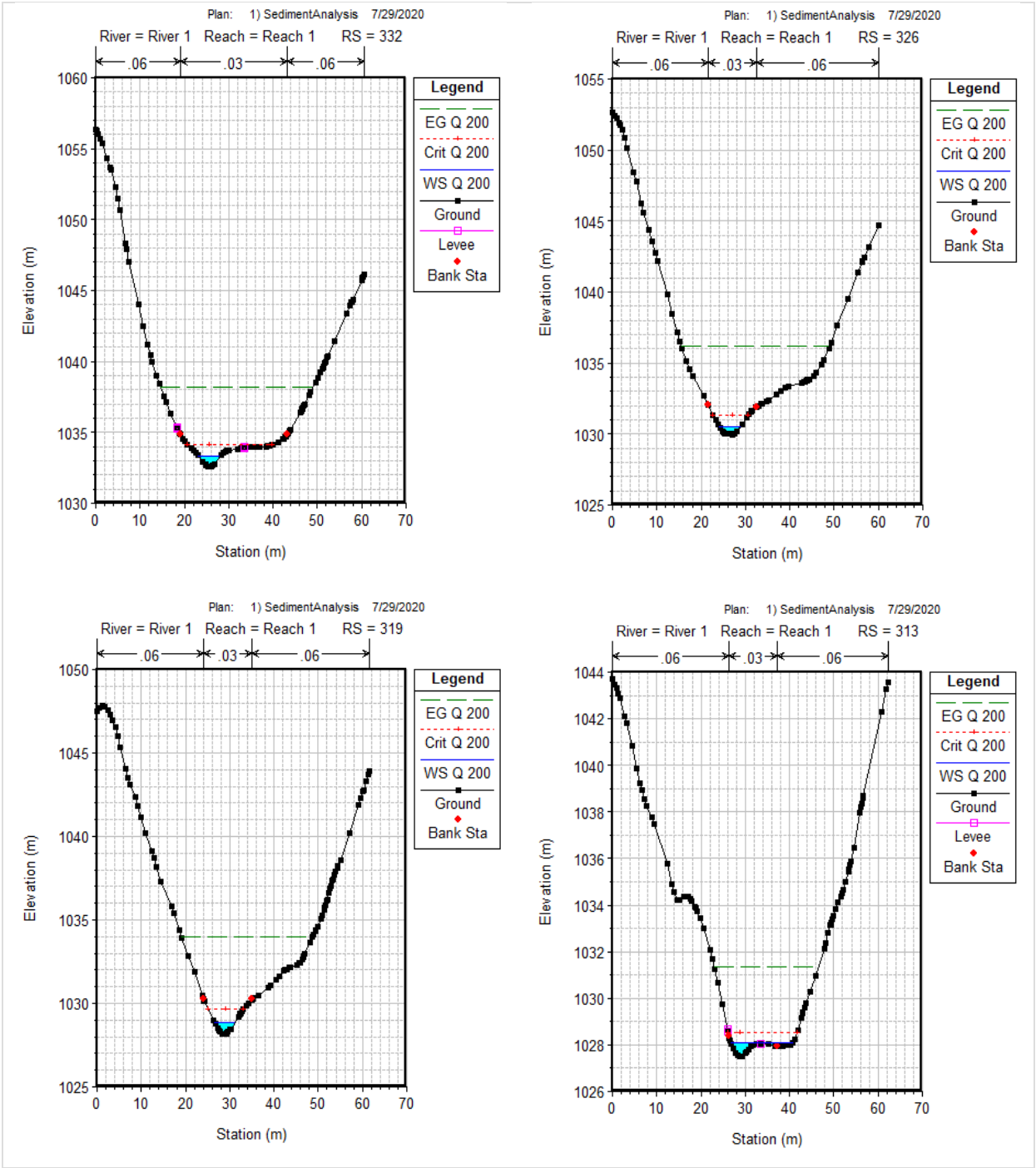
Plan: 1) SedimentAnalysis 7/29/2020
River = River 1 Reach = Reach 1 RS = 332
.06 .03 .06
Legend
EG Q 200
Crit Q 200
WS Q 200
Ground
Levee
Bank Sta
Elevation (m)
Station (m)
Plan: 1) SedimentAnalysis 7/29/2020
River = River 1 Reach = Reach 1 RS = 326
.06 .03 .06
Legend
EG Q 200
Crit Q 200
WS Q 200
Ground
Bank Sta
Elevation (m)
Station (m)
Plan: 1) SedimentAnalysis 7/29/2020
River = River 1 Reach = Reach 1 RS = 319
.06 .03 .06
Legend
EG Q 200
Crit Q 200
WS Q 200
Ground
Bank Sta
Elevation (m)
Station (m)
Plan: 1) SedimentAnalysis 7/29/2020
River = River 1 Reach = Reach 1 RS = 313
.06 .03 .06
Legend
EG Q 200
Crit Q 200
WS Q 200
Ground
Levee
Bank Sta
Elevation (m)
Station (m)

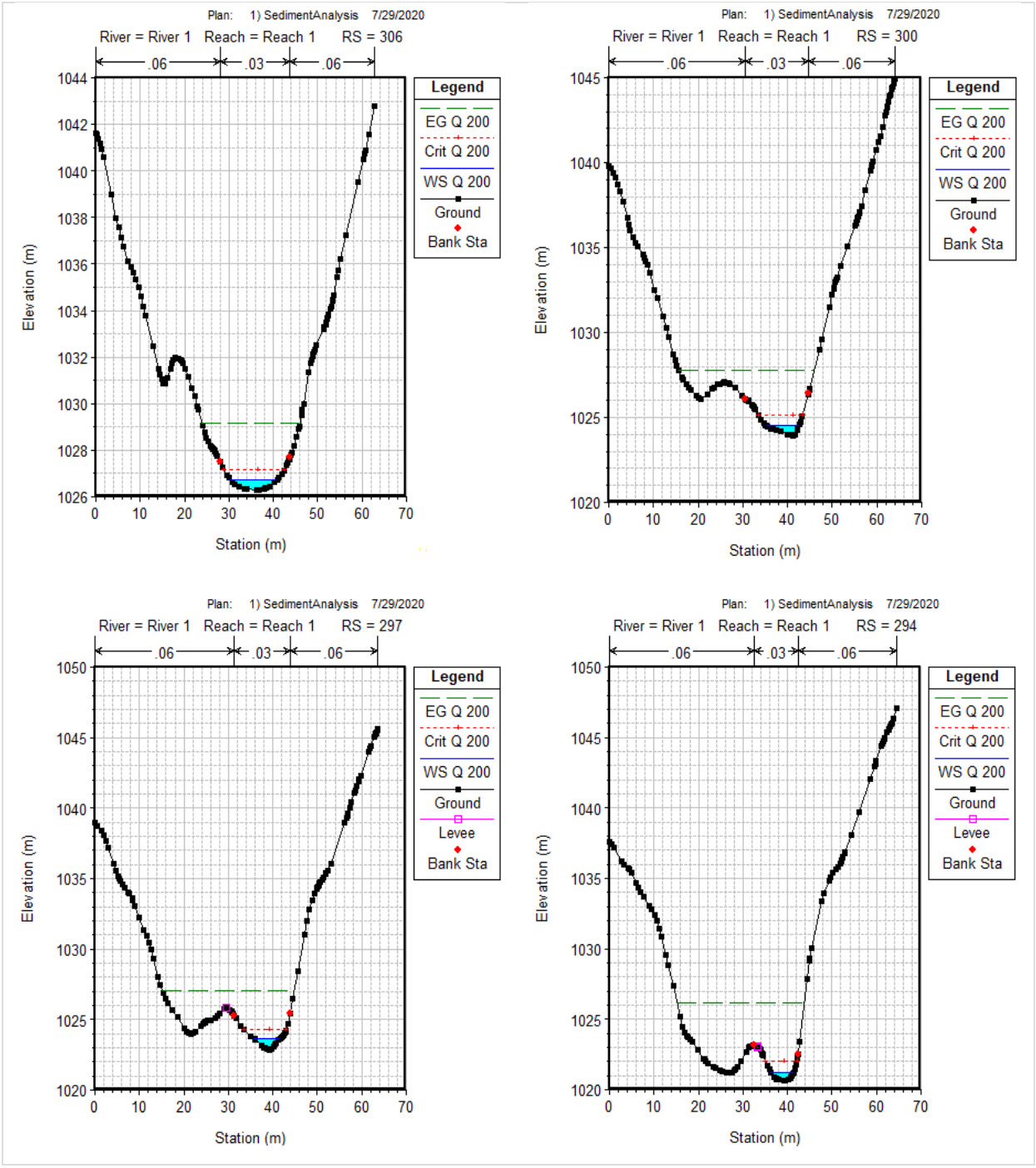
Plan: 1) SedimentAnalysis 7/29/2020
River = River 1 Reach = Reach 1 RS = 306
.06 .03 .06
Legend
EG Q 200
Crit Q 200
WS Q 200
Ground
Bank Sta
Elevation (m)
Station (m)
Plan: 1) SedimentAnalysis 7/29/2020
River = River 1 Reach = Reach 1 RS = 300
.06 .03 .06
Legend
EG Q 200
Crit Q 200
WS Q 200
Ground
Bank Sta
Elevation (m)
Station (m)
Plan: 1) SedimentAnalysis 7/29/2020
River = River 1 Reach = Reach 1 RS = 297
.06 .03 .06
Legend
EG Q 200
Crit Q 200
WS Q 200
Ground
Levee
Bank Sta
Elevation (m)
Station (m)
Plan: 1) SedimentAnalysis 7/29/2020
River = River 1 Reach = Reach 1 RS = 294
.06 .03 .06
Legend
EG Q 200
Crit Q 200
WS Q 200
Ground
Levee
Bank Sta
Elevation (m)
Station (m)

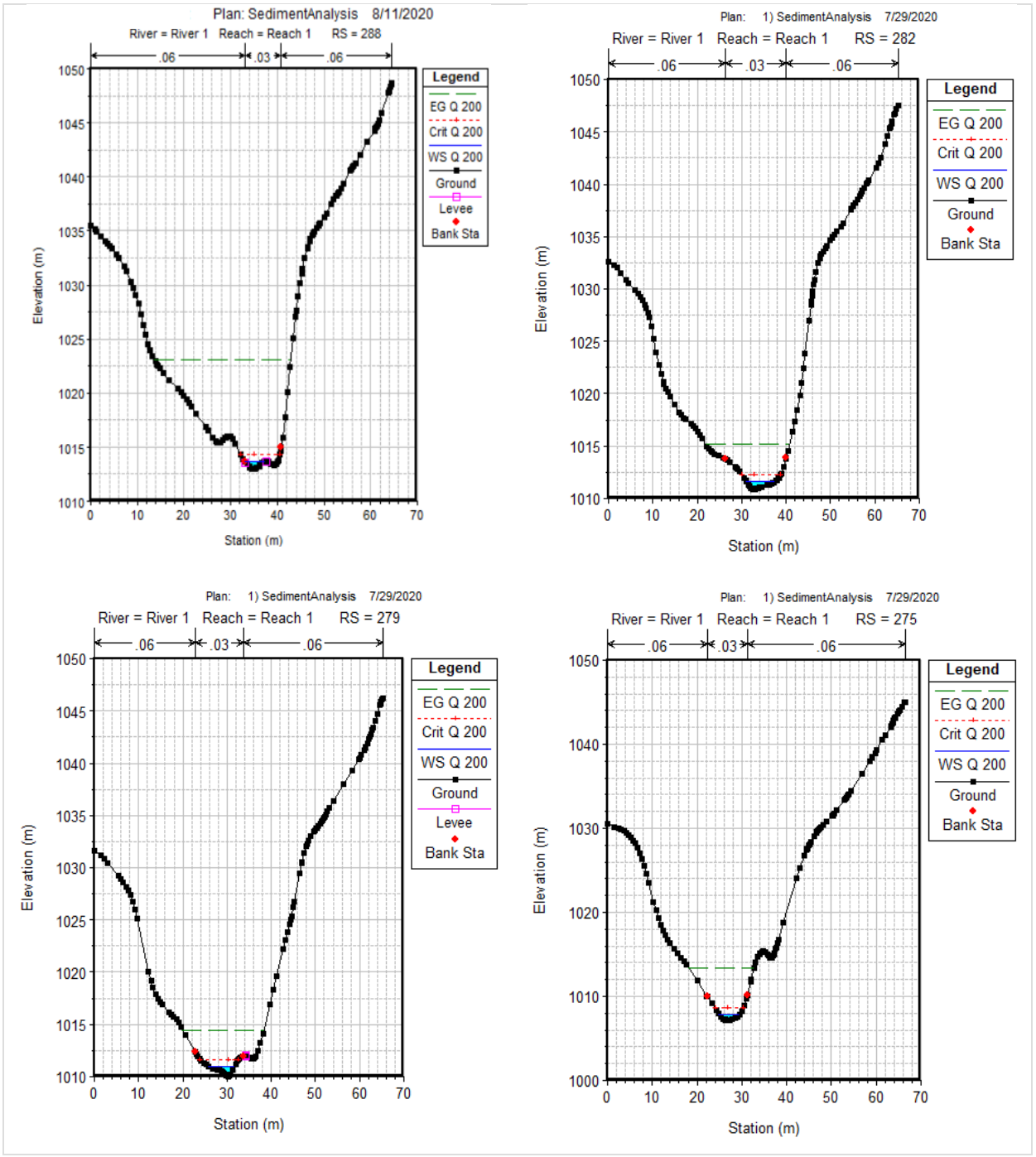
Plan: SedimentAnalysis 8/11/2020
River = River 1 Reach = Reach 1 RS = 288
.06
.03
.06
Legend
EG Q 200
Crit Q 200
WS Q 200
Ground
Levee
Bank Sta
Elevation (m)
Station (m)
Plan: 1) SedimentAnalysis 7/29/2020
River = River 1 Reach = Reach 1 RS = 282
Plan: 1) SedimentAnalysis 7/29/2020
River = River 1 Reach = Reach 1 RS = 279
Plan: 1) SedimentAnalysis 7/29/2020
River = River 1 Reach = Reach 1 RS = 275

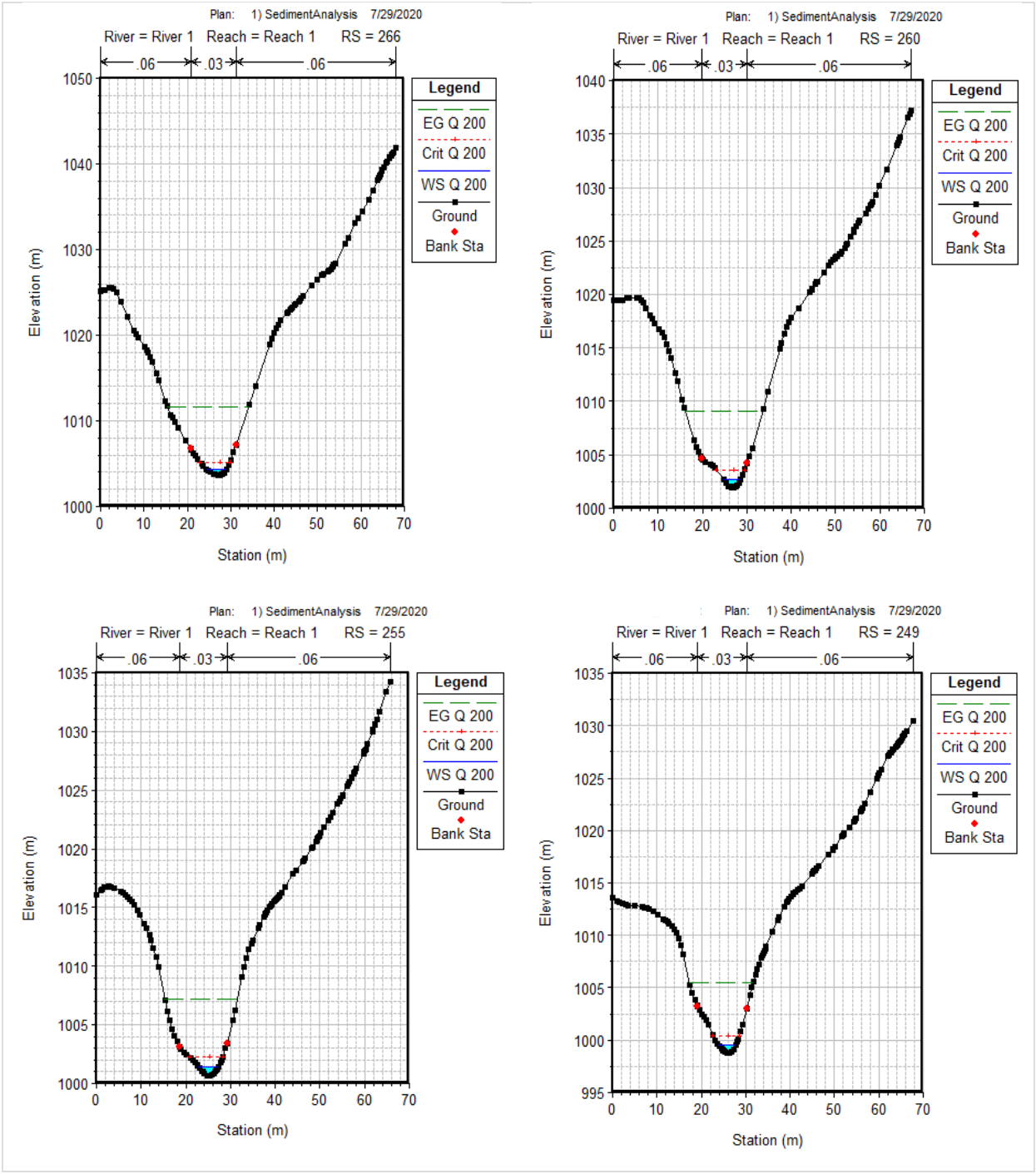
Plan: 1) SedimentAnalysis 7/29/2020
River = River 1 Reach = Reach 1 RS = 266
.06 .03 .06
Legend
EG Q 200
Crit Q 200
WS Q 200
Ground
Bank Sta
Elevation (m)
Station (m)
Plan: 1) SedimentAnalysis 7/29/2020
River = River 1 Reach = Reach 1 RS = 260
.06 .03 .06
Legend
EG Q 200
Crit Q 200
WS Q 200
Ground
Bank Sta
Elevation (m)
Station (m)
Plan: 1) SedimentAnalysis 7/29/2020
River = River 1 Reach = Reach 1 RS = 255
.06 .03 .06
Legend
EG Q 200
Crit Q 200
WS Q 200
Ground
Bank Sta
Elevation (m)
Station (m)
Plan: 1) SedimentAnalysis 7/29/2020
River = River 1 Reach = Reach 1 RS = 249
.06 .03 .06
Legend
EG Q 200
Crit Q 200
WS Q 200
Ground
Bank Sta
Elevation (m)
Station (m)

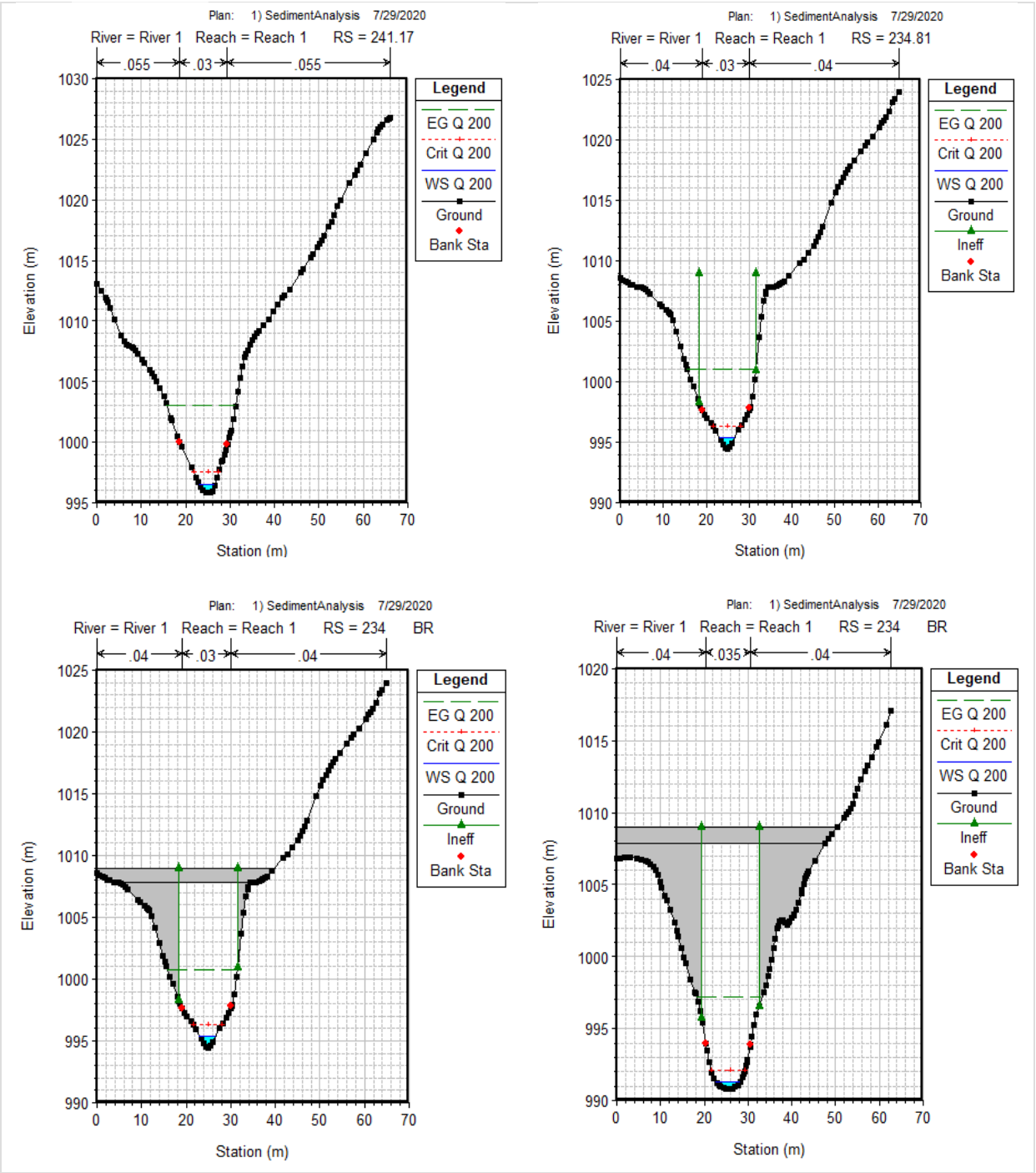
Plan: 1) SedimentAnalysis 7/29/2020
River = River 1 Reach = Reach 1 RS = 241.17
.055 .03 .055
Legend
EG Q 200
Crit Q 200
WS Q 200
Ground
Bank Sta
Elevation (m)
Station (m)
Plan: 1) SedimentAnalysis 7/29/2020
River = River 1 Reach = Reach 1 RS = 234.81
.04 .03 .04
Legend
EG Q 200
Crit Q 200
WS Q 200
Ground
Ineff
Bank Sta
Elevation (m)
Station (m)
Plan: 1) SedimentAnalysis 7/29/2020
River = River 1 Reach = Reach 1 RS = 234 BR
.04 .03 .04
Legend
EG Q 200
Crit Q 200
WS Q 200
Ground
Ineff
Bank Sta
Elevation (m)
Station (m)
Plan: 1) SedimentAnalysis 7/29/2020
River = River 1 Reach = Reach 1 RS = 234 BR
.04 .035 .04
Legend
EG Q 200
Crit Q 200
WS Q 200
Ground
Ineff
Bank Sta
Elevation (m)
Station (m)

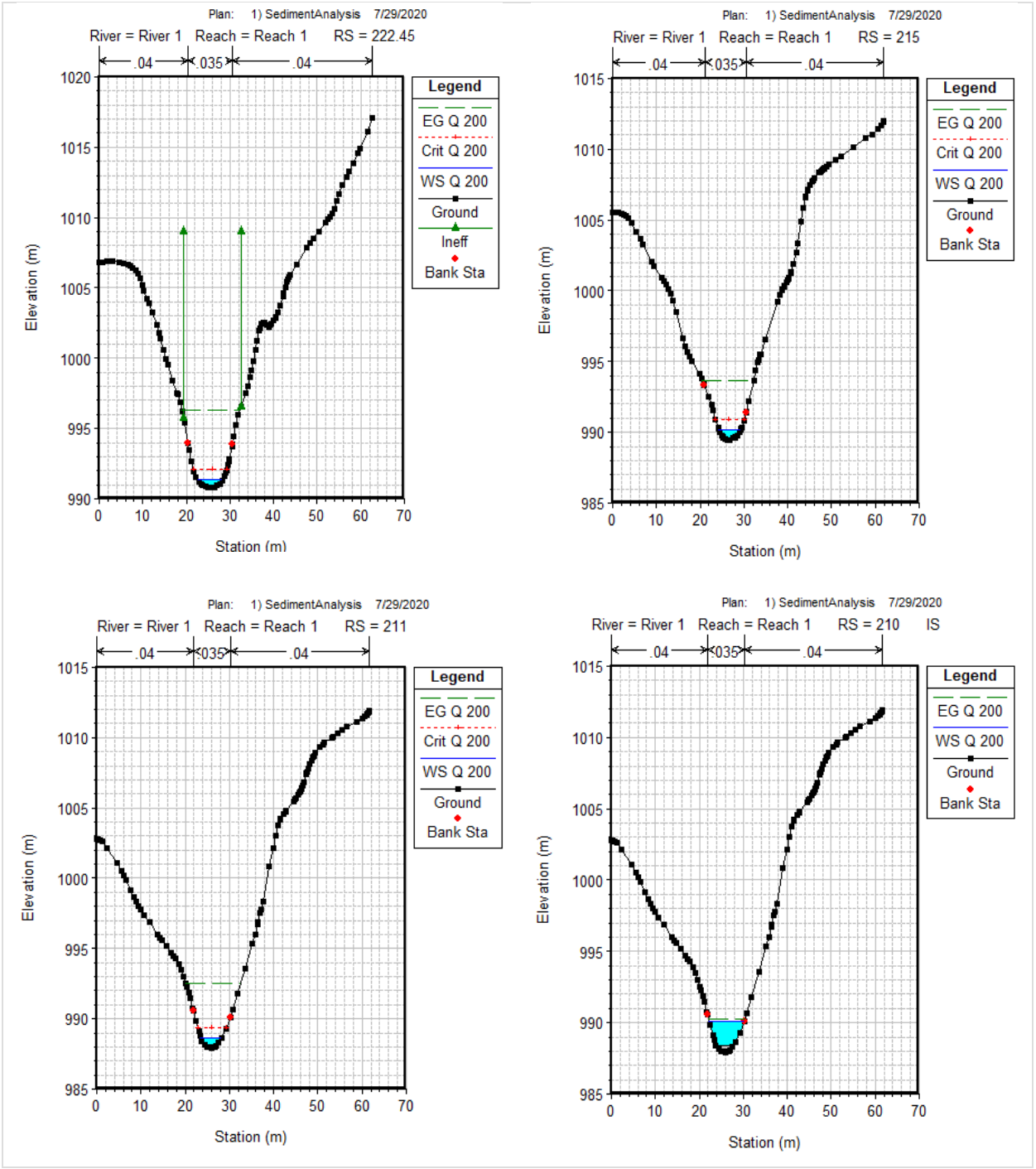
Plan: 1) SedimentAnalysis 7/29/2020
River = River 1 Reach = Reach 1 RS = 222.45
.04 .035 .04
Legend
EG Q 200
Crit Q 200
WS Q 200
Ground
Ineff
Bank Sta
Elevation (m)
Station (m)
Plan: 1) SedimentAnalysis 7/29/2020
River = River 1 Reach = Reach 1 RS = 215
.04 .035 .04
Legend
EG Q 200
Crit Q 200
WS Q 200
Ground
Bank Sta
Elevation (m)
Station (m)
Plan: 1) SedimentAnalysis 7/29/2020
River = River 1 Reach = Reach 1 RS = 211
.04 .035 .04
Legend
EG Q 200
Crit Q 200
WS Q 200
Ground
Bank Sta
Elevation (m)
Station (m)
Plan: 1) SedimentAnalysis 7/29/2020
River = River 1 Reach = Reach 1 RS = 210 IS
.04 .035 .04
Legend
EG Q 200
WS Q 200
Ground
Bank Sta
Elevation (m)
Station (m)

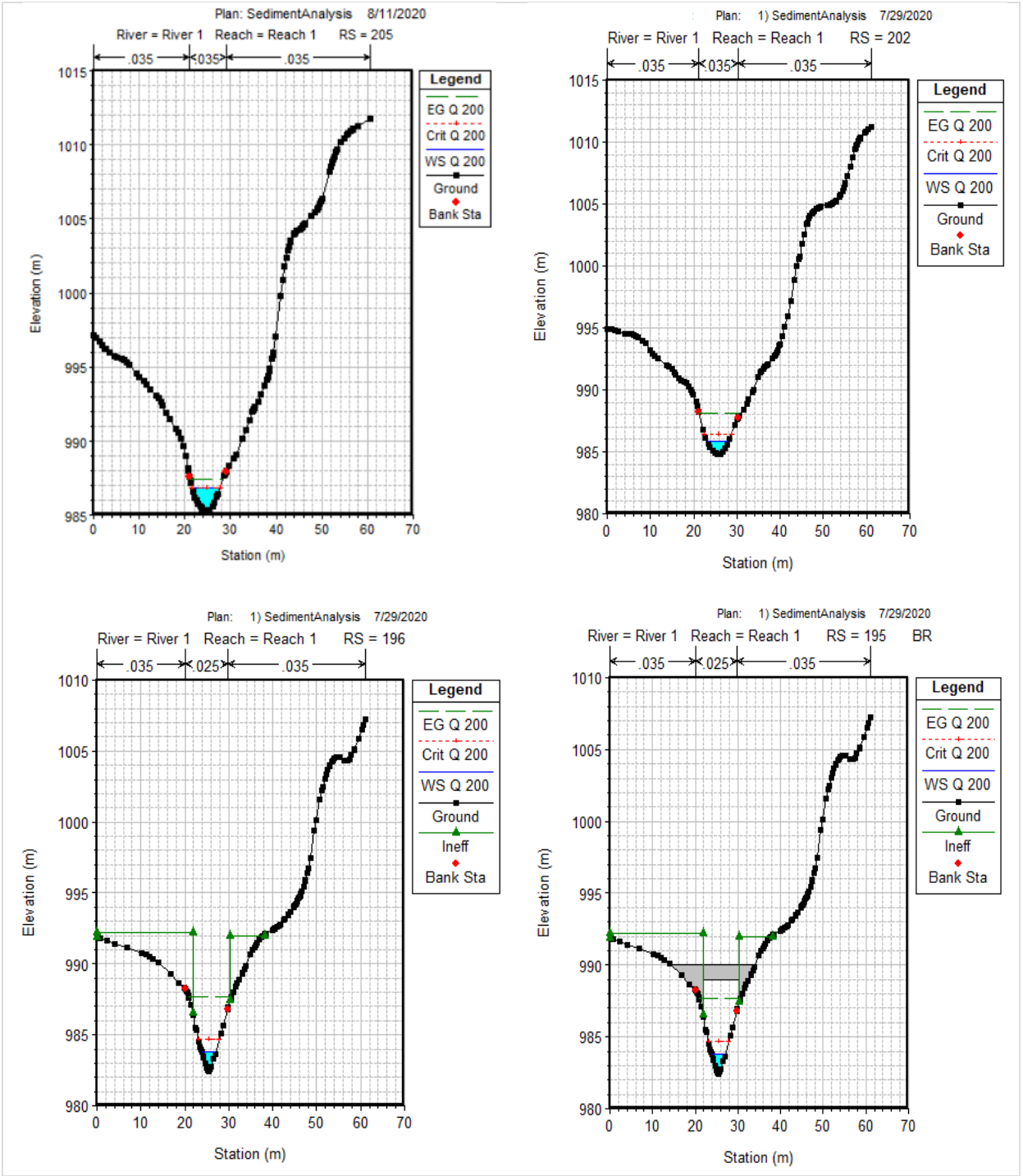
Plan: SedimentAnalysis 8/11/2020
River = River 1 Reach = Reach 1 RS = 205
.035 .035 .035
Legend
EG Q 200
Crit Q 200
WS Q 200
Ground
Bank Sta
Elevation (m)
Station (m)
Plan: 1) SedimentAnalysis 7/29/2020
River = River 1 Reach = Reach 1 RS = 202
.035 .035 .035
Legend
EG Q 200
Crit Q 200
WS Q 200
Ground
Bank Sta
Elevation (m)
Station (m)
Plan: 1) SedimentAnalysis 7/29/2020
River = River 1 Reach = Reach 1 RS = 196
.035 .025 .035
Legend
EG Q 200
Crit Q 200
WS Q 200
Ground
Ineff
Bank Sta
Elevation (m)
Station (m)
Plan: 1) SedimentAnalysis 7/29/2020
River = River 1 Reach = Reach 1 RS = 195 BR
.035 .025 .035
Legend
EG Q 200
Crit Q 200
WS Q 200
Ground
Ineff
Bank Sta
Elevation (m)
Station (m)

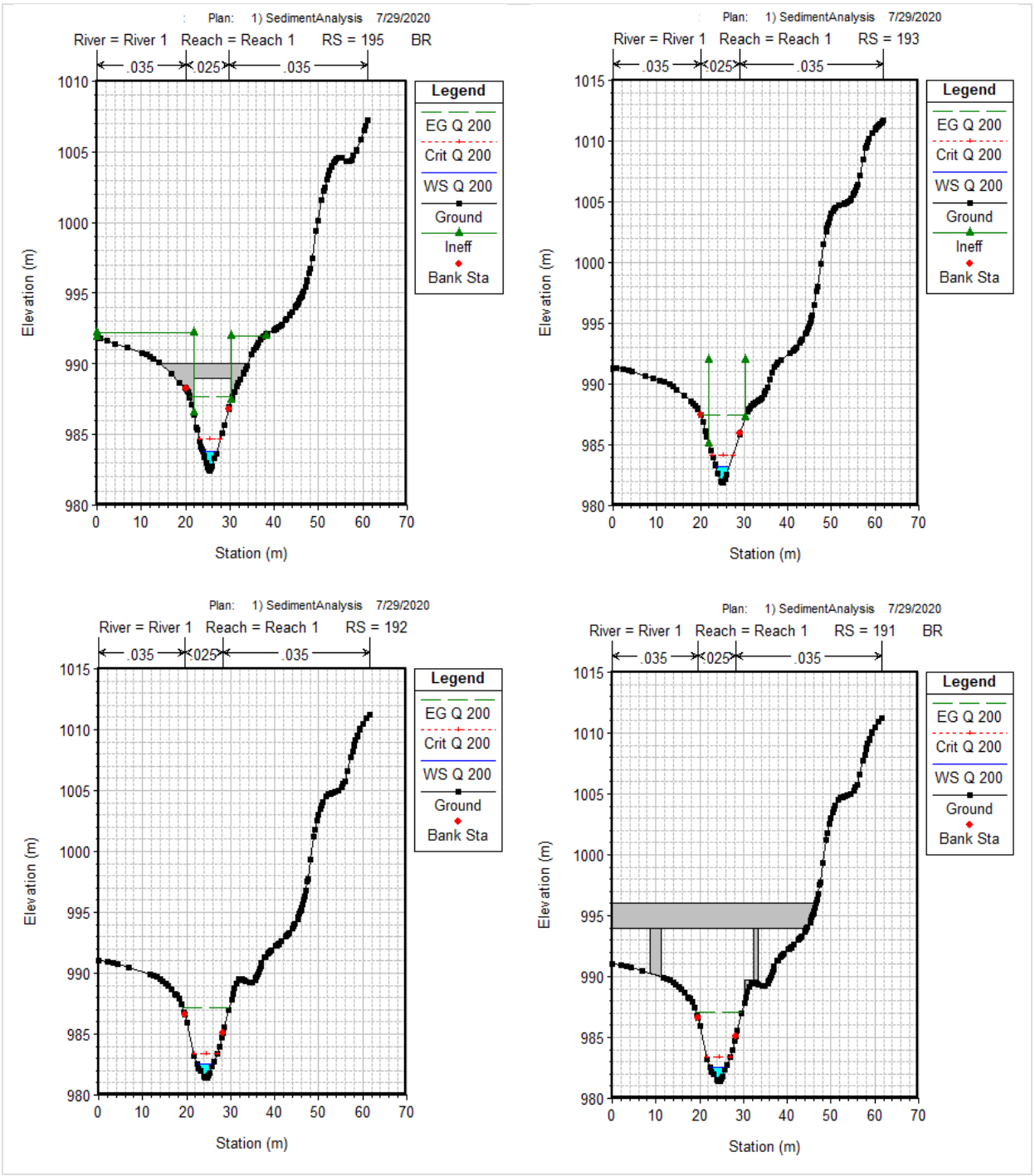
Plan: 1) SedimentAnalysis 7/29/2020
River = River 1 Reach = Reach 1 RS = 195 BR
.035 .025 .035
Legend
EG Q 200
Crit Q 200
WS Q 200
Ground
Ineff
Bank Sta
Elevation (m)
Station (m)
Plan: 1) SedimentAnalysis 7/29/2020
River = River 1 Reach = Reach 1 RS = 193
.035 .025 .035
Legend
EG Q 200
Crit Q 200
WS Q 200
Ground
Ineff
Bank Sta
Elevation (m)
Station (m)
Plan: 1) SedimentAnalysis 7/29/2020
River = River 1 Reach = Reach 1 RS = 192
.035 .025 .035
Legend
EG Q 200
Crit Q 200
WS Q 200
Ground
Bank Sta
Elevation (m)
Station (m)
Plan: 1) SedimentAnalysis 7/29/2020
River = River 1 Reach = Reach 1 RS = 191 BR
.035 .025 .035
Legend
EG Q 200
Crit Q 200
WS Q 200
Ground
Bank Sta
Elevation (m)
Station (m)

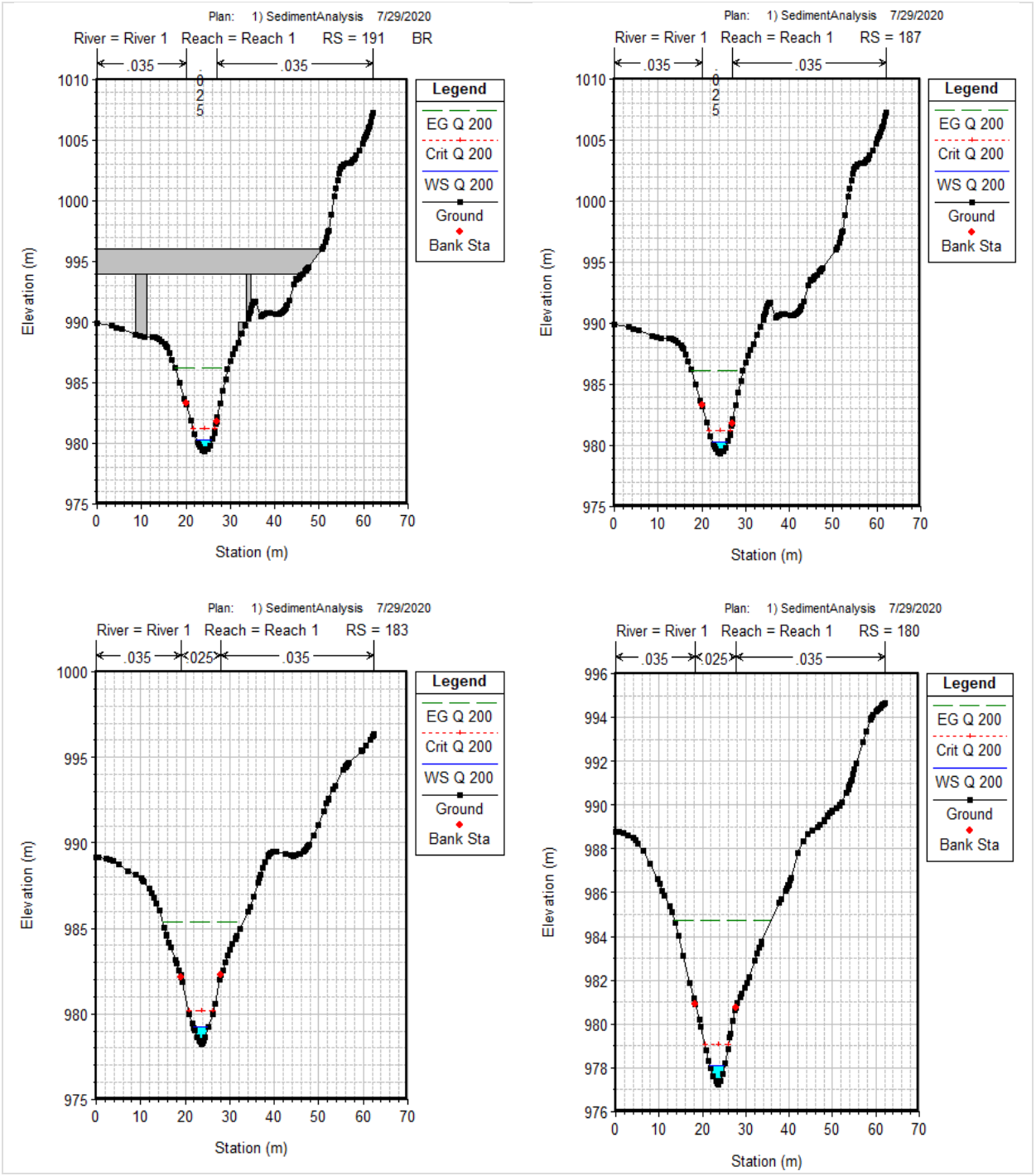
Plan: 1) SedimentAnalysis 7/29/2020
River = River 1 Reach = Reach 1 RS = 191 BR
.035
.025
.035
Legend
EG Q 200
Crit Q 200
WS Q 200
Ground
Bank Sta
Elevation (m)
Station (m)
Plan: 1) SedimentAnalysis 7/29/2020
River = River 1 Reach = Reach 1 RS = 187
.035
.025
.035
Legend
EG Q 200
Crit Q 200
WS Q 200
Ground
Bank Sta
Elevation (m)
Station (m)
Plan: 1) SedimentAnalysis 7/29/2020
River = River 1 Reach = Reach 1 RS = 183
.035
.025
.035
Legend
EG Q 200
Crit Q 200
WS Q 200
Ground
Bank Sta
Elevation (m)
Station (m)
Plan: 1) SedimentAnalysis 7/29/2020
River = River 1 Reach = Reach 1 RS = 180
.035
.025
.035
Legend
EG Q 200
Crit Q 200
WS Q 200
Ground
Bank Sta
Elevation (m)
Station (m)

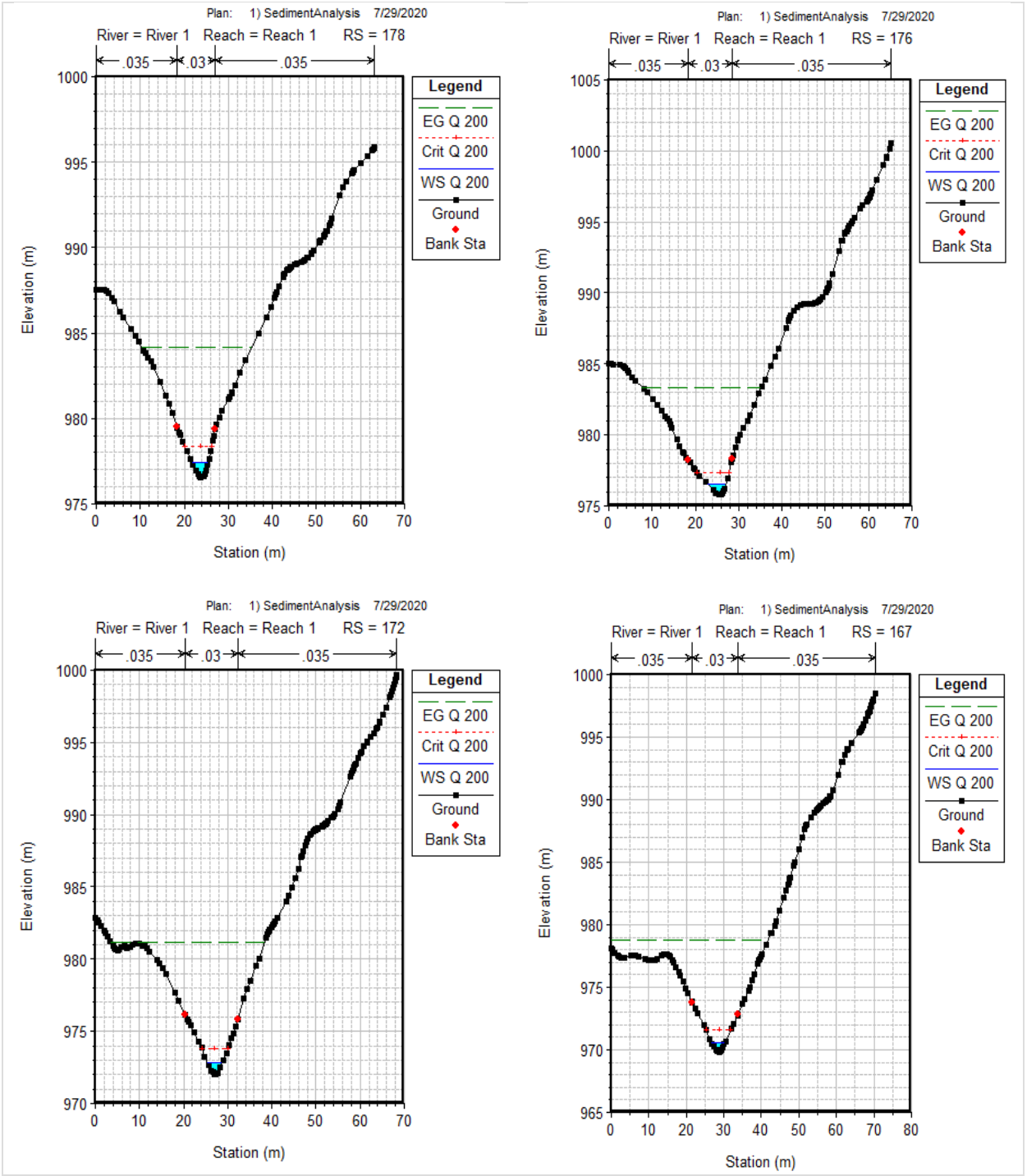
Plan: 1) SedimentAnalysis 7/29/2020
River = River 1 Reach = Reach 1 RS = 178
.035 .03 .035
Legend
EG Q 200
Crit Q 200
WS Q 200
Ground
Bank Sta
Elevation (m)
Station (m)
Plan: 1) SedimentAnalysis 7/29/2020
River = River 1 Reach = Reach 1 RS = 176
.035 .03 .035
Legend
EG Q 200
Crit Q 200
WS Q 200
Ground
Bank Sta
Elevation (m)
Station (m)
Plan: 1) SedimentAnalysis 7/29/2020
River = River 1 Reach = Reach 1 RS = 172
.035 .03 .035
Legend
EG Q 200
Crit Q 200
WS Q 200
Ground
Bank Sta
Elevation (m)
Station (m)
Plan: 1) SedimentAnalysis 7/29/2020
River = River 1 Reach = Reach 1 RS = 167
.035 .03 .035
Legend
EG Q 200
Crit Q 200
WS Q 200
Ground
Bank Sta
Elevation (m)
Station (m)

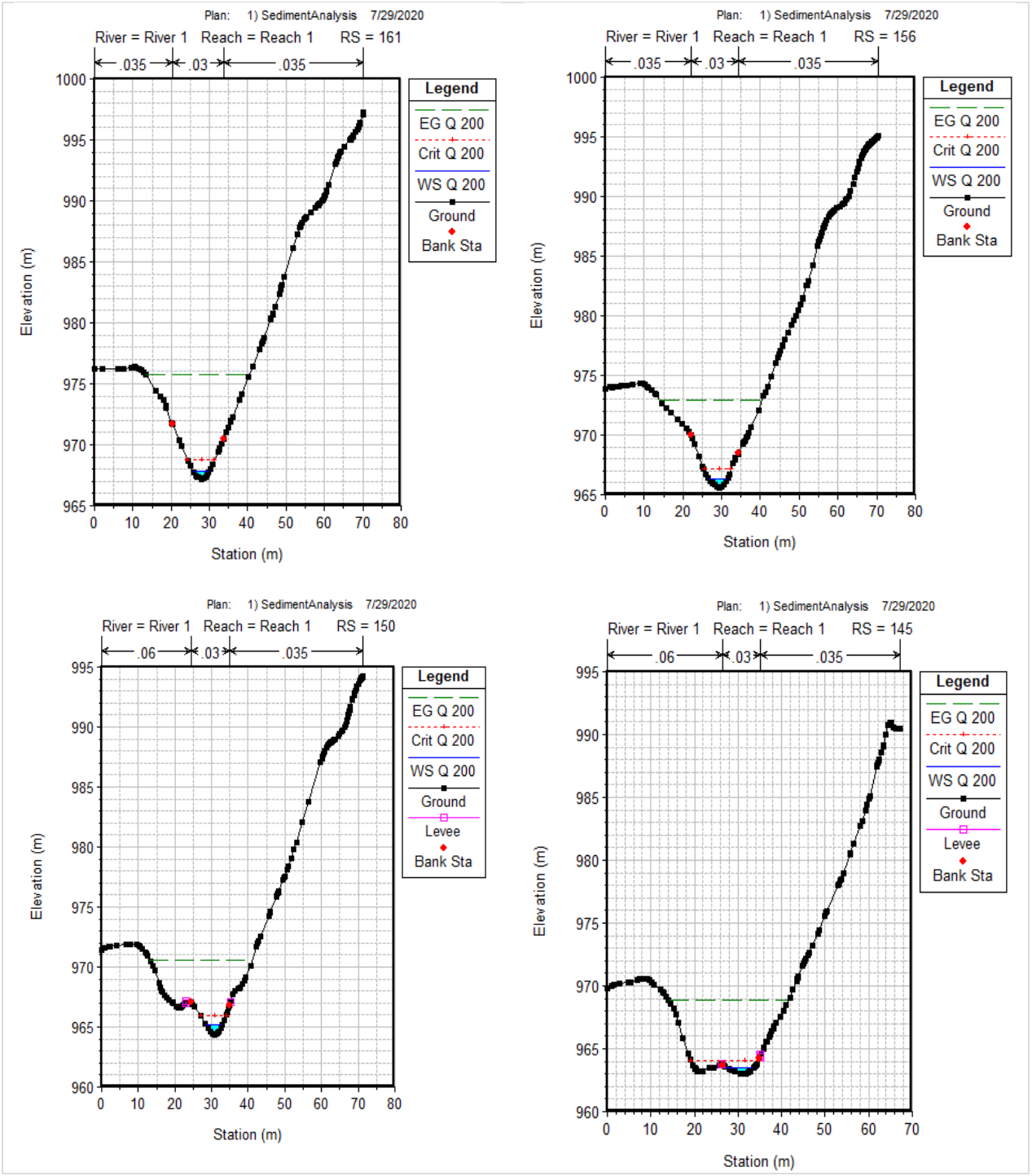
Plan: 1) SedimentAnalysis 7/29/2020
River = River 1 Reach = Reach 1 RS = 161
.035 .03 .035
Legend
EG Q 200
Crit Q 200
WS Q 200
Ground
Bank Sta
Elevation (m)
Station (m)
Plan: 1) SedimentAnalysis 7/29/2020
River = River 1 Reach = Reach 1 RS = 156
.035 .03 .035
Legend
EG Q 200
Crit Q 200
WS Q 200
Ground
Bank Sta
Elevation (m)
Station (m)
Plan: 1) SedimentAnalysis 7/29/2020
River = River 1 Reach = Reach 1 RS = 150
.06 .03 .035
Legend
EG Q 200
Crit Q 200
WS Q 200
Ground
Levee
Bank Sta
Elevation (m)
Station (m)
Plan: 1) SedimentAnalysis 7/29/2020
River = River 1 Reach = Reach 1 RS = 145
.06 .03 .035
Legend
EG Q 200
Crit Q 200
WS Q 200
Ground
Levee
Bank Sta
Elevation (m)
Station (m)

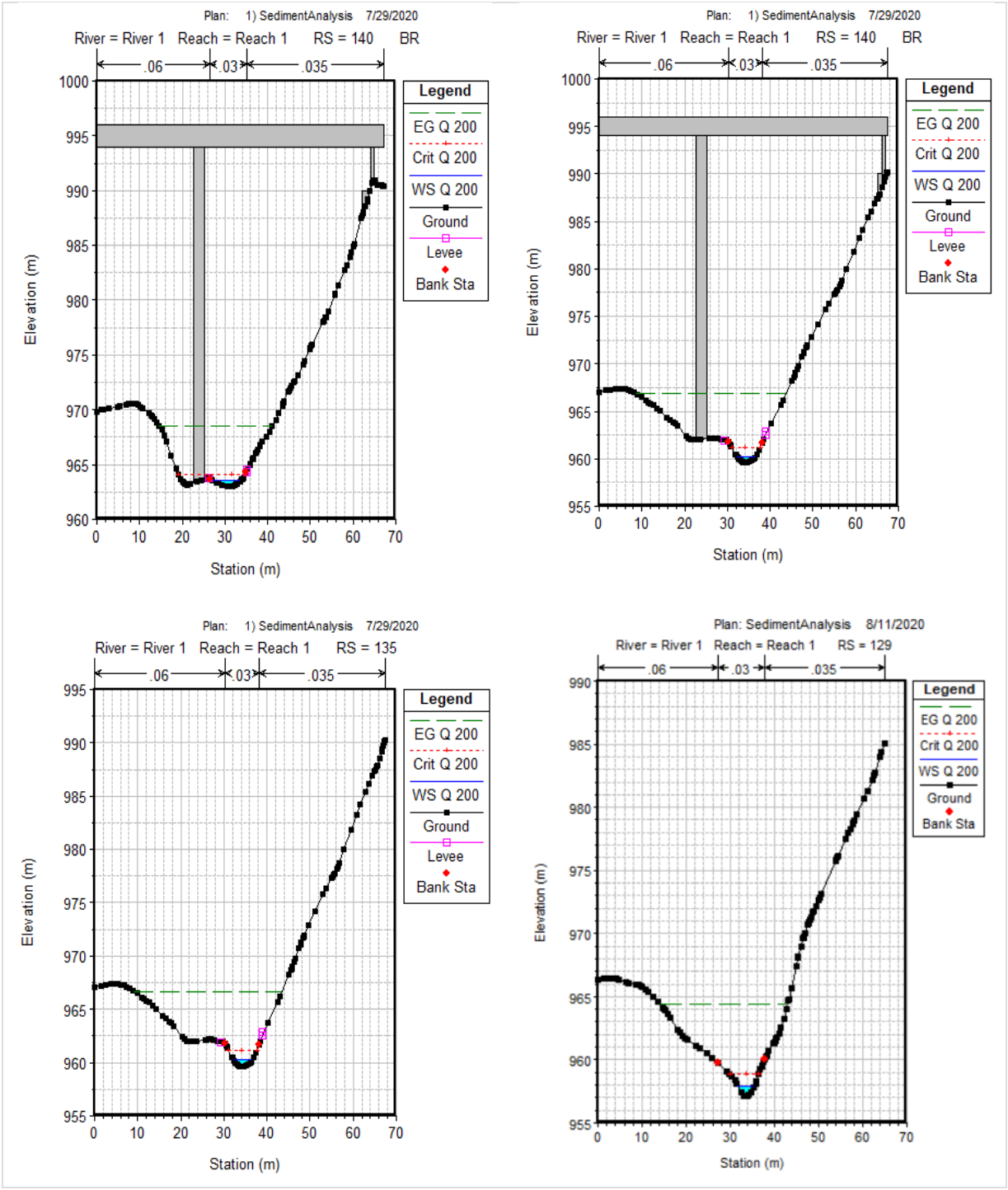
Plan: 1) SedimentAnalysis 7/29/2020
River = River 1 Reach = Reach 1 RS = 140 BR
.06
.03
.035
Legend
EG Q 200
Crit Q 200
WS Q 200
Ground
Levee
Bank Sta
Elevation (m)
Station (m)
Plan: 1) SedimentAnalysis 7/29/2020
River = River 1 Reach = Reach 1 RS = 140 BR
.06
.03
.035
Legend
EG Q 200
Crit Q 200
WS Q 200
Ground
Levee
Bank Sta
Elevation (m)
Station (m)
Plan: 1) SedimentAnalysis 7/29/2020
River = River 1 Reach = Reach 1 RS = 135
.06
.03
.035
Legend
EG Q 200
Crit Q 200
WS Q 200
Ground
Levee
Bank Sta
Elevation (m)
Station (m)
Plan: SedimentAnalysis 8/11/2020
River = River 1 Reach = Reach 1 RS = 129
.06
.03
.035
Legend
EG Q 200
Crit Q 200
WS Q 200
Ground
Bank Sta
Elevation (m)
Station (m)

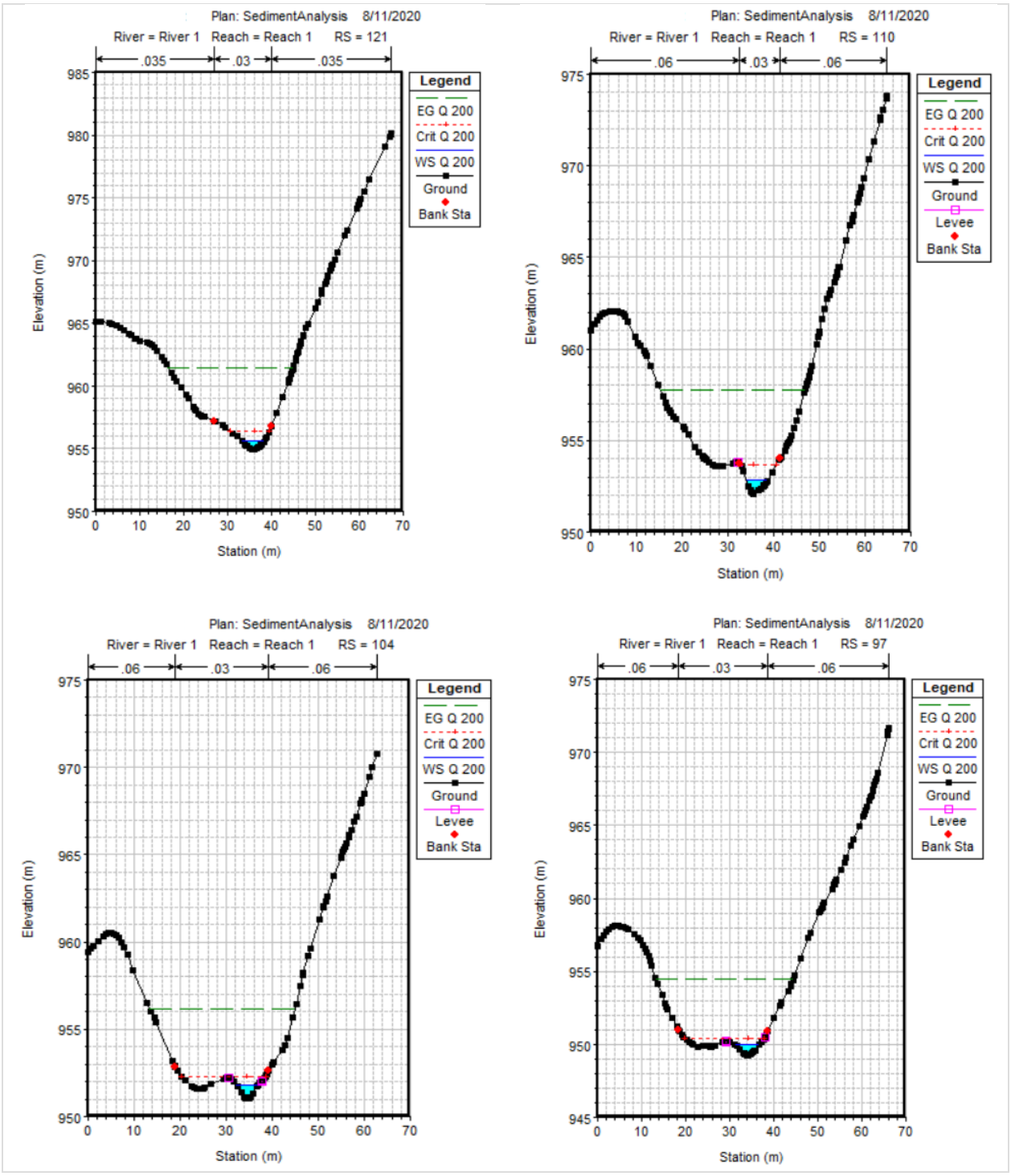
Plan: SedimentAnalysis 8/11/2020
River = River 1 Reach = Reach 1 RS = 121
.035
.03
.035
Legend
EG Q 200
Crit Q 200
WS Q 200
Ground
Bank Sta
Elevation (m)
Station (m)
Plan: SedimentAnalysis 8/11/2020
River = River 1 Reach = Reach 1 RS = 110
.06
.03
.06
Legend
EG Q 200
Crit Q 200
WS Q 200
Ground
Levee
Bank Sta
Elevation (m)
Station (m)
Plan: SedimentAnalysis 8/11/2020
River = River 1 Reach = Reach 1 RS = 104
.06
.03
.06
Legend
EG Q 200
Crit Q 200
WS Q 200
Ground
Levee
Bank Sta
Elevation (m)
Station (m)
Plan: SedimentAnalysis 8/11/2020
River = River 1 Reach = Reach 1 RS = 97
.06
.03
.06
Legend
EG Q 200
Crit Q 200
WS Q 200
Ground
Levee
Bank Sta
Elevation (m)
Station (m)

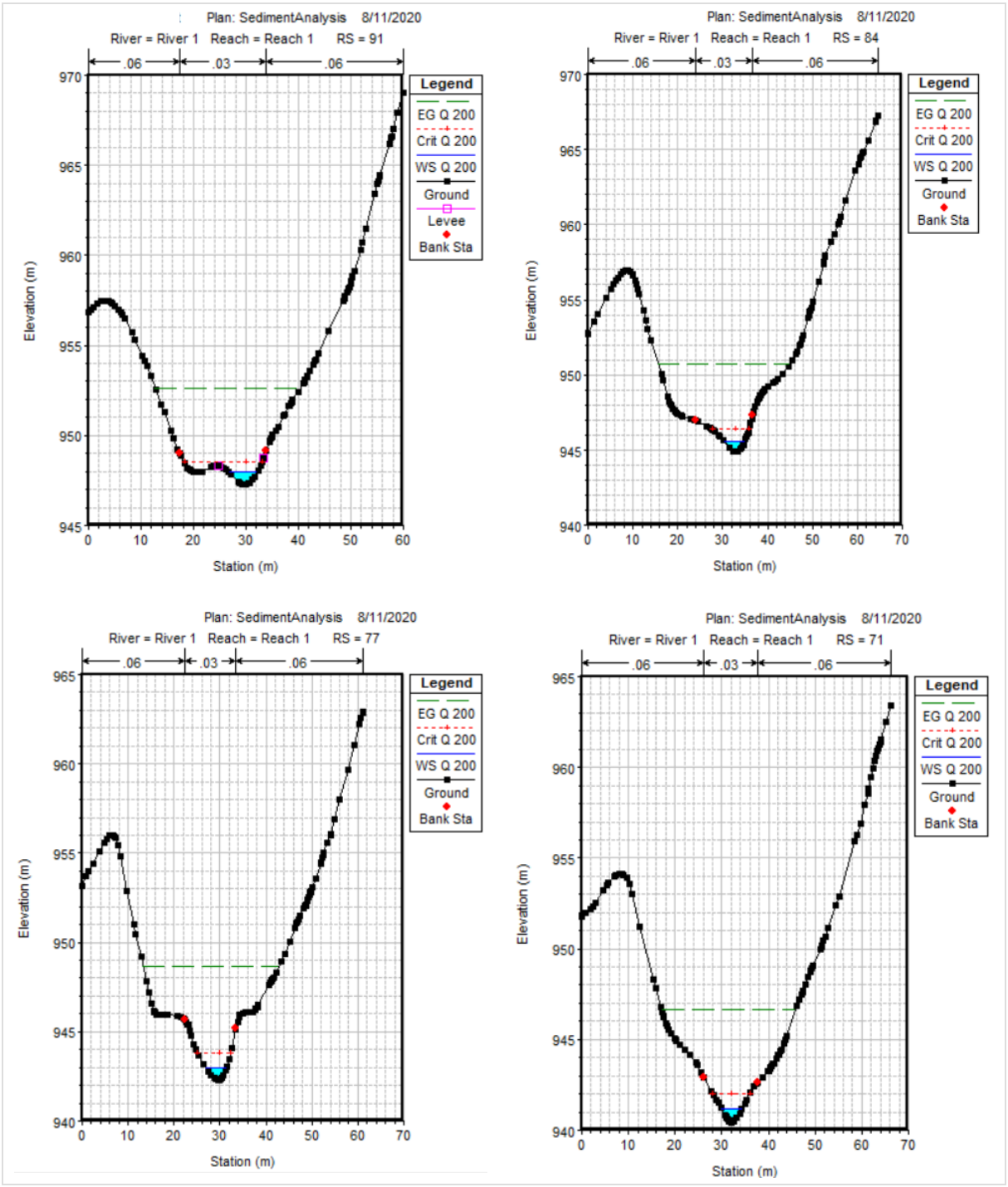
Plan: SedimentAnalysis 8/11/2020
River = River 1 Reach = Reach 1 RS = 91
.06
.03
.06
Legend
EG Q 200
Crit Q 200
WS Q 200
Ground
Levee
Bank Sta
Elevation (m)
Station (m)
Plan: SedimentAnalysis 8/11/2020
River = River 1 Reach = Reach 1 RS = 84
.06
.03
.06
Legend
EG Q 200
Crit Q 200
WS Q 200
Ground
Bank Sta
Elevation (m)
Station (m)
Plan: SedimentAnalysis 8/11/2020
River = River 1 Reach = Reach 1 RS = 77
.06
.03
.06
Legend
EG Q 200
Crit Q 200
WS Q 200
Ground
Bank Sta
Elevation (m)
Station (m)
Plan: SedimentAnalysis 8/11/2020
River = River 1 Reach = Reach 1 RS = 71
.06
.03
.06
Legend
EG Q 200
Crit Q 200
WS Q 200
Ground
Bank Sta
Elevation (m)
Station (m)

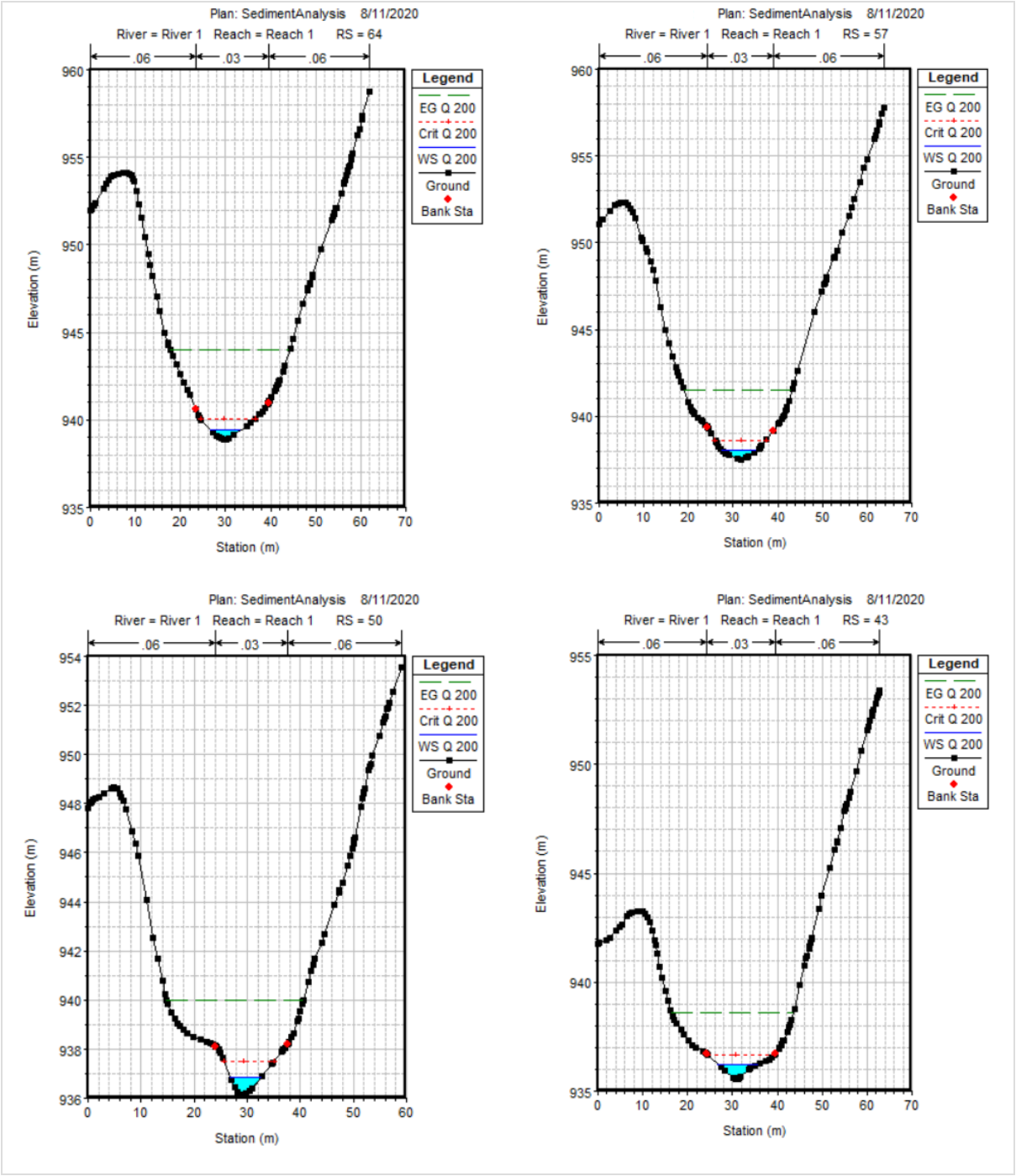
Plan: SedimentAnalysis 8/11/2020
River = River 1 Reach = Reach 1 RS = 64
.06 .03 .06
Legend
EG Q 200
Crit Q 200
WS Q 200
Ground
Bank Sta
Elevation (m)
Station (m)
Plan: SedimentAnalysis 8/11/2020
River = River 1 Reach = Reach 1 RS = 57
.06 .03 .06
Legend
EG Q 200
Crit Q 200
WS Q 200
Ground
Bank Sta
Elevation (m)
Station (m)
Plan: SedimentAnalysis 8/11/2020
River = River 1 Reach = Reach 1 RS = 50
.06 .03 .06
Legend
EG Q 200
Crit Q 200
WS Q 200
Ground
Bank Sta
Elevation (m)
Station (m)
Plan: SedimentAnalysis 8/11/2020
River = River 1 Reach = Reach 1 RS = 43
.06 .03 .06
Legend
EG Q 200
Crit Q 200
WS Q 200
Ground
Bank Sta
Elevation (m)
Station (m)

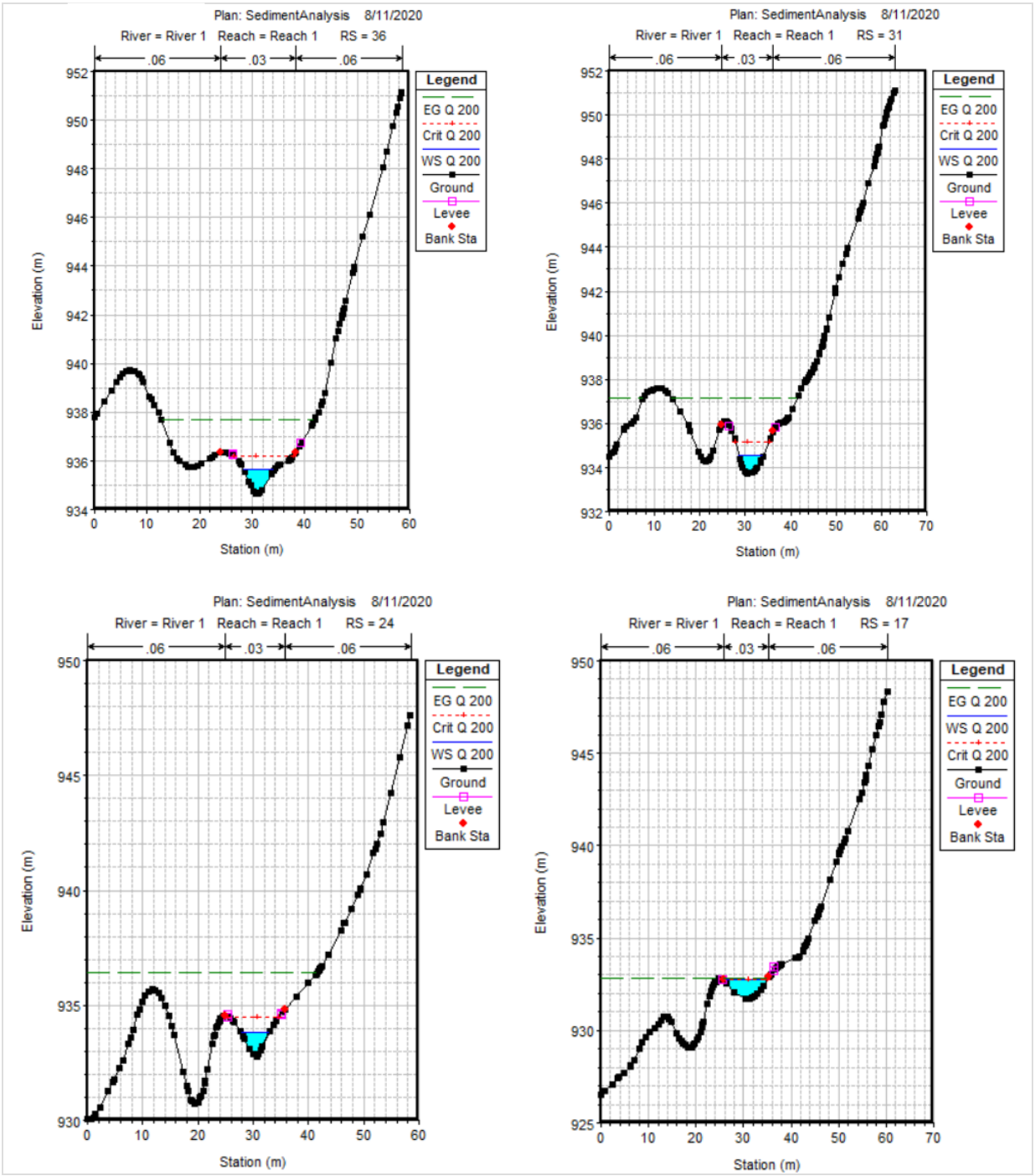
Plan: SedimentAnalysis 8/11/2020
River = River 1 Reach = Reach 1 RS = 36
.06 .03 .06
Legend
EG Q 200
Crit Q 200
WS Q 200
Ground
Levee
Bank Sta
Elevation (m)
Station (m)
Plan: SedimentAnalysis 8/11/2020
River = River 1 Reach = Reach 1 RS = 31
.06 .03 .06
Legend
EG Q 200
Crit Q 200
WS Q 200
Ground
Levee
Bank Sta
Elevation (m)
Station (m)
Plan: SedimentAnalysis 8/11/2020
River = River 1 Reach = Reach 1 RS = 24
.06 .03 .06
Legend
EG Q 200
Crit Q 200
WS Q 200
Ground
Levee
Bank Sta
Elevation (m)
Station (m)
Plan: SedimentAnalysis 8/11/2020
River = River 1 Reach = Reach 1 RS = 17
.06 .03 .06
Legend
EG Q 200
WS Q 200
Crit Q 200
Ground
Levee
Bank Sta
Elevation (m)
Station (m)

Table 21. Summary Output Table by Profile.

River Sta	Profile	Q Total (m3/s)	Min Ch El (m)	W.S. Elev (m)	Crit W.S. (m)	E.G. Elev (m)	E.G. Slope (m/m)	Vel Chnl (m/s)	Flow Area (m2)	Top Width (m)	Froude # Chl
471	Q 20	15.52	1083.38	1083.92	1084.8	1092.06	0.600	12.64	1.23	3.35	6.67
471	Q 50	17.81	1083.38	1083.96	1084.9	1092.81	0.601	13.18	1.35	3.45	6.72
471	Q 100	19.52	1083.38	1083.98	1084.97	1093.33	0.601	13.54	1.44	3.52	6.76
471	Q 200	21.23	1083.38	1084.01	1085.04	1093.84	0.601	13.89	1.53	3.59	6.79
471	Q 500	23.49	1083.38	1084.04	1085.13	1094.47	0.601	14.3	1.64	3.67	6.83
469	Q 20	15.52	1081.36	1081.92	1082.82	1090.39	0.611	12.89	1.2	3.2	6.72
469	Q 50	17.81	1081.36	1081.96	1082.93	1091.14	0.611	13.42	1.33	3.31	6.77
469	Q 100	19.52	1081.36	1081.98	1083	1091.67	0.611	13.78	1.42	3.39	6.81
469	Q 200	21.23	1081.36	1082.01	1083.07	1092.17	0.609	14.12	1.5	3.45	6.83
469	Q 500	23.49	1081.36	1082.04	1083.16	1092.8	0.607	14.53	1.62	3.53	6.85
465	Q 20	15.52	1079.56	1080.15	1081.04	1088.07	0.558	12.47	1.24	3.23	6.41
465	Q 50	17.81	1079.56	1080.19	1081.14	1088.81	0.558	13.01	1.37	3.32	6.46
465	Q 100	19.52	1079.56	1080.21	1081.22	1089.34	0.559	13.38	1.46	3.38	6.5
465	Q 200	21.23	1079.56	1080.24	1081.29	1089.84	0.560	13.72	1.55	3.44	6.53
465	Q 500	23.49	1079.56	1080.27	1081.38	1090.48	0.560	14.15	1.66	3.51	6.57
458	Q 20	15.52	1077.27	1077.83	1078.69	1086.02	0.602	12.68	1.22	3.33	6.68
458	Q 50	17.81	1077.27	1077.87	1078.79	1086.76	0.601	13.21	1.35	3.43	6.73
458	Q 100	19.52	1077.27	1077.89	1078.87	1087.28	0.601	13.57	1.44	3.5	6.76
458	Q 200	21.23	1077.27	1077.92	1078.94	1087.79	0.601	13.91	1.53	3.57	6.8
458	Q 500	23.49	1077.27	1077.95	1079.02	1088.42	0.603	14.33	1.64	3.67	6.84
450	Q 20	15.52	1074.01	1074.48	1075.18	1083.21	0.800	13.09	1.19	3.92	7.6
450	Q 50	17.81	1074.01	1074.51	1075.25	1083.94	0.806	13.6	1.31	4.11	7.69
450	Q 100	19.52	1074.01	1074.53	1075.29	1084.45	0.812	13.95	1.4	4.24	7.76
450	Q 200	21.23	1074.01	1074.55	1075.34	1084.95	0.816	14.28	1.49	4.37	7.82
450	Q 500	23.49	1074.01	1074.57	1075.39	1085.57	0.820	14.68	1.6	4.52	7.88
444	Q 20	15.52	1071.11	1071.68	1072.49	1078.71	0.513	11.75	1.32	3.6	6.19
444	Q 50	17.81	1071.11	1071.71	1072.58	1079.38	0.519	12.26	1.45	3.72	6.27
444	Q 100	19.52	1071.11	1071.74	1072.71	1079.86	0.523	12.62	1.55	3.82	6.33
444	Q 200	21.23	1071.11	1071.76	1072.76	1080.31	0.526	12.95	1.64	3.91	6.38
444	Q 500	23.49	1071.11	1071.79	1072.83	1080.89	0.531	13.36	1.76	4.02	6.45
439	Q 20	15.52	1068.17	1068.73	1069.58	1076.12	0.529	12.04	1.29	3.45	6.29
439	Q 50	17.81	1068.17	1068.77	1069.68	1076.78	0.528	12.54	1.42	3.55	6.33
439	Q 100	19.52	1068.17	1068.8	1069.75	1077.25	0.527	12.88	1.52	3.63	6.36
439	Q 200	21.23	1068.17	1068.82	1069.82	1077.7	0.526	13.19	1.61	3.7	6.39
439	Q 500	23.49	1068.17	1068.85	1069.9	1078.27	0.525	13.59	1.73	3.79	6.42

434	Q 20	15.52	1066.53	1067.14	1067.9	1073.44	0.456	11.12	1.4	3.79	5.85
434	Q 50	17.81	1066.53	1067.17	1068	1074.07	0.465	11.64	1.53	3.93	5.95
434	Q 100	19.52	1066.53	1067.2	1068.06	1074.53	0.471	11.99	1.63	4.03	6.03
434	Q 200	21.23	1066.53	1067.22	1068.12	1074.95	0.476	12.32	1.72	4.13	6.09
434	Q 500	23.49	1066.53	1067.25	1068.2	1075.5	0.483	12.72	1.85	4.25	6.16
428	Q 20	15.52	1065.21	1065.73	1066.4	1070.65	0.382	9.82	1.58	4.65	5.38
428	Q 50	17.81	1065.21	1065.76	1066.48	1071.2	0.393	10.33	1.72	4.79	5.5
428	Q 100	19.52	1065.21	1065.79	1066.54	1071.6	0.400	10.68	1.83	4.89	5.58
428	Q 200	21.23	1065.21	1065.81	1066.59	1071.98	0.406	11.01	1.93	4.99	5.65
428	Q 500	23.49	1065.21	1065.83	1066.66	1072.47	0.414	11.41	2.06	5.11	5.74
423	Q 20	15.52	1063.82	1064.37	1065	1068.52	0.314	9.03	1.72	4.93	4.88
423	Q 50	17.81	1063.82	1064.4	1065.08	1069	0.322	9.5	1.87	5.08	4.99
423	Q 100	19.52	1063.82	1064.42	1065.14	1069.34	0.328	9.83	1.99	5.18	5.07
423	Q 200	21.23	1063.82	1064.44	1065.19	1069.68	0.334	10.14	2.09	5.28	5.14
423	Q 500	23.49	1063.82	1064.47	1065.27	1070.11	0.341	10.52	2.23	5.4	5.22
416	Q 20	15.52	1061.44	1062.02	1062.57	1066.05	0.426	8.9	1.74	6.48	5.47
416	Q 50	17.81	1061.44	1062.04	1062.65	1066.48	0.425	9.33	1.91	6.57	5.53
416	Q 100	19.52	1061.44	1062.06	1062.7	1066.8	0.425	9.64	2.03	6.64	5.57
416	Q 200	21.23	1061.44	1062.08	1062.75	1067.1	0.425	9.93	2.14	6.7	5.61
416	Q 500	23.49	1061.44	1062.1	1062.81	1067.49	0.425	10.28	2.28	6.78	5.66
410	Q 20	15.52	1057.62	1058.23	1058.96	1063.43	0.351	10.1	1.54	3.98	5.19
410	Q 50	17.81	1057.62	1058.27	1059.05	1063.87	0.350	10.48	1.7	4.15	5.23
410	Q 100	19.52	1057.62	1058.29	1059.11	1064.18	0.350	10.75	1.82	4.25	5.25
410	Q 200	21.23	1057.62	1058.32	1059.17	1064.49	0.349	11	1.93	4.36	5.28
410	Q 500	23.49	1057.62	1058.35	1059.25	1064.88	0.349	11.31	2.08	4.49	5.31
403	Q 20	15.52	1053.98	1054.5	1055.19	1060.38	0.510	10.74	1.45	4.6	6.12
403	Q 50	17.81	1053.98	1054.54	1055.28	1060.84	0.502	11.12	1.6	4.78	6.13
403	Q 100	19.52	1053.98	1054.56	1055.34	1061.17	0.498	11.39	1.71	4.9	6.15
403	Q 200	21.23	1053.98	1054.58	1055.39	1061.49	0.494	11.64	1.82	5.01	6.16
403	Q 500	23.49	1053.98	1054.61	1055.47	1061.88	0.490	11.94	1.97	5.16	6.18
400	Q 20	15.52	1053.01	1053.49	1054.1	1058.57	0.538	9.98	1.56	5.81	6.16
400	Q 50	17.81	1053.01	1053.52	1054.17	1059.06	0.535	10.42	1.71	5.95	6.21
400	Q 100	19.52	1053.01	1053.54	1054.22	1059.4	0.533	10.73	1.82	6.05	6.24
400	Q 200	21.23	1053.01	1053.56	1054.27	1059.73	0.531	11.01	1.93	6.14	6.27
400	Q 500	23.49	1053.01	1053.58	1054.34	1060.15	0.528	11.35	2.07	6.27	6.31
396	Q 20	15.52	1050.71	1051.22	1051.9	1056.72	0.449	10.38	1.49	4.55	5.79
396	Q 50	17.81	1050.71	1051.25	1051.98	1057.21	0.450	10.81	1.65	4.72	5.84
396	Q 100	19.52	1050.71	1051.27	1052.04	1057.55	0.450	11.1	1.76	4.84	5.88
396	Q 200	21.23	1050.71	1051.3	1052.1	1057.89	0.449	11.37	1.87	4.94	5.91

396	Q 500	23.49	1050.71	1051.32	1052.17	1058.31	0.448	11.7	2.01	5.07	5.94
390	Q 20	15.52	1049.07	1049.57	1050.2	1053.84	0.345	9.15	1.7	5.18	5.11
390	Q 50	17.81	1049.07	1049.6	1050.29	1054.29	0.352	9.59	1.86	5.36	5.2
390	Q 100	19.52	1049.07	1049.62	1050.33	1054.62	0.356	9.9	1.97	5.48	5.27
390	Q 200	21.23	1049.07	1049.64	1050.37	1054.93	0.361	10.18	2.08	5.6	5.33
390	Q 500	23.49	1049.07	1049.67	1050.43	1055.33	0.366	10.54	2.23	5.75	5.4
384	Q 20	15.52	1047.46	1047.95	1048.49	1051.55	0.311	8.4	1.85	5.98	4.83
384	Q 50	17.81	1047.46	1047.97	1048.56	1051.93	0.319	8.81	2.02	6.21	4.93
384	Q 100	19.52	1047.46	1047.99	1048.61	1052.21	0.325	9.09	2.15	6.37	5
384	Q 200	21.23	1047.46	1048.01	1048.66	1052.48	0.330	9.36	2.27	6.52	5.07
384	Q 500	23.49	1047.46	1048.04	1048.72	1052.82	0.335	9.69	2.43	6.7	5.14
376	Q 20	15.52	1045.13	1045.68	1046.28	1049.3	0.255	8.42	1.84	5.04	4.45
376	Q 50	17.81	1045.13	1045.72	1046.36	1049.65	0.255	8.78	2.03	5.22	4.49
376	Q 100	19.52	1045.13	1045.75	1046.42	1049.89	0.256	9.02	2.17	5.35	4.52
376	Q 200	21.23	1045.13	1045.77	1046.47	1050.13	0.257	9.25	2.3	5.47	4.56
376	Q 500	23.49	1045.13	1045.8	1046.54	1050.44	0.258	9.54	2.46	5.61	4.6
369	Q 20	15.52	1043.38	1043.9	1044.48	1047.38	0.268	8.25	1.88	5.56	4.53
369	Q 50	17.81	1043.38	1043.94	1044.52	1047.72	0.269	8.61	2.07	5.75	4.58
369	Q 100	19.52	1043.38	1043.96	1044.55	1047.96	0.270	8.85	2.21	5.89	4.62
369	Q 200	21.23	1043.38	1043.98	1044.59	1048.19	0.271	9.08	2.34	6.02	4.65
369	Q 500	23.49	1043.38	1044.01	1044.63	1048.48	0.272	9.37	2.51	6.17	4.69
363	Q 20	15.52	1041.38	1041.92	1042.55	1045.68	0.264	8.58	1.81	4.94	4.53
363	Q 50	17.81	1041.38	1041.96	1042.63	1046.01	0.263	8.92	2	5.12	4.56
363	Q 100	19.52	1041.38	1041.99	1042.69	1046.26	0.262	9.15	2.13	5.24	4.58
363	Q 200	21.23	1041.38	1042.01	1042.74	1046.49	0.261	9.37	2.27	5.35	4.6
363	Q 500	23.49	1041.38	1042.04	1042.82	1046.79	0.260	9.64	2.44	5.48	4.62
357	Q 20	15.52	1039.55	1040.16	1040.83	1044.05	0.247	8.73	1.78	4.43	4.4
357	Q 50	17.81	1039.55	1040.2	1040.93	1044.4	0.245	9.08	1.96	4.57	4.42
357	Q 100	19.52	1039.55	1040.23	1040.99	1044.65	0.243	9.31	2.1	4.66	4.43
357	Q 200	21.23	1039.55	1040.26	1041.05	1044.89	0.242	9.53	2.23	4.76	4.45
357	Q 500	23.49	1039.55	1040.3	1041.13	1045.19	0.240	9.8	2.4	4.87	4.46
350	Q 20	15.52	1037.39	1037.94	1038.55	1042.18	0.338	9.12	1.7	5.13	5.06
350	Q 50	17.81	1037.39	1037.97	1038.62	1042.54	0.337	9.47	1.88	5.35	5.1
350	Q 100	19.52	1037.39	1038	1038.68	1042.8	0.336	9.7	2.01	5.5	5.12
350	Q 200	21.23	1037.39	1038.02	1038.73	1043.04	0.336	9.93	2.14	5.65	5.15
350	Q 500	23.49	1037.39	1038.05	1038.79	1043.34	0.337	10.19	2.3	5.86	5.19
344	Q 20	15.52	1035.64	1036.18	1036.83	1040.15	0.284	8.83	1.76	4.85	4.68
344	Q 50	17.81	1035.64	1036.22	1036.92	1040.53	0.281	9.2	1.94	4.95	4.7

344	Q 100	19.52	1035.64	1036.24	1036.98	1040.8	0.279	9.46	2.06	5.03	4.71
344	Q 200	21.23	1035.64	1036.27	1037.04	1041.05	0.276	9.69	2.19	5.1	4.72
344	Q 500	23.49	1035.64	1036.3	1037.12	1041.37	0.273	9.97	2.36	5.19	4.73
338	Q 20	15.52	1034.34	1034.99	1035.67	1038.71	0.219	8.54	1.82	4.23	4.16
338	Q 50	17.81	1034.34	1035.03	1035.75	1039.09	0.221	8.92	2	4.37	4.21
338	Q 100	19.52	1034.34	1035.06	1035.83	1039.36	0.222	9.18	2.13	4.47	4.25
338	Q 200	21.23	1034.34	1035.09	1035.89	1039.61	0.223	9.42	2.25	4.56	4.28
338	Q 500	23.49	1034.34	1035.13	1035.97	1039.93	0.224	9.71	2.42	4.68	4.31
332	Q 20	15.52	1032.57	1033.21	1033.92	1037.32	0.268	8.98	1.73	4.39	4.57
332	Q 50	17.81	1032.57	1033.25	1034.03	1037.69	0.269	9.33	1.91	4.59	4.62
332	Q 100	19.52	1032.57	1033.28	1034.06	1037.95	0.270	9.57	2.04	4.73	4.66
332	Q 200	21.23	1032.57	1033.31	1034.1	1038.2	0.271	9.8	2.17	4.86	4.69
332	Q 500	23.49	1032.57	1033.34	1034.14	1038.52	0.272	10.08	2.33	5.02	4.72
326	Q 20	15.52	1029.96	1030.46	1031.13	1035.26	0.365	9.71	1.6	4.59	5.25
326	Q 50	17.81	1029.96	1030.49	1031.21	1035.64	0.358	10.05	1.77	4.75	5.25
326	Q 100	19.52	1029.96	1030.52	1031.28	1035.91	0.353	10.28	1.9	4.86	5.25
326	Q 200	21.23	1029.96	1030.55	1031.34	1036.17	0.349	10.5	2.02	4.96	5.25
326	Q 500	23.49	1029.96	1030.58	1031.41	1036.49	0.345	10.77	2.18	5.1	5.26
319	Q 20	15.52	1028.16	1028.79	1029.46	1033.06	0.281	9.16	1.69	4.31	4.66
319	Q 50	17.81	1028.16	1028.83	1029.55	1033.46	0.283	9.53	1.87	4.49	4.72
319	Q 100	19.52	1028.16	1028.85	1029.61	1033.74	0.284	9.79	1.99	4.62	4.75
319	Q 200	21.23	1028.16	1028.88	1029.67	1034	0.285	10.03	2.12	4.74	4.79
319	Q 500	23.49	1028.16	1028.91	1029.74	1034.34	0.286	10.32	2.28	4.89	4.83
313	Q 20	15.52	1027.51	1028.07	1028.43	1030.51	0.389	7.06	2.43	13.99	5.03
313	Q 50	17.81	1027.51	1028.09	1028.48	1030.84	0.406	7.53	2.63	14.08	5.2
313	Q 100	19.52	1027.51	1028.1	1028.51	1031.09	0.417	7.86	2.77	14.12	5.31
313	Q 200	21.23	1027.51	1028.11	1028.54	1031.33	0.426	8.17	2.91	14.16	5.4
313	Q 500	23.49	1027.51	1028.12	1028.59	1031.63	0.436	8.54	3.08	14.22	5.5
306	Q 20	15.52	1026.28	1026.66	1027.03	1028.58	0.207	6.15	2.53	9.74	3.85
306	Q 50	17.81	1026.28	1026.68	1027.08	1028.83	0.213	6.49	2.74	9.96	3.95
306	Q 100	19.52	1026.28	1026.69	1027.12	1029.01	0.218	6.74	2.9	10.11	4.02
306	Q 200	21.23	1026.28	1026.71	1027.16	1029.19	0.222	6.97	3.05	10.25	4.08
306	Q 500	23.49	1026.28	1026.73	1027.21	1029.42	0.228	7.26	3.23	10.44	4.17
300	Q 20	15.52	1023.95	1024.47	1024.95	1027.16	0.237	7.26	2.14	7	4.2
300	Q 50	17.81	1023.95	1024.5	1025.01	1027.39	0.234	7.53	2.36	7.24	4.21
300	Q 100	19.52	1023.95	1024.52	1025.06	1027.57	0.232	7.72	2.53	7.41	4.22
300	Q 200	21.23	1023.95	1024.54	1025.11	1027.74	0.230	7.91	2.68	7.53	4.23
300	Q 500	23.49	1023.95	1024.57	1025.17	1027.96	0.227	8.15	2.88	7.66	4.24

297	Q 20	15.52	1022.84	1023.54	1024.1	1026.47	0.186	7.57	2.05	5.13	3.83
297	Q 50	17.81	1022.84	1023.58	1024.17	1026.71	0.186	7.83	2.28	5.43	3.86
297	Q 100	19.52	1022.84	1023.61	1024.23	1026.88	0.186	8	2.44	5.63	3.88
297	Q 200	21.23	1022.84	1023.64	1024.27	1027.05	0.187	8.18	2.6	5.84	3.92
297	Q 500	23.49	1022.84	1023.68	1024.34	1027.27	0.191	8.4	2.8	6.13	3.97
294	Q 20	15.52	1020.62	1021.12	1021.79	1025.58	0.337	9.35	1.66	4.78	5.06
294	Q 50	17.81	1020.62	1021.16	1021.87	1025.84	0.316	9.58	1.86	4.9	4.96
294	Q 100	19.52	1020.62	1021.19	1021.93	1026.02	0.304	9.73	2.01	4.98	4.9
294	Q 200	21.23	1020.62	1021.22	1021.99	1026.2	0.293	9.88	2.15	5.07	4.85
294	Q 500	23.49	1020.62	1021.26	1022.07	1026.43	0.281	10.07	2.33	5.17	4.79
288	Q 20	15.52	1012.97	1013.53	1014.16	1022.22	0.690	13.05	1.19	3.46	7.11
288	Q 50	17.81	1012.97	1013.57	1014.23	1022.6	0.674	13.3	1.34	3.72	7.08
288	Q 100	19.52	1012.97	1013.6	1014.29	1022.86	0.664	13.47	1.45	3.91	7.07
288	Q 200	21.23	1012.97	1013.63	1014.34	1023.07	0.673	13.61	1.56	4.2	7.13
288	Q 500	23.49	1012.97	1013.66	1014.4	1023.31	0.708	13.76	1.71	4.7	7.29
282	Q 20	15.52	1010.9	1011.39	1012.04	1017.55	0.616	10.99	1.41	5.02	6.62
282	Q 50	17.81	1010.9	1011.42	1012.11	1018.02	0.611	11.38	1.56	5.24	6.65
282	Q 100	19.52	1010.9	1011.44	1012.17	1018.35	0.606	11.64	1.68	5.39	6.67
282	Q 200	21.23	1010.9	1011.46	1012.22	1018.59	0.593	11.83	1.79	5.54	6.64
282	Q 500	23.49	1010.9	1011.49	1012.28	1018.82	0.568	11.99	1.96	5.74	6.55
279	Q 20	15.52	1010.02	1010.78	1011.43	1015.56	0.380	9.68	1.6	4.61	5.24
279	Q 50	17.81	1010.02	1010.82	1011.52	1016.01	0.389	10.1	1.76	4.84	5.34
279	Q 100	19.52	1010.02	1010.84	1011.58	1016.33	0.393	10.38	1.88	4.99	5.4
279	Q 200	21.23	1010.02	1010.86	1011.63	1016.6	0.393	10.61	2	5.14	5.43
279	Q 500	23.49	1010.02	1010.9	1011.7	1016.88	0.388	10.83	2.17	5.34	5.43
275	Q 20	15.52	1007.14	1007.68	1008.43	1013.88	0.481	11.03	1.41	4.09	6
275	Q 50	17.81	1007.14	1007.72	1008.52	1014.34	0.469	11.39	1.56	4.23	5.99
275	Q 100	19.52	1007.14	1007.75	1008.59	1014.66	0.462	11.65	1.68	4.34	5.98
275	Q 200	21.23	1007.14	1007.77	1008.65	1014.94	0.453	11.86	1.79	4.44	5.96
275	Q 500	23.49	1007.14	1007.81	1008.73	1015.25	0.438	12.08	1.94	4.55	5.9
266	Q 20	15.52	1003.66	1004.17	1004.94	1011.55	0.613	12.03	1.29	3.94	6.72
266	Q 50	17.81	1003.66	1004.21	1005.04	1012.05	0.596	12.41	1.44	4.09	6.69
266	Q 100	19.52	1003.66	1004.23	1005.11	1012.41	0.585	12.67	1.54	4.19	6.67
266	Q 200	21.23	1003.66	1004.26	1005.17	1012.73	0.573	12.89	1.65	4.29	6.64
266	Q 500	23.49	1003.66	1004.29	1005.24	1013.1	0.557	13.14	1.79	4.42	6.6
260	Q 20	15.52	1001.92	1002.57	1003.37	1008.33	0.362	10.62	1.46	3.5	5.25
260	Q 50	17.81	1001.92	1002.62	1003.47	1008.87	0.365	11.07	1.61	3.63	5.31
260	Q 100	19.52	1001.92	1002.64	1003.54	1009.24	0.366	11.38	1.72	3.72	5.35
260	Q 200	21.23	1001.92	1002.67	1003.61	1009.6	0.366	11.65	1.82	3.8	5.37

260	Q 500	23.49	1001.92	1002.71	1003.69	1010.02	0.365	11.97	1.96	3.9	5.39
255	Q 20	15.52	1000.69	1001.3	1002.04	1006.28	0.325	9.88	1.57	3.95	5
255	Q 50	17.81	1000.69	1001.34	1002.13	1006.79	0.330	10.34	1.72	4.09	5.09
255	Q 100	19.52	1000.69	1001.37	1002.2	1007.15	0.334	10.65	1.83	4.19	5.14
255	Q 200	21.23	1000.69	1001.39	1002.26	1007.49	0.337	10.93	1.94	4.28	5.18
255	Q 500	23.49	1000.69	1001.43	1002.34	1007.91	0.339	11.28	2.08	4.4	5.23
249	Q 20	15.52	998.77	999.41	1000.19	1004.52	0.310	10.01	1.55	3.61	4.88
249	Q 50	17.81	998.77	999.46	1000.29	1005.01	0.312	10.44	1.71	3.73	4.93
249	Q 100	19.52	998.77	999.49	1000.36	1005.36	0.313	10.73	1.82	3.82	4.97
249	Q 200	21.23	998.77	999.52	1000.43	1005.69	0.314	11.01	1.93	3.89	4.99
249	Q 500	23.49	998.77	999.55	1000.51	1006.11	0.314	11.34	2.07	3.98	5.02
241.17	Q 20	15.52	995.81	996.44	997.27	1002.03	0.334	10.47	1.48	3.36	5.04
241.17	Q 50	17.81	995.81	996.49	997.38	1002.52	0.332	10.88	1.64	3.46	5.05
241.17	Q 100	19.52	995.81	996.52	997.45	1002.87	0.330	11.16	1.75	3.53	5.06
241.17	Q 200	21.23	995.81	996.55	997.53	1003.21	0.329	11.42	1.86	3.6	5.08
241.17	Q 500	23.49	995.81	996.59	997.62	1003.62	0.328	11.75	2	3.68	5.09
234.81	Q 20	15.52	994.45	995.29	996.1	999.99	0.250	9.6	1.62	3.25	4.35
234.81	Q 50	17.81	994.45	995.33	996.2	1000.46	0.255	10.03	1.78	3.38	4.42
234.81	Q 100	19.52	994.45	995.37	996.28	1000.8	0.258	10.32	1.89	3.48	4.47
234.81	Q 200	21.23	994.45	995.4	996.35	1001.12	0.261	10.59	2	3.56	4.51
234.81	Q 500	23.49	994.45	995.44	996.44	1001.53	0.264	10.93	2.15	3.68	4.56
234		Bridge									
222.45	Q 20	15.52	990.79	991.26	991.87	995.28	0.442	8.87	1.75	5.35	4.96
222.45	Q 50	17.81	990.79	991.29	991.95	995.72	0.447	9.31	1.91	5.48	5.03
222.45	Q 100	19.52	990.79	991.31	992.01	996.03	0.450	9.61	2.03	5.56	5.08
222.45	Q 200	21.23	990.79	991.33	992.07	996.33	0.451	9.9	2.15	5.64	5.12
222.45	Q 500	23.49	990.79	991.36	992.14	996.71	0.454	10.25	2.29	5.73	5.17
215	Q 20	15.52	989.42	990.1	990.69	992.81	0.203	7.29	2.13	4.72	3.47
215	Q 50	17.81	989.42	990.14	990.77	993.16	0.211	7.69	2.31	4.86	3.56
215	Q 100	19.52	989.42	990.17	990.84	993.42	0.215	7.99	2.44	4.92	3.62
215	Q 200	21.23	989.42	990.19	990.9	993.68	0.220	8.27	2.57	4.97	3.67
215	Q 500	23.49	989.42	990.23	990.98	994.01	0.225	8.61	2.73	5.03	3.74

211	Q 20	15.52	987.95	988.56	989.18	991.7	0.246	7.85	1.98	4.55	3.8
211	Q 50	17.81	987.95	988.61	989.28	992.03	0.247	8.19	2.17	4.68	3.84
211	Q 100	19.52	987.95	988.64	989.34	992.28	0.248	8.45	2.31	4.76	3.87
211	Q 200	21.23	987.95	988.66	989.41	992.52	0.250	8.69	2.44	4.83	3.9
211	Q 500	23.49	987.95	988.7	989.49	992.83	0.253	9	2.61	4.92	3.95
210		Inl Struct									
205	Q 20	15.52	985.22	986.62	986.62	987.08	0.015	2.99	5.19	5.78	1.01
205	Q 50	17.81	985.22	986.72	986.72	987.21	0.015	3.1	5.74	5.96	1.01
205	Q 100	19.52	985.22	986.79	986.79	987.3	0.015	3.18	6.14	6.08	1.01
205	Q 200	21.23	985.22	986.85	986.86	987.39	0.015	3.24	6.55	6.2	1.01
205	Q 500	23.49	985.22	986.93	986.94	987.5	0.015	3.33	7.05	6.35	1.01
202	Q 20	15.52	984.82	985.86	986.2	986.95	0.051	4.63	3.35	4.99	1.8
202	Q 50	17.81	984.82	985.94	986.3	987.08	0.049	4.73	3.77	5.21	1.78
202	Q 100	19.52	984.82	986	986.36	987.17	0.047	4.8	4.07	5.37	1.76
202	Q 200	21.23	984.82	986.05	986.43	987.26	0.046	4.87	4.36	5.51	1.75
202	Q 500	23.49	984.82	986.12	986.51	987.37	0.044	4.95	4.75	5.68	1.73
196	Q 20	15.52	982.42	983.68	984.42	986.61	0.085	7.58	2.05	2.89	2.87
196	Q 50	17.81	982.42	983.78	984.55	986.75	0.079	7.63	2.33	3.09	2.8
196	Q 100	19.52	982.42	983.85	984.63	986.84	0.076	7.67	2.55	3.23	2.76
196	Q 200	21.23	982.42	983.91	984.71	986.94	0.073	7.71	2.75	3.37	2.72
196	Q 500	23.49	982.42	983.99	984.81	987.05	0.069	7.75	3.03	3.53	2.67
195		Bridge									
193	Q 20	15.52	981.88	983.02	983.84	986.39	0.098	8.14	1.91	2.69	3.09
193	Q 50	17.81	981.88	983.11	983.96	986.54	0.092	8.2	2.17	2.85	3
193	Q 100	19.52	981.88	983.18	984.05	986.65	0.087	8.25	2.37	2.95	2.94
193	Q 200	21.23	981.88	983.24	984.12	986.75	0.084	8.29	2.56	3.06	2.89
193	Q 500	23.49	981.88	983.33	984.23	986.87	0.080	8.33	2.82	3.21	2.84
192	Q 20	15.52	981.4	982.39	983.14	986.18	0.129	8.63	1.8	3.26	3.71
192	Q 50	17.81	981.4	982.46	983.25	986.34	0.120	8.72	2.04	3.44	3.61
192	Q 100	19.52	981.4	982.51	983.34	986.45	0.115	8.79	2.22	3.56	3.56
192	Q 200	21.23	981.4	982.56	983.4	986.55	0.110	8.85	2.4	3.67	3.5
192	Q 500	23.49	981.4	982.62	983.5	986.68	0.104	8.92	2.63	3.8	3.42
191		Bridge									
187	Q 20	15.52	979.35	980.12	980.95	985.14	0.188	9.92	1.56	3.18	4.52
187	Q 50	17.81	979.35	980.18	981.06	985.35	0.175	10.07	1.77	3.31	4.4
187	Q 100	19.52	979.35	980.23	981.14	985.49	0.167	10.16	1.92	3.4	4.32
187	Q 200	21.23	979.35	980.27	981.21	985.63	0.160	10.25	2.07	3.49	4.25

187	Q 500	23.49	979.35	980.33	981.31	985.79	0.152	10.35	2.27	3.61	4.16
183	Q 20	15.52	978.24	979.1	979.94	984.37	0.203	10.16	1.53	3.14	4.65
183	Q 50	17.81	978.24	979.16	980.05	984.62	0.193	10.35	1.72	3.3	4.58
183	Q 100	19.52	978.24	979.2	980.13	984.79	0.186	10.47	1.87	3.41	4.52
183	Q 200	21.23	978.24	979.25	980.2	984.95	0.180	10.58	2.01	3.5	4.46
183	Q 500	23.49	978.24	979.3	980.29	985.13	0.171	10.7	2.2	3.61	4.38
180	Q 20	15.52	977.24	978	978.85	983.69	0.225	10.56	1.47	3.13	4.92
180	Q 50	17.81	977.24	978.05	978.95	983.97	0.214	10.77	1.65	3.28	4.84
180	Q 100	19.52	977.24	978.1	979.02	984.15	0.207	10.9	1.79	3.39	4.79
180	Q 200	21.23	977.24	978.14	979.1	984.33	0.201	11.03	1.93	3.49	4.74
180	Q 500	23.49	977.24	978.19	979.19	984.54	0.193	11.16	2.1	3.62	4.68
178	Q 20	15.52	976.57	977.28	978.11	983.11	0.356	10.7	1.45	3.32	5.17
178	Q 50	17.81	976.57	977.33	978.22	983.42	0.338	10.92	1.63	3.46	5.08
178	Q 100	19.52	976.57	977.37	978.29	983.62	0.327	11.07	1.76	3.56	5.02
178	Q 200	21.23	976.57	977.41	978.36	983.82	0.317	11.21	1.89	3.65	4.97
178	Q 500	23.49	976.57	977.45	978.44	984.04	0.305	11.36	2.07	3.78	4.9
176	Q 20	15.52	975.77	976.41	977.17	982.28	0.402	10.73	1.45	3.7	5.48
176	Q 50	17.81	975.77	976.45	977.26	982.61	0.388	10.99	1.62	3.89	5.43
176	Q 100	19.52	975.77	976.49	977.32	982.84	0.379	11.16	1.75	4.02	5.4
176	Q 200	21.23	975.77	976.52	977.38	983.05	0.370	11.32	1.88	4.14	5.37
176	Q 500	23.49	975.77	976.56	977.45	983.29	0.359	11.5	2.04	4.3	5.32
172	Q 20	15.52	972.02	972.71	973.59	980.05	0.469	12	1.29	3.03	5.87
172	Q 50	17.81	972.02	972.76	973.7	980.45	0.452	12.28	1.45	3.18	5.81
172	Q 100	19.52	972.02	972.8	973.77	980.72	0.440	12.47	1.57	3.28	5.76
172	Q 200	21.23	972.02	972.83	973.84	980.98	0.430	12.64	1.68	3.38	5.73
172	Q 500	23.49	972.02	972.87	973.93	981.27	0.417	12.84	1.83	3.51	5.67
167	Q 20	15.52	969.84	970.49	971.33	977.48	0.477	11.71	1.33	3.37	5.96
167	Q 50	17.81	969.84	970.54	971.43	977.98	0.469	12.09	1.47	3.52	5.96
167	Q 100	19.52	969.84	970.57	971.5	978.32	0.464	12.34	1.58	3.62	5.96
167	Q 200	21.23	969.84	970.6	971.56	978.64	0.458	12.56	1.69	3.73	5.96
167	Q 500	23.49	969.84	970.63	971.65	979.02	0.450	12.83	1.83	3.86	5.94
161	Q 20	15.52	967.21	967.77	968.55	974.42	0.493	11.43	1.36	3.78	6.09
161	Q 50	17.81	967.21	967.8	968.64	974.98	0.490	11.86	1.5	3.92	6.12
161	Q 100	19.52	967.21	967.83	968.71	975.36	0.487	12.15	1.61	4.02	6.13
161	Q 200	21.23	967.21	967.85	968.77	975.71	0.483	12.42	1.71	4.11	6.15
161	Q 500	23.49	967.21	967.89	968.85	976.15	0.479	12.73	1.84	4.23	6.16
156	Q 20	15.52	965.58	966.2	966.92	971.62	0.398	10.32	1.5	4.17	5.49
156	Q 50	17.81	965.58	966.23	967	972.16	0.404	10.79	1.65	4.32	5.57

156	Q 100	19.52	965.58	966.26	967.06	972.54	0.407	11.1	1.76	4.42	5.62
156	Q 200	21.23	965.58	966.28	967.12	972.9	0.409	11.4	1.86	4.52	5.67
156	Q 500	23.49	965.58	966.31	967.2	973.35	0.411	11.75	2	4.65	5.72
150	Q 20	15.52	964.38	965.05	965.76	969.45	0.274	9.28	1.67	4.05	4.62
150	Q 50	17.81	964.38	965.09	965.86	969.93	0.282	9.74	1.83	4.2	4.71
150	Q 100	19.52	964.38	965.12	965.92	970.27	0.287	10.05	1.94	4.3	4.78
150	Q 200	21.23	964.38	965.14	965.98	970.6	0.291	10.34	2.05	4.4	4.84
150	Q 500	23.49	964.38	965.18	966.06	971.01	0.296	10.7	2.2	4.53	4.9
145	Q 20	15.52	963.01	963.47	963.91	967.8	0.412	9.22	1.68	5.85	5.49
145	Q 50	17.81	963.01	963.49	963.96	968.24	0.417	9.64	1.85	6.05	5.57
145	Q 100	19.52	963.01	963.51	964	968.55	0.421	9.94	1.96	6.19	5.64
145	Q 200	21.23	963.01	963.53	964.04	968.85	0.424	10.21	2.08	6.32	5.69
145	Q 500	23.49	963.01	963.55	964.08	969.23	0.428	10.55	2.23	6.49	5.75
140		Bridge									
135	Q 20	15.52	959.59	960.16	960.91	965.62	0.390	10.35	1.5	4.07	5.44
135	Q 50	17.81	959.59	960.2	961.01	966.06	0.385	10.71	1.66	4.22	5.45
135	Q 100	19.52	959.59	960.23	961.07	966.37	0.379	10.97	1.78	4.3	5.45
135	Q 200	21.23	959.59	960.26	961.13	966.68	0.374	11.22	1.89	4.37	5.45
135	Q 500	23.49	959.59	960.29	961.22	967.06	0.369	11.53	2.04	4.46	5.44
129	Q 20	15.52	957.1	957.81	958.62	963.23	0.325	10.32	1.5	3.42	4.97
129	Q 50	17.81	957.1	957.85	958.72	963.7	0.321	10.71	1.66	3.5	4.96
129	Q 100	19.52	957.1	957.89	958.79	964.04	0.321	10.98	1.78	3.58	4.98
129	Q 200	21.23	957.1	957.92	958.86	964.36	0.321	11.24	1.89	3.67	5
129	Q 500	23.49	957.1	957.96	958.94	964.76	0.321	11.55	2.03	3.79	5.03
121	Q 20	15.52	954.98	955.52	956.19	960.32	0.367	9.71	1.6	4.61	5.27
121	Q 50	17.81	954.98	955.55	956.27	960.8	0.371	10.15	1.75	4.77	5.35
121	Q 100	19.52	954.98	955.57	956.33	961.14	0.372	10.45	1.87	4.87	5.39
121	Q 200	21.23	954.98	955.59	956.39	961.46	0.373	10.72	1.98	4.97	5.42
121	Q 500	23.49	954.98	955.62	956.45	961.85	0.374	11.05	2.13	5.09	5.46
110	Q 20	15.52	952.06	952.75	953.41	956.72	0.253	8.83	1.76	4.3	4.41
110	Q 50	17.81	952.06	952.79	953.51	957.14	0.256	9.24	1.93	4.43	4.48
110	Q 100	19.52	952.06	952.81	953.58	957.44	0.258	9.53	2.05	4.53	4.52
110	Q 200	21.23	952.06	952.84	953.64	957.73	0.261	9.79	2.17	4.63	4.57
110	Q 500	23.49	952.06	952.87	953.72	958.09	0.264	10.12	2.32	4.75	4.62
104	Q 20	15.52	951.02	951.73	952.25	955.29	0.209	8.36	1.86	4.32	4.07
104	Q 50	17.81	951.02	951.77	952.25	955.67	0.215	8.74	2.04	4.51	4.16
104	Q 100	19.52	951.02	951.8	952.26	955.94	0.220	9.01	2.17	4.65	4.22
104	Q 200	21.23	951.02	951.83	952.29	956.19	0.226	9.25	2.29	4.84	4.29

104	Q 500	23.49	951.02	951.86	952.33	956.52	0.230	9.56	2.46	4.99	4.35
97	Q 20	15.52	949.27	949.89	950.31	953.66	0.261	8.6	1.8	4.81	4.49
97	Q 50	17.81	949.27	949.92	950.35	954.01	0.264	8.95	1.99	5.04	4.55
97	Q 100	19.52	949.27	949.95	950.38	954.25	0.268	9.19	2.12	5.23	4.6
97	Q 200	21.23	949.27	949.98	950.41	954.48	0.270	9.39	2.26	5.41	4.64
97	Q 500	23.49	949.27	950.01	950.44	954.78	0.276	9.67	2.43	5.66	4.72
91	Q 20	15.52	947.26	947.86	948.41	951.86	0.278	8.86	1.75	4.72	4.64
91	Q 50	17.81	947.26	947.9	948.46	952.2	0.278	9.18	1.94	4.94	4.68
91	Q 100	19.52	947.26	947.92	948.49	952.43	0.278	9.4	2.08	5.1	4.71
91	Q 200	21.23	947.26	947.95	948.52	952.65	0.277	9.6	2.21	5.25	4.72
91	Q 500	23.49	947.26	947.98	948.57	952.93	0.277	9.85	2.38	5.43	4.75
84	Q 20	15.52	944.87	945.5	946.19	949.94	0.291	9.33	1.66	4.21	4.74
84	Q 50	17.81	944.87	945.54	946.28	950.29	0.287	9.65	1.85	4.39	4.75
84	Q 100	19.52	944.87	945.57	946.34	950.53	0.284	9.86	1.98	4.51	4.76
84	Q 200	21.23	944.87	945.6	946.4	950.76	0.282	10.06	2.11	4.64	4.76
84	Q 500	23.49	944.87	945.64	946.47	951.05	0.279	10.31	2.28	4.79	4.77
77	Q 20	15.52	942.31	942.89	943.59	947.78	0.343	9.79	1.59	4.26	5.12
77	Q 50	17.81	942.31	942.93	943.68	948.16	0.336	10.13	1.76	4.41	5.12
77	Q 100	19.52	942.31	942.96	943.74	948.43	0.332	10.36	1.88	4.52	5.12
77	Q 200	21.23	942.31	942.99	943.8	948.67	0.327	10.56	2.01	4.62	5.12
77	Q 500	23.49	942.31	943.02	943.87	948.99	0.323	10.82	2.17	4.75	5.11
71	Q 20	15.52	940.45	941.1	941.82	945.68	0.289	9.48	1.64	3.99	4.72
71	Q 50	17.81	940.45	941.14	941.91	946.08	0.289	9.85	1.81	4.16	4.77
71	Q 100	19.52	940.45	941.17	941.97	946.37	0.289	10.1	1.93	4.28	4.79
71	Q 200	21.23	940.45	941.2	942.03	946.63	0.289	10.32	2.06	4.39	4.82
71	Q 500	23.49	940.45	941.23	942.1	946.97	0.289	10.6	2.22	4.54	4.85
64	Q 20	15.52	938.88	939.36	939.9	943.09	0.345	8.55	1.82	6.2	5.04
64	Q 50	17.81	938.88	939.39	939.97	943.47	0.352	8.94	1.99	6.45	5.14
64	Q 100	19.52	938.88	939.41	940.01	943.74	0.356	9.21	2.12	6.62	5.2
64	Q 200	21.23	938.88	939.43	940.06	943.99	0.359	9.46	2.24	6.79	5.25
64	Q 500	23.49	938.88	939.45	940.11	944.31	0.363	9.76	2.41	7	5.32
57	Q 20	15.52	937.52	937.99	938.45	940.73	0.254	7.34	2.11	7.25	4.34
57	Q 50	17.81	937.52	938.01	938.52	941.05	0.261	7.72	2.31	7.49	4.44
57	Q 100	19.52	937.52	938.03	938.56	941.27	0.265	7.97	2.45	7.65	4.5
57	Q 200	21.23	937.52	938.05	938.61	941.49	0.269	8.21	2.58	7.81	4.56
57	Q 500	23.49	937.52	938.07	938.67	941.76	0.274	8.51	2.76	8.01	4.63
50	Q 20	15.52	936.12	936.78	937.31	939.34	0.158	7.09	2.19	5.38	3.55
50	Q 50	17.81	936.12	936.82	937.4	939.61	0.160	7.4	2.41	5.59	3.6

50	Q 100	19.52	936.12	936.84	937.45	939.8	0.161	7.62	2.56	5.74	3.64
50	Q 200	21.23	936.12	936.87	937.5	939.99	0.163	7.82	2.71	5.88	3.68
50	Q 500	23.49	936.12	936.9	937.57	940.23	0.165	8.08	2.91	6.06	3.72
43	Q 20	15.52	935.53	936.16	936.56	938.06	0.154	6.1	2.54	7.87	3.43
43	Q 50	17.81	935.53	936.19	936.61	938.29	0.163	6.41	2.78	8.32	3.54
43	Q 100	19.52	935.53	936.21	936.65	938.44	0.169	6.62	2.95	8.67	3.62
43	Q 200	21.23	935.53	936.23	936.69	938.6	0.175	6.82	3.11	9	3.7
43	Q 500	23.49	935.53	936.25	936.73	938.8	0.183	7.07	3.32	9.4	3.8
36	Q 20	15.52	934.65	935.52	936.03	937.24	0.080	5.81	2.67	5.17	2.58
36	Q 50	17.81	934.65	935.58	936.11	937.43	0.080	6.03	2.95	5.41	2.61
36	Q 100	19.52	934.65	935.61	936.16	937.56	0.080	6.18	3.16	5.59	2.62
36	Q 200	21.23	934.65	935.65	936.2	937.68	0.081	6.32	3.36	5.8	2.65
36	Q 500	23.49	934.65	935.69	936.26	937.84	0.083	6.49	3.62	6.08	2.69
31	Q 20	15.52	933.74	934.41	934.96	936.71	0.122	6.72	2.31	5.02	3.16
31	Q 50	17.81	933.74	934.46	935.04	936.91	0.118	6.93	2.57	5.18	3.14
31	Q 100	19.52	933.74	934.5	935.1	937.04	0.115	7.06	2.76	5.3	3.12
31	Q 200	21.23	933.74	934.53	935.17	937.17	0.113	7.19	2.95	5.41	3.1
31	Q 500	23.49	933.74	934.58	935.24	937.33	0.110	7.34	3.2	5.55	3.09
24	Q 20	15.52	932.79	933.7	934.26	935.92	0.105	6.6	2.35	4.53	2.93
24	Q 50	17.81	932.79	933.75	934.36	936.14	0.104	6.83	2.61	4.75	2.95
24	Q 100	19.52	932.79	933.79	934.43	936.28	0.104	6.99	2.79	4.9	2.96
24	Q 200	21.23	932.79	933.83	934.49	936.42	0.104	7.13	2.98	5.05	2.97
24	Q 500	23.49	932.79	933.88	934.58	936.6	0.103	7.31	3.21	5.24	2.98
17	Q 20	15.52	931.7	932.76	932.76	933.09	0.010	2.55	6.1	9.24	1
17	Q 50	17.81	931.7	932.79	932.79	932.79	0.000	0.16	90.58	34.29	0.06
17	Q 100	19.52	931.7	932.79	932.79	932.79	0.000	0.18	90.58	34.29	0.07
17	Q 200	21.23	931.7	932.79	932.79	932.79	0.000	0.2	90.58	34.29	0.08
17	Q 500	23.49	931.7	932.79	932.79	932.79	0.000	0.22	90.58	34.29	0.08